PLASMA MAGNETOSPHERE AROUND COMPACT OBJECTS

S.C. TRIPATHY

Ph. D. THESIS
JUNE 1991

PHYSICAL RESEARCH LABORATORY
AHMEDABAD
INDIA

PLASMA MAGNETOSPHERE AROUND COMPACT OBJECTS

S.C. TRIPATHY

PHYSICAL RESEARCH LABORATORY
AHMEDABAD
INDIA

A THESIS
SUBMITTED TO THE GUJARAT UNIVERSITY
FOR THE DEGREE OF
DOCTOR OF PHILOSOPHY

JUNE 1991

DECLARATION

I hereby declare that the contents of this thesis represent original work and they have not formed the basis for the award of any degree or diploma by any University or Institution.

Author

S.C. Tripathy
Physical Research Laboratory
Ahmedabad - 380 009
India.

Certified by

Thesis Supervisor

A. C. Das
Theoretical Physics Division
Physical Research Laboratory
Ahmedabd - 380 009
India.

DEDICATED TO

My Parents

and

My Teachers

Contents

Acknowledgements

I wish to express my profound gratitude to Professor A.C. Das, my thesis supervisor for his expert guidance, constant encouragement and affection. His deep physical insight has rescued me out of many seemingly endless problems on several occasions. I am quite fortunate to have been associated with him. I am grateful to him for all his help and timely advices.

It is a pleasure to explicitly acknowledge the singular influence of my academic advisor Professor A.R. Prasanna. His devotion to the Theory of General Relativity as well as his research contributions have been a continuing source of inspiration for me. I am extremely thankful to him for introducing me to GTR and its wide ranging applications in astrophysical scenarios. I value greatly my association as well as my collaboration with him.

I am indebted to the Director, Professor R.K. Varma for many fruitful discussions and valuable advices. My sincere thanks are also due to Professor Vijay Sheorey and Dr. Suhasini Rao for many helpful discussions on different aspects of numerical analysis. I gratefully acknowledge the extensive help rendered by Sitaram both academically and otherwise. It was my good fortune as a student to have had a series of excellent teachers in Physics and I would like to particularly thank Swaren Maharaj from whom I have learnt a lot.

I wish to record my heart-felt thanks to Professors Lynden-Bell of Institute of Astronomy, Cambridge, Marek Abramowicz of ICTP, Trieste and Jiří Bičák of Charles University, Prague for many interesting discussions. I also wish to acknowledge Professors Vinod Kishan and Bhaskar Datta of IIA, Bangalore for many stimulating discussions.

My friend and colleague Bhaskaran has been extremely helpful at different stages of my research work and it is a pleasure to thank him. I would like to specially thank Dwivediji, although a late joiner, for his critical suggestions. I enjoyed greatly the collaborative work carried out with both of them. I have been benefited extensively from endless discussions and arguments with Kishku. He introduced me to the eigenvalue techniques, which I have

extensively applied in my calculations. My special thanks to him. My sincere thanks to Sai for introducing me to TEX and for giving all possible help, ever smilingly.

I am quite fortunate to have the intimate friendship with Rekha right from the beginning days of PRL. Although her regular e-mails have been quite refreshing, I miss her delightful company a lot. My affectionate thanks to her for all that she has done for me. I am indebted to Professor Jain and Mrs. Jain for all their affection and love and for creating a homely atmosphere away from my home. My thanks are due to Anand and Usha for their wonderful company. My Bhabi's encouraging letters have kept my spirits high in many a difficult times and I owe her a lot.

Special thanks are due to my friends and colleagues at PRL, particularly Bhaskaran, Dwivediji, Kishku, Manoj, Sunil and Subrat who read the evolving manuscript and made numerous helpful corrections and suggestions. I profusely thank Mathew and Supriya for their endless efforts in bringing the diagrams into this neat form. I thank Debashish, Krishnan, Sam and Somesh for their sincere help in the final rites of my thesis.

I wish to thank Ajay, Durga, Jerry, Raju and Shwetketu for being nice friends. My thanks are due to Ganguly, Guru, Himadri, Manohar Lal, Gufran, Shisir, Lambodar, Vasif, Viswa and Murali for their cheerful company. Ramani deserves a special mention for his energetic commotion and self-less help. It is pleasant to recollect the lively after dinner talks with Bhaskaran, Kishku, Raju, Sateesh, Subba, Debi and Mathew. I thank Sheela and Reeta for their jovial company.

I wish to thank the staff of Library, Computer Center and Canteen for their cooperation and excellent services. I am thankful to Messers. Ranpura and Bhavsar for their skillful work. My grateful thanks to Rajagopalan for typing the figure captions neatly.

Last, but not the least, I am thankful to all those who have directly or indirectly helped me in my work.

Research Publications

1. Equilibrium structure for a plasma magnetosphere around a compact object, Prasanna A.R., **S.C. Tripathy** and A.C. Das, 1989, J. Astrophys. Astr., **10**, 21.

2. Accreting Magnetofluid Around a Compact Object with a Dipolar Magnetic Field - A Newtonian Analysis, **S.C. Tripathy**, A.R. Prasanna and A.C. Das, 1990, Mon. Not. R. astr. Soc., **246**, 384.

3. Plasma Disc Around a Slowly Rotating Compact Object, P.Bhaskaran, **S.C. Tripathy** and A.R. Prasanna, 1990, J. Astrophys. Astr., **11**, 461.

4. Plasma Instability at the Inner Edge of the Accretion Disc: **S.C. Tripathy**, C.B. Dwivedi, A.C. Das and A.R. Prasanna, PRL-TH /91-1 (Pre-print).

5. Radial- Azimuthal Instability at the Inner edge of the Accretion Disc (in preparation).

Abstract

When a star or a planet has an associated magnetic field, the space surrounding the object is strongly influenced by the magnetic field. The magnetic field acts as a barrier to charged particles that travel towards the central object because gyrating motions of the particles deflect direction of the flight. Due to this effect, plasma from external origin tends to be excluded from vicinity of the magnetised objects. As a result, a cavity is carved out around a magnetised object in the domain of the streaming plasma. The cavity inside which magnetic field lines are confined is called the magnetosphere of the central object.

The study of magnetospheres around accreting compact objects started with the discovery of the quasars, Active Galactic Nuclei (AGN's) and X-ray sources. Most of the energy emitted by these objects is in the range of 10^{38} *-*10^{45} *ergs/sec. The main energy generation mechanism is believed to be the accretion of matter onto highly collapsed stars, a scenario where gravitation, the main binding force of the universe is in operation. If the matter being attracted has angular momentum with respect to the central star, it forms a disc around it. The large scale structure and the dynamics of such discs is important physically, as many of the observable properties like pulse shapes, spectra, spin-up rate and intensity fluctuations depend on it.*

The earliest of the theoretical models of such accretion discs, which took into account, self-consistently, various physical parameters, was due to Shakura & Sunyaev [33]. Subsequently, several variations of this model have been considered depending upon the particular scenario where the model was applied, but a firm theoretical basis for these models is yet to be established. One of the factors is the non-inclusion of the role of magnetic fields in the discussion of the dynamics of the plasma flow. It is believed that most of the matter in the universe is in plasma state. The motion of ions and electrons in the plasma environment circling the central star would produce currents and the associated magnetic fields. One of the earliest discussions that explains qualitatively the influence of the magnetic field on the inner edge of the magnetosphere, in the context of the accretion disk model for compact X-ray sources, is due to Pringle [114]. Bisnovatyi-Kogan [101] had considered the effects of magnetic field on the accreting magnetofluid and found that there could be an increase in the efficiency of radiation emission.

As accretion is synonymous to gravitation, it is quite natural to realise the importance of general relativity in discussing the structure and stability of magnetospheric plasma around a compact object [11]. Although, the Newtonian description may be satisfactory for describing the motion of the magnetofluid in the magnetosphere of a neutron star, it would not be adequate for the case of plasma flow around black holes. Thus, it is very important to consider the dynamics and stability of magnetospheric plasma in the presence of electromagnetic fields on curved space time.

In this work, we have taken up the study of the dynamical equilibrium and stability of magnetospheric plasma around a compact object including the effects of general relativity through the analysis of the MHD equations self consistently. With

this motivation, we have developed the dynamical equations for a magnetofluid surrounding a central compact object in a curved background geometry. The governing equations are solved for several special cases of velocity and magnetic field distributions. The analysis reveals explicitly the inter-dependence of certain physical parameters like seed magnetic field, outer disc density, finite conductivity and continuous pressure distribution on the equilibrium configurations of the magnetofluid.

Instability studies, as a source for different kinds of radiation processes especially X-rays from accretion discs, are very important. We have analysed the instabilities of different modes that can be supported by the plasma in accretion discs. One of the key features of this investigation, in the frame work of a local analysis, is the existence of plasma instabilities like Kelvin-Helmholtz, Rayleigh-Taylor and magnetosonic modes.In addition, we have also observed one other mode which may be excited due to the finite conductivity of the plasma in the disc. To understand the structure of various unstable modes, we have also carried out, a global analysis in the frame work of a complete numerical model.

Chapter 1

INTRODUCTION

The study of structure of magnetosphere around accreting compact objects is central to the understanding of a wide variety of cosmic high energy sources. Most of the energy emitted by these sources is in the form of X-rays in the range of 10^{36} ergs-s^{-1} to 10^{45} ergs-s^{-1} and is supplied by the accretion of matter to the surface of the compact objects like neutron stars or black holes. If the central compact object has an intrinsic magnetic field, the magnetic field influences the incoming magnetofluid and eventually the motion is completely governed by the field. Finally, the matter ends up on the surface of the central star either by flowing along the field lines or by diffusing across it due to turbulence or instabilities. If the matter being attracted has angular momentum with respect to the central body, it forms a disc around it. The large scale structures and dynamics of such plasma magnetospheres are of fundamental importance and the current interest lies in understanding of structure and properties of these magnetospheres in order to explain many of the observable properties.

It is also of great significance to understand the interaction between the magnetosphere of a neutron star and the surrounding accretion disc with regard to

the formation of binary radio pulsars and the origin of quasi-periodic oscillations (QPO) from low mass X-ray binaries. In this context, it is necessary to investigate different modes of instabilities that could arise in discs supported by the gas and magnetic pressure around compact objects under general perturbations. Although numerous models with several variations have been proposed for different scenarios, equilibrium structures and the corresponding stability analysis including the effects of self-consistent magnetic fields are still in its infancy.

In this thesis, we have studied the self-consistent equilibrium configurations and stability criteria for a plasma magnetosphere around compact objects in the presence of magnetic and gravitational fields both in Newtonian and relativistic formalisms. With this motivation, we have developed the dynamical equations for a magnetofluid surrounding a central compact object in a curved background geometry. Subsequently, these equations are applied to analyse the dynamical equilibrium and stability of a few configurations.

In this chapter, a brief description of the magnetospheric models associated with disc accretion is presented. We start with the preliminaries in Section 1. The basic need for studying such models is stressed in Section 2. Section 3 highlights the role of general relativity and magnetic fields in such studies. An overview of theoretical models with special emphasis on those incorporating magnetic fields is given in Section 4. The role of plasma instabilities is illustrated in Section 5. A brief summary of the structure and stability of thick disc models is presented in Section 6. The aim and scope of the thesis is briefly outlined in Section 7.

1.1 Preliminaries

When a star or a planet has an intrinsic magnetic field, the space surrounding the object is strongly influenced by the magnetic field. The magnetic field acts as a barrier to charged particles that travel towards the central object because gyrating motions of the particles deflect direction of the flight. Due to this effect, plasma from external origin tends to be excluded from the vicinity of the magnetized objects. As a result, a cavity is formed around a magnetized object in the domain of the streaming plasma. The cavity inside which magnetic field lines are confined, is called the magnetosphere of the central object. The term 'magnetosphere' was introduced, in the terrestrial context by Gold [1]. The magnetosphere of an object, according to his definition, is the region of space surrounding the object within which the object's magnetic field exerts a dominant influence upon the motion of the plasma. Since the magnetic field controls the plasma flow and *viceversa*, the two ways of defining the magnetosphere are essentially equivalent.

The study of magnetospheres can be broadly classified into two types *viz.* planetary or terrestrial magnetosphere (Fig. 1.1) and magnetosphere around compact objects (Fig.1. 2). The planetary magnetospheres are formed by the interaction of the solar wind with the intrinsic magnetic fields of the planets. The physical mechanisms that operate in planetary magnetospheres are more or less well understood. Many basic plasma processes and instabilities such as the reconnection of magnetic field lines, wave particle interactions, double layers and Kelvin-Helmholtz (K-H) instability occur in planetary magnetospheres. Although, some of these fundamental concepts have been already applied for the understanding of physical processes around compact objects, these concepts need to be extensively examined in the case of plasma magnetospheres around compact objects and its interaction with the

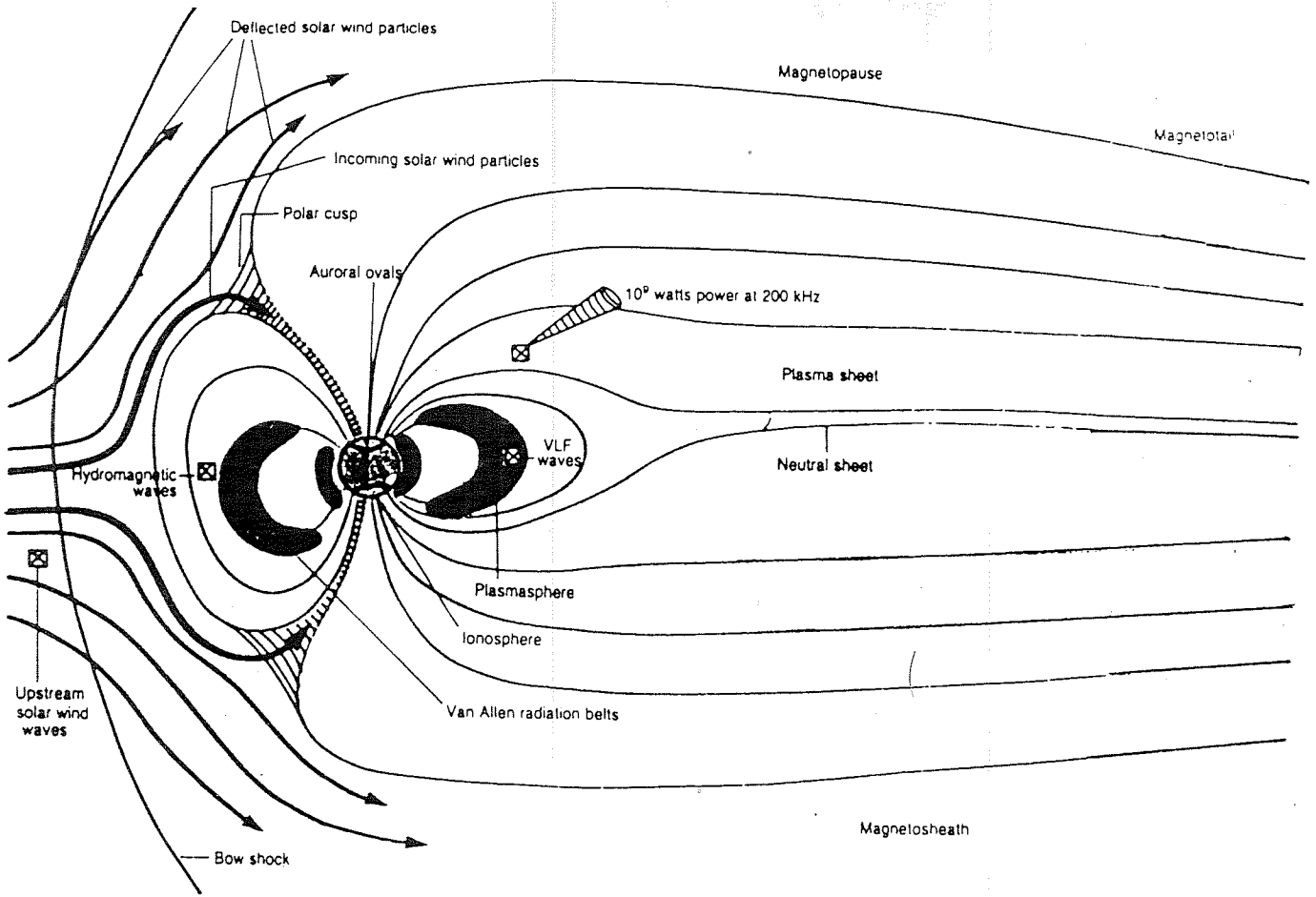

Figure 1.1. **Earth's magnetosphere.** The sketch above shows important features of the plasmas and waves in the magnetic fields that surround the Earth. (Source: Lanzerotti & Kirmigis, 1985, Phys. Today, 11, 24).

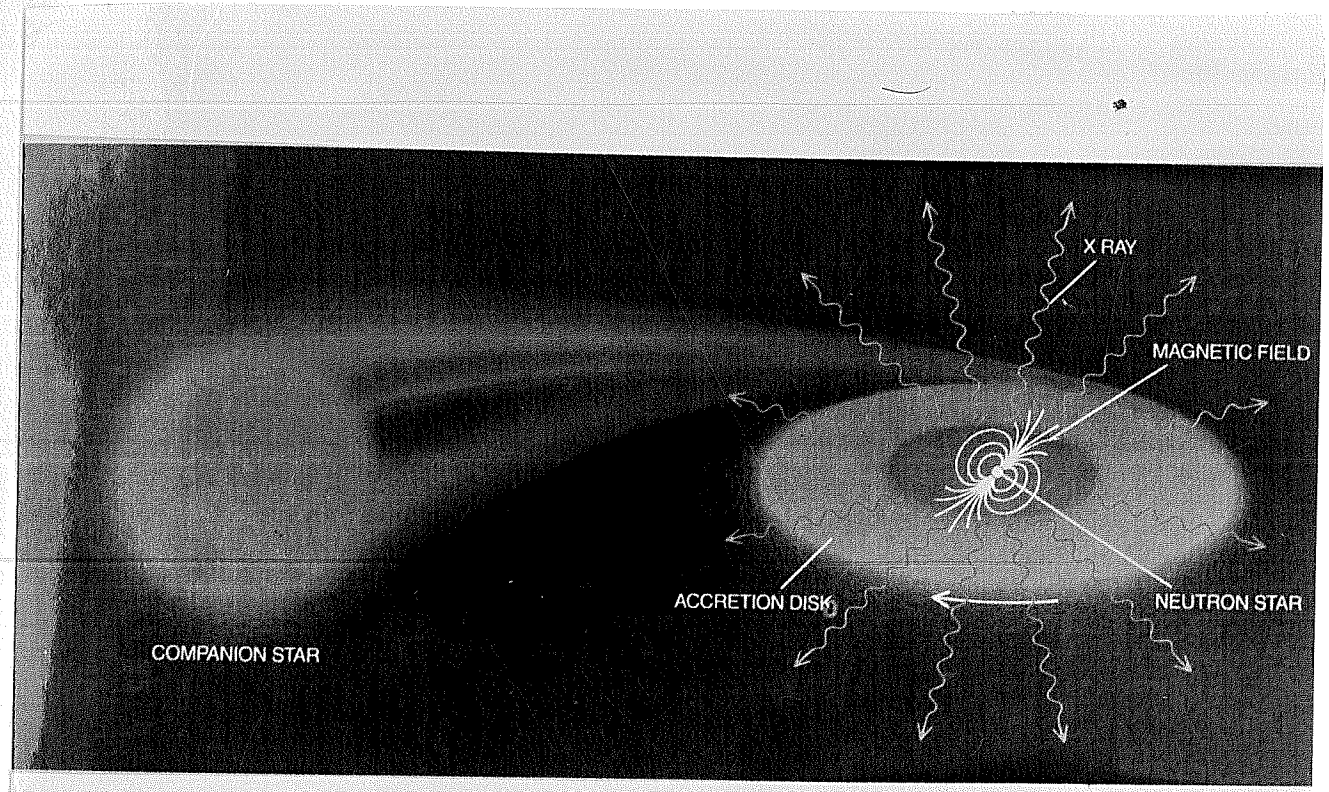

Figure 1.2: An artistic picture of a spinning neutron star having an accretion disc and being orbited by a companion star. (Source: J. Shaham, 1987, Sci. American., **256(2)**, 50)

the accretion discs.

The study of magnetospheres around accreting compact objects started with the discovery of the quasars, active galactic nuclei (AGN) and X-ray sources. Most of the energy emitted by these objects is in the range of 10^{38} -10^{45} ergs-s^{-1}. The main energy generation mechanism is believed to be the accretion of matter onto highly collapsed stars, a scenario where gravitation, the main binding force of the universe is in operation. A simple back-of-envelope estimate will illustrate this point. For a body of mass M_g and radius R, the amount of potential energy released by the accretion of mass M on to its surface is

$$\Delta E_{acc} = \frac{GM_gM}{R}, \tag{1.1.1}$$

and the luminosity is given by

$$L_{acc} = \frac{GM_g\dot{M}}{R}, \tag{1.1.2}$$

where G is the gravitational constant and $\dot{M}$ is the accretion rate . If the accreting body is a neutron star (NS) with radius R = 10 km and mass $M_g = M_\odot$, the solar mass, then $\Delta E_{acc} = 10^{20}$ ergs/accreted gram and this energy is released mainly in the form of electromagnetic energy. Since the observed X-ray luminosity is in the range of 10^{36} to 10^{38} ergs-s^{-1}, equation (1.1.2) implies

$$\dot{M} = 10^{-7}M_\odot/M_g \quad \text{for a white dwarf} \tag{1.1.3}$$

$$\dot{M} = 10^{-9}M_\odot/M_g \quad \text{for a neutron star.} \tag{1.1.4}$$

For the case of accretion onto black holes, the validity of luminosity relation is questionable. The main objection arises from the fact that the radius does not refer to a hard surface and once the matter enters the event horizon, it cannot escape out

of the black hole. This uncertainty in the luminosity relationship is parameterized by the introduction of a dimensionless quantity η called the efficiency factor,

$$L_{acc} = \frac{2\eta G M_g \dot{M}}{R} \tag{1.1.5}$$

$$= \eta \dot{M} c^2, \tag{1.1.6}$$

where $R = 2GM/c^2$ have been used for the black hole radius.

The study of magnetospheres of accreting neutron stars began with the discovery of bright pulsating X-ray sources in the galaxy in 1972 by Schreier *et al.* [2] & Tananbaum *et al.* [3]. These rotating magnetic neutron stars accrete matter from a binary companion and should not be confused with the pulsars (pulsating radio sources) in which the primary energy source and the physical conditions are completely different. The plasma environment of neutron star magnetospheres which ranges from low density winds with little rotation to very high density Keplerian accretion discs, are considerably different than those of the known planetary magnetospheres, all of which are immersed in solar wind. In spite of this contrasting nature, the principal differences between the two types of magnetospheres may be traced to a relatively few factors:

1. the strong gravitational field, which traps the plasma far outside the magnetosphere and controls its flow to the stellar surface,

2. the large mass flux into the magnetosphere, which stresses the outer magnetosphere and produces a relatively high plasma density throughout,

3. the high density, which makes the plasma collisional or quasi-collisional and leads to rapid cooling,

4. the intense radiation field, which quickly cools the plasma and can produce forces even larger than gravity and,

5. the rapid rotation of the plasma and the magnetosphere, which stretches the outer magnetosphere and strongly affects the plasma flow pattern.

In describing the dynamics of mass outflow from the companion and its subsequent capture by the compact star, two broad cases *viz.* spherical accretion and accretion from a disc can be distinguished. These cases can be illustrated by considering a binary system whose orbits are circular. This is usually a good approximation since tidal effects tend to circularize the azimuthal eccentric orbits on time scales short compared to the time over which mass transfer occurs. The effective gravitational potential (Roche potential) of the binary system is given by,

$$\Phi(r) = -\frac{GM_1M_\odot}{\mid \mathbf{r} - \mathbf{r_1} \mid} - \frac{GM_2M_\odot}{\mid \mathbf{r} - \mathbf{r_2} \mid} - \frac{1}{2}(\omega \times \mathbf{r})^2, \tag{1.1.7}$$

where $\mathbf{r_1}$ and $\mathbf{r_2}$ are the position vectors of the centers of the two stars with masses M_1 and M_2. Fig. 1.3 depicts the equipotential surfaces of $\Phi(r)$ in the orbital plane. The most interesting and important feature of this diagram is the figure-of-eight area which is called the Roche lobe. The lobes join at the inner Lagrangian point L_1 which is a saddle point of $\Phi(r)$ and it facilitates mass transfer from one side to the other. On the basis of the relative sizes of the Roche lobe to the companion star, the above mentioned accretion processes are distinguished which we define below.

1.1.1 Spherical accretion

If the companion star is much smaller than the Roche lobe, then the matter flowing out from the star as a stellar wind is captured by the gravitational field of the

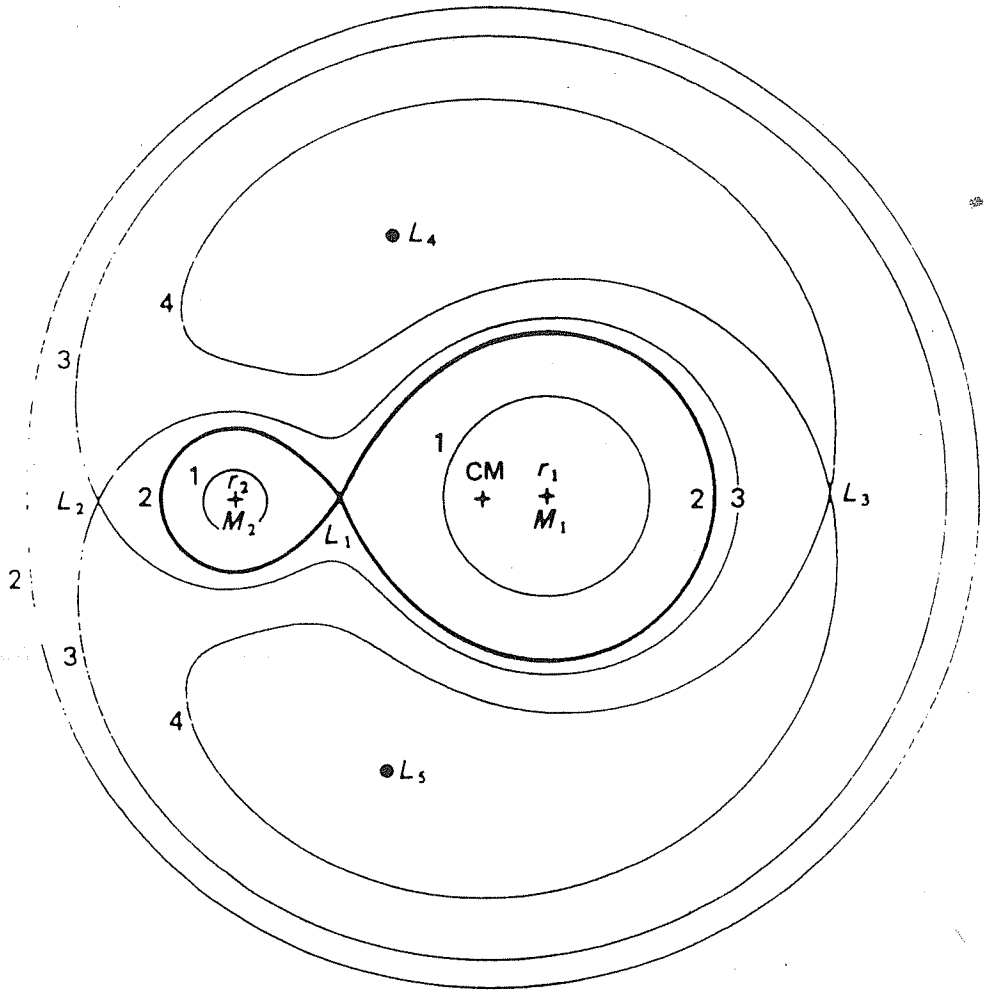

Figure 1.3. Sections in the orbital plane of the Roche equipotentials $\Phi(r)$ = constant, for a binary system with mass ratio $q = M_2/M_1 = 0.2$. Shown are the centre of mass (cm) and Lagrange points L_1-L_5. The equipotentials are labelled 1-4 in order of increasing $\Phi(R)$. Adopted from Frank et al. [34].

compact object from the gravitational sphere of influence whose radius is given by

$$R = \frac{GM_g}{2V^2}, \tag{1.1.8}$$

where V is the flow speed of the stellar wind. This case was studied by Hoyle & Lyttleton [4] and later by Bondi [5] three decades ago and presently, this is referred to as *spherical accretion* (Fig. 1.4a).

1.1.2 Disc accretion

On the other hand, if the companion star fills its Roche Lobe (Roche lobe overflow), matter from the normal star transfers through the Lagrangian point L_1 to the compact object. As a consequence of this process, the accreting matter has considerable angular momentum so that the matter cannot accrete directly onto the compact object. Instead it forms a disc from which the matter spirals slowly as the angular momentum is removed by tangential stresses, either viscous or magnetic. This case is universally referred to as *disc accretion* (Fig. 1.4b).

1.2 Why magnetospheric models ?

Theoretical models of a magnetosphere aim to describe the configuration of the magnetic field and the dynamics of the plasma flow within the magnetosphere. The existence of Eddington limit for luminosity (an upper bound on the luminosity at which radiation pressure on free electron balances gravity) which signifies the importance of forces other than gravity, suggests that the dynamics of the flow may not be very simple. In addition to the intrinsic scientific interest of the problem, there are several reasons for developing the magnetospheric models of compact objects:

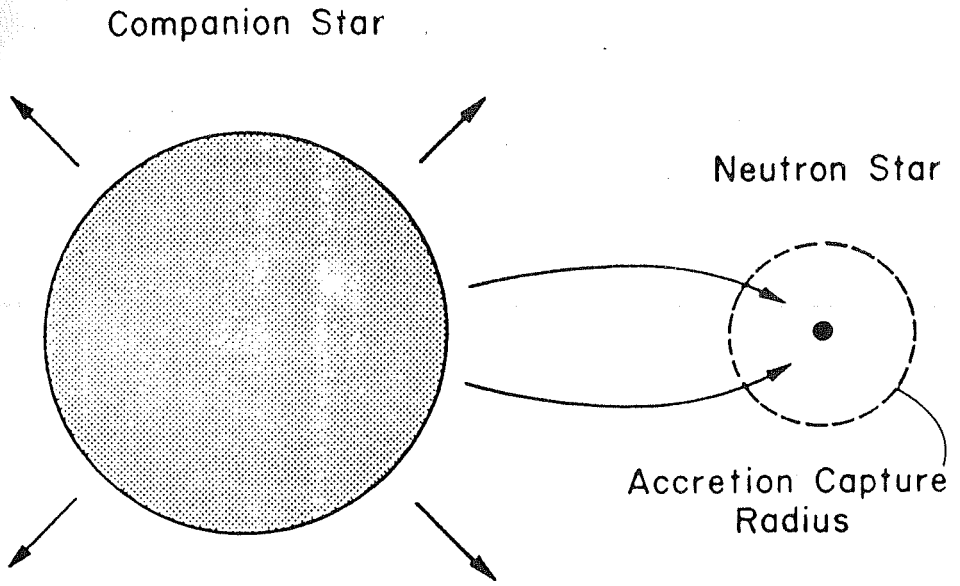

Figure 1.4. (a) WIND-FED STAR ($\omega_p \lesssim 1$)

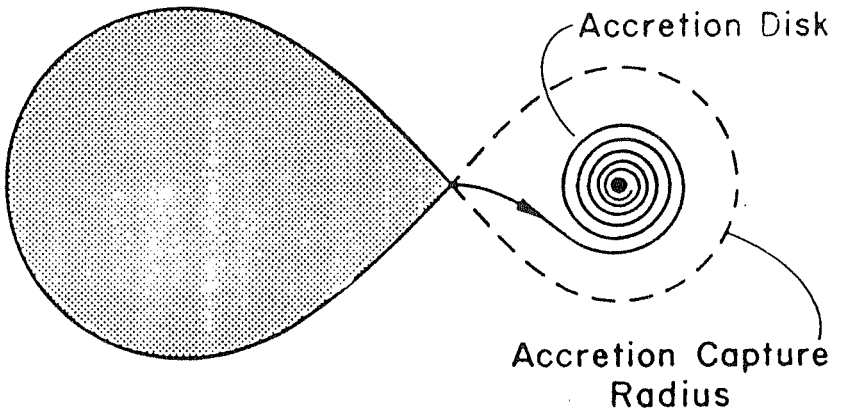

Figure 1.4. (b) DISK-FED STAR ($\omega_p = 1$)

1. Understanding of the observable properties of the X-ray sources like pulse shapes, spectra, spin up rates and intensity fluctuations which depend on the structure of the magnetosphere.

2. To ensure that mass transfer rate is adequate to sustain the luminosity.

3. To understand the possible ways of losing angular momentum and the application of torque on the compact object which would provide quantitative estimates of rate of change of period for comparison with observations.

4. Properties of the plasma within the magnetosphere for a detailed calculation of the emitted radiation.

5. Detailed description of the accretion flow to explain the observed spectral distribution of the radiation produced.

6. Plasma instabilities and their associated time scales in the magnetosphere to explain the formation of bursts, X-ray emissions, variabilities of AGN's and possibly millisecond pulsars.

Many published theoretical models, in the past, have attempted to explain various features of the observations. However, more sophisticated models of the dynamical properties of the accreting matter and the transfer of angular momentum as well as the response of the compact object itself are still required to understand the whole variety of observations. Although many excellent review articles (Vasyliunas [6], Börner [7], Hayakawa [8], Wiita [9], Fumiaki [10], Prasanna [11]) have been published, we cite here, for the sake of completeness, a brief summary of the research work done with special emphasis on the role of magnetic fields in both Newtonian formalism and on curved background geometry.

1.3 Importance of general relativity and magnetic field

The influence of gravity in the study of accretion process is self evident. To give a flavour, we consider a simple example which will bring out the importance of gravitation in accretion dynamics. Consider a blob of gas (plasma) which approaches a rotating neutron star with approximately radial velocity. Even far from the magnetosphere, the plasma is gravitationally bound to the star due to the nature of the gravitational force and it will remain so until it enters the magnetosphere. Even in the case of disc accretion, model calculations indicate that the bulk of the plasma that reaches the magnetospheric boundary will be accreted to the stellar surface. Thus, it is to be emphasized that due to gravity the plasma cannot escape from the potential well of the compact object and has to follow only one path - to fall into the central star.

As accretion is synonymous to gravitation, it is quite natural to realise the importance of general relativity in discussing the structure and stability of magnetospheric plasma around a compact object (for a review, see Prasanna[11]). The significance of general relativity in accretion process was independently cited by Zeldovich [12] and Salpeter [13] in 1964 while discussing the accretion of interstellar matter by massive objects for producing high luminosities. In the case of accretion onto black holes, it is well known that the accreted material would finally fall into its center and emit part of its energy as radiation. In the absence of the magnetic field, the transformation of kinetic energy into radiation is very small but this gets enhanced in the presence of the magnetic field due to the intense synchrotron radiation (Bishnovyati-Kogan [14]). A clue to the relevance of magnetic field in the

accretion process was obtained from the study of charged particle motion on curved space-time geometry (Prasanna [15]). Even, in the presence of a weak magnetic field, the investigation for the motion of a charged particle in Schwarzschild geometry (Prasanna & Varma [16]) demonstrated that there exists stable orbits as close as 2.1m against the limit of 6m in the absence of magnetic fields. A further study by Chakrabarty & Prasanna [17] showed the possible existence of thick disc structures due to the interaction of magnetic and intense gravitational fields. This analysis also revealed that the formation of cusp is possible only when the gravitational field is described by the general relativistic formalism and not in the Newtonian theory. The cusp, where the angular momentum induced by the gravity of the central source equals the angular momentum of the source itself, was shown (Abramowicz *et al.* [18]) to exist between the marginally bound (r = 4m) and marginally stable (r = 6m) time like orbits in the Schwarzschild geometry.

Although black holes do not have an intrinsic magnetic field, the analysis of Galeev *et al.* [19] showed that as a result of stretching of the interstellar magnetic fields, the field gets amplified and becomes dynamically important. The motion of the plasma would then produce currents and associated magnetic fields in the disc. These ordered magnetic fields in accretion discs around black holes may have a completely different role in the formation of narrow jets seen in many extra-galactic radio sources. Although a widely favoured idea for the origin of these jets is based on the occurrence of narrow, essentially empty vortex funnels in accretion flows (Lynden-Bell [20]), an alternative proposal involving magnetic fields in which jets are electrodynamically accelerated due to the unipolar induction dynamo effect, has also been considered (Lovelace *et al.* [21]; Blandford [22]; Blandford *et al.* [23]).

In the realm of observations, the evidence to include the effects of general

relativity is progressively increasing. Malkan *et al.* [24] showed that the best fit for the quasar emission spectra could be obtained by including the general relativistic effects of redshift and focusing. Paczynski [25] attributed the QPO phenomenon to the unsteady flow of the accreting matter in the inner region of a thick accretion disc and conjectured that the oscillations may be due to the general relativistic effect.

The above description clearly illustrates the importance of magnetic field in the dynamics of plasma flow around compact objects. It also highlights the fact that the Newtonian formalism is not adequate for the analysis of accretion flow around black holes although it may be satisfactory for characterizing the motion of the magnetofluid in the magnetosphere of a neutron star.

Hence, it is imperative to consider the role of magnetic fields in a curved back ground geometry for the analysis of accretion flows around magnetospheres of compact objects. With this prime motivation, we have investigated the self-consistent structures and stability of plasma magnetospheres around compact objects in the frame work of a complete relativistic model including magnetic fields.

1.4 Historical perspective

The study of accretion had its foundations in the late thirties with the publication of a paper by Hoyle & Lyttleton [4]. This key note paper which has an interesting title "The effect of interstellar matter on climatic variations" contains the first derivation of the accretion rate for a star moving through cold gas. The next important step in the development of accretion theory was the paper by Bondi [5] where a full analytic solution for the fluid flow was derived. The real emphasis on building self-consistent models of accretion discs started in the sixties with two fundamental astrophysical

discoveries: quasars and X-ray sources with extremely large luminosities (10^{38} - 10^{45} ergs-s^{-1}). From the variability associated with these objects, it was immediately known that the radiation is being emitted from comparatively small regions ($r \sim$ 1 pc). Even before the detection of X-ray sources, Hayakawa [26] had suggested that close binary stars may be detectable as X-ray objects because of the mass accretion. The role of accretion discs in binary sources was recognized by Novikov & Zeldovich [27], Shklovsky [28] and Prendergest & Burbidge [29] and subsequently the importance of disc accretion onto a massive black hole was pointed out by Lynden-Bell [30] with special reference to the center of our galaxy and by Lynden-Bell and Rees [31] with application to AGN. The discovery in 1971 of the source Cen X-3 (Giaconni *et al.*, Schreier *et al.* [32,2]) and Her X-1 (Tananbaum [3]) by the Uhuru satellite exhibiting eclipses and periodic doppler variations of the pulsation period ushered in a new era in the study of accretion dynamics. A detailed model with a computation of the emission spectrum was later published by Shakura and Sunyaev [33] which is now referred to as the standard α-disc model in the literature and is discussed in great length by Frank *et al.* [34]. The other earlier models which need special mention are due to Novikov & Thorne [35] and Thorne [36] where they elucidated the effects of general relativity on the inner regions of the accretion disc. Subsequently, several variations of the standard model and many other models have been published but a firm theoretical confirmation with observations is yet to be achieved.

With the success of accretion theory being applied to X-ray sources, quasars and AGN, it is natural for the theory to gain a prominent role in the standard astrophysical scenarios. At present, the theory of accretion enters into the realm of various classes of objects like cataclysmic variables (CVs), X-ray binaries and AGN

(seyfert nuclei, quasars and blazars) and possibly the still mysterious gamma ray sources.

1.5 Survey of models

Accretion disc, at present, is the only important model capable of explaining radiation and some of the observed properties from high energy astrophysical objects. As a result, these models have gained tremendous popularity in astrophysical community. However, due to the extreme conditions prevailing in and around the compact object, a single comprehensive model describing all the major aspects of the magnetosphere around accreting compact objects is yet to emerge. The development of accretion theory could be broadly classified into two major sections *viz.* (i) the seminal ones (ii) the ones that are fundamentally important in establishing accretion as a basic mechanism for energy generation. Some of the important papers covering these aspects are now available in a collected volume (Treves *et al.* [37].)

The first quantitative models of accreting neutron star magnetospheres were those developed by Pringle and Rees [38], Davidson and Ostriker [39] and Lamb, Pethick and Pines [40]. Various features of these models were subsequently developed by Baan and Treves [41], and Elsner and Lamb [42]. Plasma flow inside the magnetosphere has also been studied by Ghosh, Lamb and Pethick [43] and by Scharlemann [44]. The basic models, as reviewed by Vasyliunas [6] can be classified into four broad headings *viz*

- the early models in which the size of the magnetosphere is estimated from the simple pressure balance conditions and the accreting matter is postulated to enter the magnetosphere through a pair of funnels at the pole,

- closed magnetospheric models in which the matter enters the magnetosphere through instabilities at its inner boundary,
- plasma flow inside the magnetosphere and,
- magnetospheric models associated with disc accretion.

However, in the next section, we confine our discussion specifically to disc accretion models which are primarily relevant to our work.

1.5.1 Disc Accretion

As noted earlier, an accretion disc would form if the incoming matter possesses significant angular momentum during the Roche lobe overflow. Accretion from such a disc is possible only when the angular momentum is transported away by dissipative processes. The total luminosity during such processes in a steady state (Frank *et al.* [34]) is

$$L_{disc} = \frac{GM_g\dot{M}}{2R}, \tag{1.5.1}$$

where $\dot{M}$ is the accretion rate. It is to be noted that this disc luminosity is just half of the accretion luminosity (equation 1.1.2) which is obtained when all the kinetic energy of the infalling matter is given up at the stellar surface. The other half of the energy is to be radiated at the magnetospheric boundary (magnetopause or inner boundary) between the accretion disc and the compact object. The estimate of the size of the magnetosphere was obtained by Davidson & Ostriker [39] and Baan & Treves [41] based on the concept first proposed by Chapman and Ferraro in 1933 and extensively applied in the terrestrial magnetosphere. To a first approximation, the radial distance R_{CF} (Chapman-Ferraro radius) from the compact object to the

magnetopause may be estimated by equating the pressure of the dipole magnetic field to the gas pressure of the accreting matter *i.e.*

$$\frac{B^2_{dipole}}{8\pi} = P_{disc}. \tag{1.5.2}$$

In the case of spherical accretion, the radius is found to be

$$\frac{R_{CF}}{R} = \frac{\mu}{4L} V_{ff} \phi \zeta, \tag{1.5.3}$$

where μ is the dipole moment of the compact object, L is the luminosity, $V_{ff} = (2GM/r)^{\frac{1}{2}}$ is the free fall velocity, ϕ is the area over which the accreting matter enters the magnetosphere and ζ signifies the ratio between the average flow speed and free fall velocity at the magnetopause. Using the same concept of pressure balance, Pringle and Rees [38] estimated this distance for a disc accretion and found that this occurs at the radius,

$$r_p = 0.89 \left[\frac{rV_r}{hV_{ff}}\right]^{\frac{2}{7}} l_0, \tag{1.5.4}$$

where V_r is the inward radial drift velocity in the disc, h is the disc semi-thickness, and l_0 is a characteristic length which appears in nearly all estimates of the size of accreting neutron star magnetospheres. Since, above and below the disc, the pressure is assumed to be very small, the magnetosphere is expected to extend to larger distances over the disc's mid-plane and the equilibrium configuration requires the matter pressure at the top and bottom of the disc to balance the magnetic field.

The details of the accretion process in the region where the magnetic field dominates the dynamics have been studied by several investigators. The general description of plasma flow from the disc midplane to the surface is quite complex and still not very well understood. Further, there is no consensus regarding several basic questions. This could be probably attributed to two rather different types of

models that have been considered. In one approach to the problem, the accretion disc is presumed to be threaded by stellar magnetic field. In contrast, the other approach is based on the assumption that the disc matter (plasma) is characterized by an infinite conductivity. As a result, the disc is considered to be diamagnetic and the stellar field is completely excluded from the disc. We discuss, in the next section, the main merits and demerits of these models.

Accretion discs could also be broadly divided into two distinct classes based on their geometrical shapes. If the disc flow is confined closely to the orbital plane then, as a first approximation, one can regard the disc as a two dimensional gas flow, such a configuration is called a thin disc. In cylindrical geometry (R,ϕ,z), a disc is defined to be thin, if h $\ll$ R, where h is the vertical height of the disc. In terms of the dynamics, a disc is said to be thin if the local Keplerian velocity turns out to be supersonic, *i.e.*

$$C_s \ll \left(\frac{GM}{R}\right)^{\frac{1}{2}} \tag{1.5.5}$$

where C_s is the local sound speed. The above descriptions may be violated in the innermost region of accretion discs around stellar black holes and neutron stars where the accretion rate approaches the limiting value specified by the Eddington luminosity. In this case, the thin disc approximation breaks down near the central object. We will discuss the case of thin disc accretion first and then go over to the discussion of thick discs in Sect. 1.5.3.

1.5.2 Thin Disc

Lamb, Pethick & Pines [40] were the first to assume that the plasma entering the magnetosphere would be rapidly threaded by the magnetic field and showed that the plasma would then be forced to flow along the field lines. Fig. 1.5a depicts

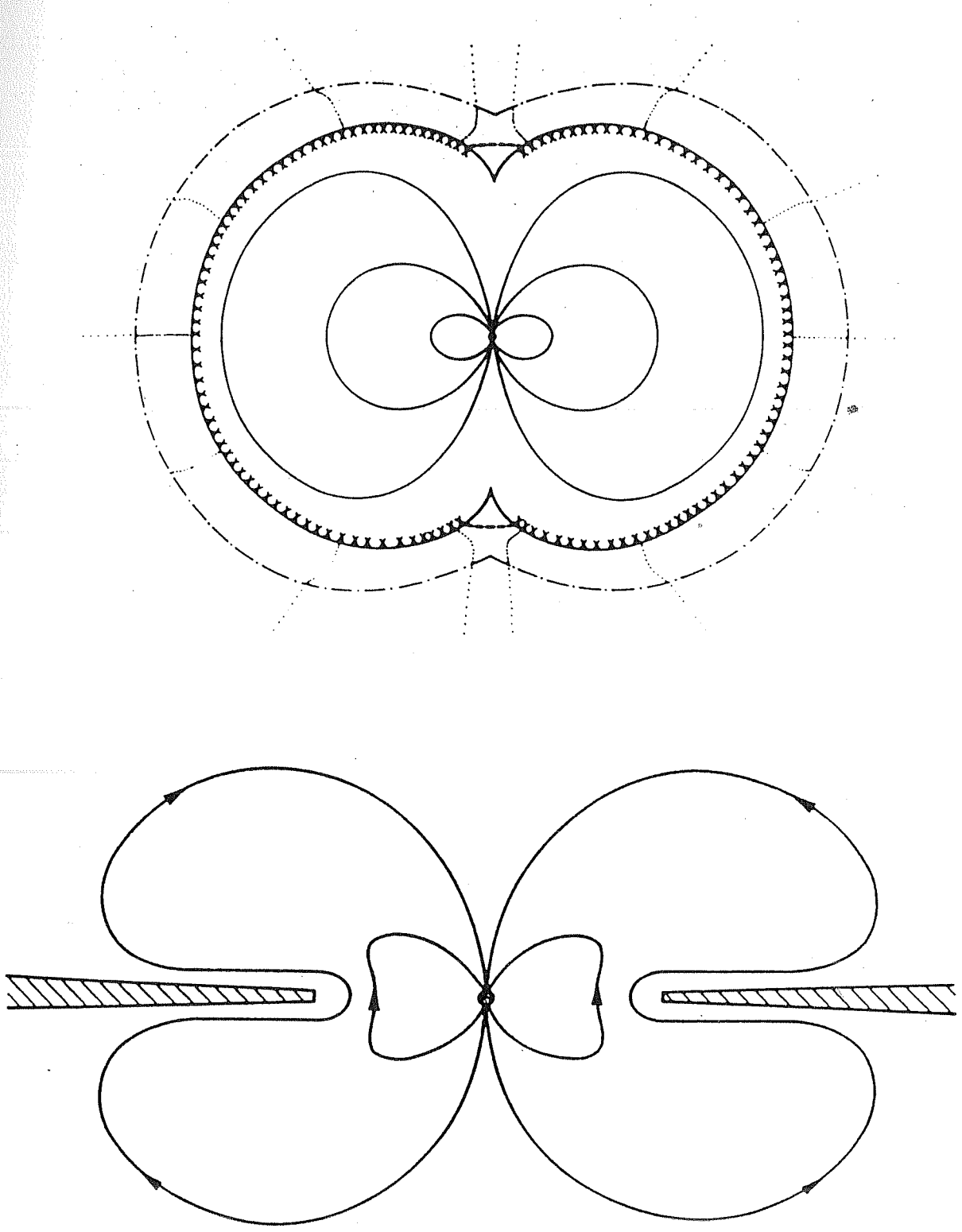

Figure 1.5. (a) The shape of the accreting magnetosphere in case of closed magnetospheric models. Adopted from Arons & Lea [84].
(b) Sketch of closed magnetosphere in case of disc accretion. Adopted from Lamb [46].

schematically the magnetosphere for a case where the magnetic field lines are assumed to be closed. Scharlemann [44] emphasized the importance of the shape of the field lines threading the plasma in controlling the flow of plasma from the inner edge of the disc to the neutron star. Assuming that the stellar magnetic field is completely excluded from the disc by screening currents which are represented by a current ring of radius R_{CF}, he discusses the possible mechanisms *viz.* K-H and Rayleigh-Taylor (R-T) instabilities through which the plasma can flow to the stellar surfaces either along the field lines or through the equatorial magnetosphere. Ichimaru [45] proposed a model of disc accretion in which the inner radius of the disc is determined by a static pressure balance condition but modified in an attempt to include the effect of gravity and centrifugal force acting on the plasma in the boundary layer between the disc and the magnetosphere. However, all these models are mostly qualitative in nature and several questions have been raised on the validity of the inherent assumptions (Lamb [46]). The most important of all, concerns the complete screening of the stellar magnetic field from the disc.

Towards a more quantitative decsription, Lamb and his collaborators have considered, in detail, disc accretion onto a magnetic neutron star. The initial model of Lamb *et al.* [40] takes into account the effects of stellar rotation and the magnetic field. In the case of a neutron star, the theory shows that the accreting material is channeled toward the magnetic poles of the star and forms a hot spot on entering the stellar atmosphere. The resulting radiation emerges from the neighbourhood of the stellar surface in a strongly angular pattern with a spectrum which depends on the nature of the accretion flow process and the configuration of the magnetic field inside the magnetosphere of a rotating neutron star (Ghosh & Lamb [47]). Assuming that the star is an aligned slow rotator and that the accreting plasma becomes threaded

by the stellar magnetic field near the magnetospheric boundary, they investigated the flow of matter and the configuration of the magnetic field inside the Alfv́en surface. In the absence of pressure and electrical resistivity, this analysis concluded that the flow within Alfv́en surface is well described by the magnetohydrodynamic (MHD) equations and that the matter moves along the field lines when viewed from the frame co-rotating with the star. As a special case, they considered a Keplerian disc flow outside the magnetosphere. Contrary to the earlier belief regarding the source of the excess energy dissipated in the disc as being the rotational energy of the star, they showed that this energy comes mainly from the transition zone between the disc and the magnetosphere. These studies were later extended by Ghosh *et al.* [48,49]. The study emphasized that the stellar magnetic field cannot be completely screened by disc plasma due to turbulent diffusion, development of K-H instability and reconnection of small scale fields within the disc. The resulting configuration projected on the meridional plane is qualitatively shown in Fig. 1.5b. The major uncertainty concerning this model is the question of magnetic field line reconnection in the disc and it is not clear if the field lines could be adequately simulated by introducing an effective resistivity (Lamb [46]; Börner [7]; Kaburaki [50]). In addition, all these models do not derive the self-consistent magnetic field structures.

In a model similar to Schralemann [44], Aly [51] obtained an exact analytical solution for a thin disc consisting of a perfectly conducting plasma which excludes the stellar field from the interior of the disc. The general structure of steady accretion discs with magnetic fields, in the limit of infinite conductivity was also analysed by Horiuchi *et al.* [52,53]. The results showed the existence of three critical points (surfaces) the Alfv́en, slow and fast points (surfaces) where the poloidal components

of accretion velocity equal the phase velocities of the Alfv́en, slow and fast waves respectively. In a follow-up paper, Horiuchi [54] solved the vertical force equation under the approximation of a geometrically thin disc and concluded that for a treatment of sub-Alfv́enic flow in the disc, one needs to study magnetic disc consisting of a viscous plasma with finite conductivity. Anzer *et al.* [55] computed the changes in the vertical structure of an accretion disc brought about by an external magnetic field and found that a high probability exists for the occurance of instabilities at the magnetospheric boundary due to the inversion of the density profile.

In a different approach, Kaburaki [50,56] considered structure of thin Keplerian accretion discs threaded by magnetic fields including the finite electrical conductivity of the plasma. Assuming that the vertical and radial structures separate out, Kaburaki [50] obtained disc solutions with two parameters R_m and $\triangle$ which represent magnetic Reynold's number and half thickness of the disc respectively. But, as he points out the calculations are not self-consistent due to the fact that one gets two different expressions for the radial velocity. In addition, the electric field solutions do not satisfy the Faraday's law and we believe this to be an artifact of the scaling used in his calculation. However, the calculations revealed that the pressure term has a contribution comparable to gravity and hence one cannot neglect the pressure gradients in the dynamical equations in the presence of magnetic fields. In a follow up paper, he [56] included the pressure term in the equation of radial force balance and also considered the flow along the meridional direction. As a result, he obtained self-consistent radial velocity but the inconsistency in the above mentioned Maxwell's equation still remained.

Lightman and Eardley [57] tested the stability of a thin orbiting accretion disc near a black hole and found that the disc is always secularly unstable on

time scales of a few seconds or less. As an alternative model, they formulated a detailed self-consistent model for magnetic viscosity. The equilibrium structure for the accretion of matter without pressure into a gravitating center of a black hole for (a) a laminar disc with the Coulomb mechanism of diffusion and (b) a turbulent disc, was calculated by Bisnovyati-Kogan & Ruzmaikin [58,59]. This study was further elaborated by Bisnovyati-Kogan [14] where a self-consistent two-dimensional MHD solution for a chaotic and ordered magnetic field in the gas along with the spectra of radiation was computed. However, this study was restricted to a case where the matter falling to the collapsar (black hole) was assumed to have no angular momentum and no poloidal magnetic field ($V^{\phi} = 0$ and $B_{\phi} = 0$). Lovelace *et al.* [60] has proposed a general theory for relativistic ideal MHD flows around a black hole or a rotating magnetized neutron star. This theory leads to an autonomous second order partial Grad-Shafranov equation (a well known equation in fusion plasmas) for the magnetic flux function and needs sophisticated numerical codes for its solution. As a particular example they obtained solutions for a simplified case of a disc around neutron stars with no poloidal flow ($V_P = 0$) and no toroidal magnetic field ($B_{\phi} = 0$). The above theory was later generalised to include steady axisymmetric flow around a Schwarzschild black hole (Mobarry & Lovelace [61]). Although, this work derived a virial equation and discussed the stability of the motion of a charged test particle in the presence of an electromagnetic field, the model does not present any specific equilibrium solution.

In a completely different formalism, Prasanna & Chakraborty [62], and Chakrabarty & Prasanna [63] analyzed structure and stability of fluid discs around a Schwarzschild black hole and observed that

1. the inner edge of the disc can not lie within 4m,

2. if the inner edge of the disc lies within 4m and 6m, then the outer edge must lie beyond 2a/(a-4), where a is the radius of the inner edge defined in units of m ($m = MG/c^2$),

3. there exists no restriction on outer edge, if the inner edge is at or beyond 6m,

4. in the case of a pressureless disc, the structure is stable if the inner edge is greater than 6m,

5. an ordinary perfect fluid disc rotating around central source is stable under radial perturbations.

The dynamics of accretion disc and its emerging radiation flux in the presence of electromagnetic fields on curved space time for several special cases of azimuthal velocity distributions was obtained by Prasanna & Bhaskaran [64] and Bhaskaran & Prasanna [65] A subsequent analysis by Bhaskaran & Prasanna [66] including the radial velcocity component of the flow revealed the inter-dependence of different physical parameters like outer density, seed magnetic field and finite conductivity on the continuous pressure distributions of the disc configurations. An analysis for a disc around a slowly rotating compact object was also carried out by Bhaskaran *et al.* [67] which demonstrated the influence of co- and counter rotation at the inner edge of the disc . However, all these analyses were confined to the thin disc limit ($\theta = \pi/2$).

Most of the studies mentioned above were carried out for thin discs with assumptions that (i) there are no pressure gradient forces (ii) the angular momentum distribution is Keplerian and (iii) the accretion rate is sub-Eddington. In case, the luminosity exceeds the Eddington limit, the inner regions of the disc get blown up by radiation pressure giving rise to thick disc configurations. In the next section,

we focus our attention on these models.

1.5.3 Thick disc

Geometrical thick accretion discs are believed to form when the accretion rate $\dot{M}$ is super critical (super Eddington, $L > L_E$) and are bright candidates for SS-433, active galactic nuclei and QPO sources. The interior properties of the radiation dominated thick accretion discs are determined by three dimensional, transonic, dissipative general relativistic hydrodynamics and its study is still in a developing stage. This is because the structure of accretion flow with $\dot{M} > \dot{M}_E$ is considerably more complicated than the structure of $\dot{M} \ll \dot{M}_E$ flows described by the standard thin accretion disc model. The complexity is caused by several physical processes which are assumed to be absent for thin accretion disc. The most notable feature is the angular momentum flow which no longer remains Keplerian. Work on the equilibrium distributions of perfect black holes showed that as long as the radiation pressure is not negligible, material near a black hole probably would not follow Keplerian orbits and would tend to have a nearly constant specific angular momentum. This is due to the inherent properties of discs with $\dot{M} > \dot{M}_E$, where both horizontal and vertical pressure gradients determine equilibrium as against the case of thin discs where only the vertical gradient is dynamically important. As a result, the structures of thick discs have to be described by a set of complicated partial differential equations. The most complex part of modelling thick discs is the inner most region, due to the transonic nature of the accretion flow and to the formation of cusp at the inner boundary (topological peculiarity of the equipotential surfaces, Abramowicz [68]). As a consequence, there have been only a few attempts to solve the complete equations.

In discussing quasars and double radio galaxies, Lynden-Bell [20] showed that the accreting material could form a pair of very deep vortices or whirlpools along the rotation axis through which relativistic plasma could be shut out, thus producing the frequently observed radio jets. Subsequent works have attempted to build more complex pictures of these thick accretion discs to elucidate the luminosities, to estimate the possible acceleration and collimation of the beams and analyze the stability. Following the earlier works of Fishbone & Moncrief [69] and Abramowicz *et al.* [18], Paczynski [70] developed a full-fledged disc model. To describe the gravitational field of the central compact source, he used a pseudo-Newtonian potential instead of a complete relativistic calculation. In these models, hydrostatic equilibrium was presumed which is equivalent to taking the orbital velocity of the fluid much greater than the radial velocity. This concept was subsequently verified in an analysis of flow through a cusp where it was found that the sonic point for the in-flowing fluid is located closer to the inner edge of the disc. The study of Jaroszynski et al. [71] who performed general relativistic calculations for both the Schwarzschild and Kerr metric showed that the thick discs implied $\alpha \ll 1$ in the standard picture or conversely if $\alpha \ll 1$, then disc has to be treated as physically thick. Although the existence of super critical discs does depend on relativistic effects, the analysis carried out by Abramowicz *et al.* [72] showed that fairly good results could be obtained by assuming a purely Newtonian treatment where the parameter of the model depends on the ratio of the inner to the outer radii. The other significant highlights of this analysis was that for super-Eddington accretion rate, the luminosity does not grow in proportion to the accretion rate but more slowly as

$$L \propto log\dot{M}. \tag{1.5.6}$$

The specific models including accretion flows were proposed by Paczynski [73] who assumed that the accretion flow is confined to a thin surface layer of the disc and concluded that for high enough accretion rates, dynamical instabilities could affect part of the disc. Assuming the viscous processes to be significant in the same thin layer Paczynski and Abramowicz [74] showed that both these models produced maximal equatorial temperature around 10^7 K. In different analyses, Kuwahara [75,76] considered all the flow components of the matter and calculated axisymmetric structures of relativistic tori around Schwarzschild and Kerr black holes. The results showed that for the existence of thick disc configurations, the radial velocity of the flow must be subsonic throughout the whole torus.

From the above studies of disc dynamics both in the limit of thin and thick discs, it is evident that the theories of thin accretion discs are reasonably well understood as compared to that of thick discs. However, the theories of thin accretion discs including self-consistent magnetic fields, finite conductivity of the plasma and all the velocity flow patterns are just emerging. But, as the theory is becoming more concrete and detail, it is giving rise to new problems. It turns out from the study of Kaburaki [50] that in the case of thin discs with magnetic fields the pressure gradient is as large as the gravitational force. Thus, whether the magnetic accretion discs can be really in a Keplerian orbit (which is one of the assumptions in the study of thin discs) is questionable (Kaburaki [56]).

In the case of thick discs, most of the calculations have been carried out for fluid discs without self-consistent magnetic fields. But, we saw that magnetic fields help in bringing the matter nearer to the compact object. Also, for modelling extragalactic jets, one has to take into account the magnetic fields. We investigate in subsequent chapters the importance of magnetic fields in disc configurations around

magnetospheres of compact objects.

1.6 Plasma instabilities in the accretion disc

The motivation for studying the stability of accretion flows lies in the possibility of its relevance to

- magnetic field penetration into the disc,
- mass transport inside the magnetosphere through the inner boundary,
- outbursts of dwarf novae,
- the rapid time variability of compact X-ray sources (X-ray bursters and QPO's),
- variability of active galactic nuclei.

In addition, there are several other reasons which necessitate the study of instabilities of accretion discs. The primary reason is to find out if the steady state models are stable against small perturbations or the growth rates of instabilities could completely disrupt the equilibrium structures. Another important reason for this study, is to gain quantitative information about the viscosity parameter which controls the time dependence behaviour of the steady flow (Pringle [77]).

It has been found that thin accretion discs quite generally fall prey to unstable modes of oscillations. Two types of instabilities (secular and thermal) of radiation pressure dominant discs have been investigated by Lightman [57]; Pringle [78]; and Shakura & Sunyaev [79]. Even when the gas pressure is dominant, the disc becomes thermally unstable owing to hydrogen ionisation (Hoshi [80]). Both thermal and viscous instabilities have been extensively studied regarding outbursts

of dwarf novae (Bath [81]). More general analyses conclude that instabilities of the above types could significantly affect almost any thin accretion disc model and are difficult to avoid (Wiita [9]). But, the analysis of Abramowicz *et al.* [82] shows that the mass loss from the inner edges of the discs could stabilize the innermost regions of the thin accretion discs.

The outstanding question of plasma entry into the magnetosphere in magnetically closed models can, probably, be answered by plasma instabilities at the inner boundary. Some attempts have been made in this direction. The most plausible mechanism which pushes matter inside the inner edge is believed to be caused by the interchange instability at the magnetopause (Elsner & Lamb [42]; Lamb & Elsner [83] and Arons & Lea [84]). This instability arises due to accumulation of matter at the inner edge supported by gravity against magnetic field, a situation well known to be unstable and goes by the name of Rayleigh-Taylor instability. Ghosh & Lamb [47] invoked the K-H instability in the context of field penetration into the magnetic disc. The study of Anzer & Börner [85,86] showed that the velocity discontinuity between the low density magnetic field and the disc drives the Kelvin-Helmholtz instability and initially grows on a time scale much shorter than the radial drift time.

The stability of thick accretion discs is a subject of very active research at present. The initial study of Papaloizou and Pringle [87] [88] demonstrated that non-accreting perfect fluid tori orbiting a Newtonian center of gravity are subject to violent global non-axisymmetric instability. However, the subsequent studies showed that stabilization could occur by (i) inclusion of accretion flow (Blaes et.al. [89]) and (ii) self gravity (Goodman & Narayan [90]). It was also pointed out that the growth rate of the instability is too low to be of any astrophysical

significance and decreases with increasing width of the torus (Robinson [91]). A possible explanation for the quasi-periodic oscillations observed in some galactic X-ray sources has also been proposed (Vanderklis [92]) in terms of oscillations in the inner region of a thick accretion disc which partially obscures the X-ray source. In addition, a qualitative argument by Treves *et al.* [93] suggests a limit cycle behaviour between thick and thin accretion discs when the mass supply rate from the secondary star is higher than the critical value of $2 \times 10^{-2}\ \dot{M}_E$ for $M = M_\odot$. It is conjectured that this occurs due to the alternate expansion and cooling of the disc. However, more theoretical and 3-dimensional hydrodynamic simulations need to be carried out before any final conclusion on the stability of thick discs is arrived at.

1.7 Aim and scope of the thesis

Although a substantial progress has been achieved in the study of thin and thick accretion discs since its inception, many major aspects remain to be investigated. A fully self-consistent MHD calculation is yet to be realized and the stability of these discs is still very much an open question. Thus our main objective, in this thesis, is to obtain fully self- consistent solutions of structure of magnetic accretion discs around magnetosphere of compact objects including the possible effects of general relativity. The motivation for working in the relativistic framework came from the fact that cusps between the marginally bound and marginally stable orbits could form only in relativistic treatment. Furthermore, the charged particle motion in the presence of a weakly magnetized fields demonstrated that the stable orbits could be pushed much closer to the compact object. As the existence of cusps nearer to the central star is of vital importance in the theory of accretion discs, we

were inspired to look for solutions of magnetohydrodynamic equations on a general curved background space-time. Thus, we have taken up the study of dynamical structure and stability of accretion discs both in the limit of thin and thick disc configurations to answer some of the yet unanswered questions.

The rest of the thesis is divided into the following chapters. A general formalism for the study of plasma magnetosphere in a relativistic formalism is presented in Chapter 2. The two subsequent chapters are devoted to equilibrium structures around compact objects. The equilibrium configuration in Chapter 3 manifests the general relativistic effects with particular emphasis on the nature of the Keplerian flow. Chapter 4 treats a more complicated flow pattern including the effects of finite conductivity of the plasma in Newtonian formalism. A general stability analysis of the equilibrium structures of Chapter 4 is presented in Chapter 5. The conclusions and open problems are summarized in Chapter 6.

Chapter 2

MATHEMATICAL FORMULATION

2.1 Dynamics of magnetofluid in relativistic formalism

In this Chapter, we develop the complete set of basic mathematical equations in the relativistic domain for the study of structure, dynamics and stability of the magnetofluid around non-rotating compact objects. This general theory is applicable, for example, to the detailed calculation of plasma accretion flows involving appreciable magnetic fields and to the determintion of the electrodynamically driven jets. However, in this analysis, we confine ourselves only to the study of plasma motion around the compact objects. In Section 2, we derive the equations governing the equilibrium and in Section 3, we cite the linear perturbation equations.

2.2 Equations of structure

In the previous chapter, the analysis of dynamics of plasma flow around compact objects emphasized the role of magnetic fields and associated currents produced by

the motion of the magnetofluid. In a realistic astrophysical situation involving a neutron star, the electromagnetic field is generated by the currents on its surface while for a blackhole it may be due to the ring currents in plasma discs surrounding the object. In addition, interstellar magnetic field would also be present. Thus, in the relativistic formalism, it is appropriate to look for solutions of Einstein-Maxwell's equations which are asymptotically flat and have non-zero dipole moment even in the absence of rotation of the central compact object. In general, these system of equations are formidable to solve. However, there are some solutions obtained by perturbation techniques under the assumption that the electromagnetic field energy is small compared to the mass energy of the gravitating source. As a result, the electromagnetic field does not affect the background geometry but the background geometry modifies the electromagnetic field. These fields, in general, are referred to as the painted fields. In this frame work, we will consider the complete set of dynamical equations that govern the flow of the magnetofluid with the following assumptions.

(i) The disc is not massive in comparison with the central object such that the space-time structure supporting the disc is entirely governed by the central object.

(ii) The energy associated with the electromagnetic field (test field) produced in and around the disc is negligible compared to the mass of the central object such that the field does not affect the geometry but itself gets modified by the geometry.

The equation of motion for such a system is obtained through the laws of conservation of energy and momentum expressed through the covariant equations

(Prasanna [94])

$$T_i^j{}_{;j} = 0, \tag{2.2.1}$$

where T_i^j is the appropriate energy momentum tensor and the covariant derivative is taken with respect to the background metric. In general, the geometry of the spacetime should be obtained by solving the set of Einstein equations $G_{ij} = T_{ij}$, where

$$T_i^j = m_i^j - \frac{4\pi}{c} E_i^j \ . \tag{2.2.2}$$

The matter part m_i^j, and the electromagnetic stress tensor E_i^j are defined as

$$m_i^j = \left(\rho + \frac{p}{c^2}\right) U_i U^j - \frac{p}{c^2}\delta_i^j, \tag{2.2.3}$$

and

$$E_i^j = \left(F_{ik}F^{jk} - \frac{1}{4}\delta_i^j F_{kl}F^{kl}\right). \tag{2.2.4}$$

Here ρ, p and U^i are the density, the hydrostatic pressure, and the time like four velocity vector respectively. Assuming the background geometry to be given by the metric

$$ds^2 = g_{ij}\, dx^i\, dx^j., \tag{2.2.5}$$

we have the normalisation condition for the fluid four velocity $\left(U^i = \frac{dx^i}{ds}\right)$,

$$g_{ij} = U^i U^j = \pm 1, \tag{2.2.6}$$

where the choice of the sign depends on the signature of the metric. In addition, the antisymmetric field tensor F_{ij} is defined through the vector potential as

$$F_{ij} = A_{j;i} - A_{i;j} \ . \tag{2.2.7}$$

The complete system of coupled equations are obtained by adding the covariant Maxwell's equations

$$F^{ij}{}_{;j} = -\frac{4\pi}{c} J^i, \tag{2.2.8}$$

$$F_{[ij,k]} = 0. \tag{2.2.9}$$

The current density J^i is defined through the covariant expression of Ohm's law

$$J^i = c\epsilon U^i + \sigma F^i{}_j U^j, \tag{2.2.10}$$

where ϵ is the charge density measured locally, and σ is the electrical conductivity of the fluid. With these definitions, we can now split the conservation law (equation 2.2.1) as,

the equation of continuity (mass conservation)

$$\rho_{;j} U^j + \left(\rho + \frac{p}{c^2}\right) U^j_{;j} = \frac{1}{c^3} F_{ik} J^k U^i, \tag{2.2.11}$$

and the momentum equation

$$\left(\rho + \frac{p}{c^2}\right) U^i{}_{;j}\, U^j + \left(\frac{p}{c^2}\right) ;j \left(U^i U^j - g^{ij}\right) = \frac{1}{c^3}(F^i{}_k - F_{lk} U^i U^l) J^k. \tag{2.2.12}$$

Using the spatial 3-velocity V^α, defined through the relation $U^\alpha = U^0 \frac{V^\alpha}{c}$, these systems of equations in terms of currents can be rewritten as,
the equation of continuity

$$\begin{aligned}\left(\rho + \frac{p}{c^2}\right) & \left[V^\alpha_{,\alpha} + c\,\Gamma^\alpha_{0\alpha} - \left(\Gamma^0_{0\alpha} - \Gamma^\beta_{\beta\alpha}\right) V^\alpha - \Gamma^0_{\alpha\beta} \frac{V^\alpha V^\beta}{c} \right] + \frac{\partial}{\partial t}\left(\rho - \frac{p}{c^2}\right) \\ & + V^\alpha \frac{\partial}{\partial x^\alpha}\left(\rho - \frac{p}{c^2}\right) + \frac{1}{c^2 (U^0)^2}\left(g^{00}\frac{\partial p}{\partial t} + c g^{0\alpha}\frac{\partial p}{\partial x^\alpha}\right) \\ & + \frac{1}{c^2 (U^0)^2}\left[F^0_k J^k - 2 F_{ik} J^k U^i U^0\right] = 0, \end{aligned} \tag{2.2.13}$$

and the equation of momentum balance

$$\left(\rho + \frac{p}{c^2}\right) \quad \left(U^0\right)^2 \left[\frac{\partial V^\alpha}{\partial t} + V^\beta \frac{\partial V^\alpha}{\partial x^\beta} + c^2 \left(\Gamma^\alpha_{00} - \frac{V^\alpha}{c}\Gamma^0_{00}\right)\right.$$

$$+ \quad 2c\, V^{\beta}\left(\Gamma^{\alpha}_{0\beta} - \frac{V^{\alpha}}{c}\Gamma^{0}_{0\beta}\right) + V^{\beta}V^{\gamma}\left(\Gamma^{\alpha}_{\beta\gamma} - \Gamma^{0}_{\beta\gamma}\frac{V^{\alpha}}{c}\right)\Big]$$

$$+ \quad \left(g^{0i}\frac{V^{\alpha}}{c} - g^{\alpha i}\right)\frac{\partial p}{\partial x^{i}} + \left(F^{0}{}_{k}\frac{V^{\alpha}}{c} - F^{\alpha}{}_{k}\right)\frac{J^{k}}{c} = 0, \qquad (2.2.14)$$

where *greek* indices take values 1, 2 and 3 while latin ones take values 0, 1, 2 and 3 ($x^0 = ct$). These equations (2.2.13 & 2.2.14) together with the set of Maxwell's equations (2.2.8 & 2.2.9) constitute the system of equations governing the structure of a magnetofluid disc around a gravitating source which is in equilibrium under the influence of

(i) the gravitational field produced by the background geometry,

(ii) the centrifugal force produced by the rotating disc, and

(iii) the self-consistent electromagnetic field produced by the moving magnetofluid.

The formulation described above is applicable to any given metric, but we restrict our analysis to the case of Schwarzschild background geometry (static, spherically symmetric) representing the gravitational field of a non-rotating compact object of mass M. The form of the metric in spherical co-ordinate system (r,θ, ϕ) is,

$$ds^2 = \left(1 - \frac{2m}{r}\right)c^2dt^2 - \left(1 - \frac{2m}{r}\right)^{-1}dr^2 - r^2\left(d\theta^2 - \sin^2\theta d\phi^2\right), \qquad (2.2.15)$$

where $m = \frac{GM}{c^2}$ with G and c denoting the gravitational constant and velocity of light respectively. We write the equations in terms of Local Lorentz Frame (LLF) components defined by the orthogonal tetrad appropriate to the Schwarzschild metric as,

$$\lambda^{i}_{(a)} = diag\left[\left(1 - \frac{2m}{r}\right)^{-1/2}, \left(1 - \frac{2m}{r}\right)^{1/2}, \frac{1}{r}, \frac{1}{\sin\theta}\right], \qquad (2.2.16)$$

alongwith

$$
\begin{aligned}
F_{(a)(b)} &= \lambda^{i}_{(a)}\lambda^{k}_{(b)}F_{ik}, \\
J^{(a)} &= \lambda^{(a)}_{i}J^{i}, \\
E_{(\alpha)} &= F_{(\alpha)(t)}, \\
B_{(\alpha)} &= \epsilon_{\alpha\beta\gamma}F_{(\beta)(\gamma)} \text{ (no summation)},
\end{aligned}
\tag{2.2.17}
$$

where $\epsilon_{\alpha\beta\gamma}$ is the Levi-Civita symbol. Using these definitions, the electromagnetic field components can be explicitly written as

$$
\begin{aligned}
F_{(r)(\theta)} &= \frac{1}{r}\left(1-\frac{2m}{r}\right)^{\frac{1}{2}}F_{r\theta}, \\
F_{(r)(t)} &= F_{rt}, \\
F_{(\theta)(\phi)} &= \frac{1}{r^2\sin\theta}F_{\theta\phi}, \\
F_{(\theta)(t)} &= \frac{1}{r}\left(1-\frac{2m}{r}\right)^{-\frac{1}{2}}F_{\theta t}, \\
F_{(\phi)(r)} &= \frac{1}{r\sin\theta}\left(1-\frac{2m}{r}\right)^{\frac{1}{2}}F_{\phi r}, \\
F_{(\phi)(t)} &= \frac{1}{r\sin\theta}\left(1-\frac{2m}{r}\right)^{-\frac{1}{2}}F_{\phi t}.
\end{aligned}
\tag{2.2.18}
$$

Using the same tetrad (equation 2.2.16), one can also express the 3-velocity V in terms of local Lorentz components as given by

$$
\begin{aligned}
V^{r} &= \left(1-\frac{2m}{r}\right)V^{(r)}, \\
V^{\theta} &= \left(1-\frac{2m}{r}\right)^{\frac{1}{2}}\frac{V^{(\theta)}}{r}, \\
V^{\phi} &= \left(1-\frac{2m}{r}\right)^{\frac{1}{2}}\frac{V^{(\phi)}}{r\sin\theta}.
\end{aligned}
\tag{2.2.19}
$$

Thus, the complete set of equations that govern the dynamics of a quasi-neutral magnetofluid ($n_i = n_e$; $\epsilon = 0$) around a compact object are given by,

the equations of momentum balance

$$\left(\rho + \frac{p}{c^2}\right) \left[\frac{DV^{(r)}}{Dt} + \frac{mc^2}{r^2}\left(1 - \frac{V^{(r)^2}}{c^2}\right) - \frac{1}{r}\left(1 - \frac{2m}{r}\right)\left(V^{(\theta)^2} + V^{(\phi)^2}\right)\right]$$
$$= -\left(1 - \frac{V^2}{c^2}\right)\left[\left(1 - \frac{2m}{r}\right)\frac{\partial p}{\partial r} + \frac{V^{(r)}}{c^2}\frac{\partial p}{\partial t}\right.$$
$$\left. + \left(1 - \frac{2m}{r}\right)^{\frac{1}{2}}\frac{1}{c}\left\{F_{(r)(i)}J^{(i)} + \frac{V^{(r)}}{c}F_{(t)(\alpha)}J^{(\alpha)}\right\}\right], \qquad (2.2.20)$$

$$\left(\rho + \frac{p}{c^2}\right) \left[\frac{DV^{(\theta)}}{Dt} + \left(1 - \frac{3m}{r}\right)\frac{V^{(r)}V^{(\theta)}}{r} - \left(1 - \frac{2m}{r}\right)^{\frac{1}{2}}\frac{\cot\theta}{r}V^{(\phi)^2}\right]$$
$$= -\left(1 - \frac{V^2}{c^2}\right)\left[\left(1 - \frac{2m}{r}\right)^{\frac{1}{2}}\frac{1}{r}\frac{\partial p}{\partial \theta} + \frac{V^{(\theta)}}{c^2}\frac{\partial p}{\partial t}\right.$$
$$\left. + \left(1 - \frac{2m}{r}\right)^{\frac{1}{2}}\frac{1}{c}\left\{F_{(\theta)(i)}J^{(i)} + \frac{V^{(\theta)}}{c}F_{(t)(\alpha)}J^{(\alpha)}\right\}\right], \qquad (2.2.21)$$

$$\left(\rho + \frac{p}{c^2}\right) \left[\frac{DV^{(\phi)}}{Dt} + \left(1 - \frac{3m}{r}\right)\frac{V^{(r)}V^{(\phi)}}{r} + \left(1 - \frac{2m}{r}\right)^{\frac{1}{2}}\frac{\cot\theta}{r}V^{(\phi)}V^{(\theta)}\right]$$
$$= -\left(1 - \frac{V^2}{c^2}\right)\left[\left(1 - \frac{2m}{r}\right)^{\frac{1}{2}}\frac{1}{r\sin\theta}\frac{\partial p}{\partial \phi} + \frac{V^{(\phi)}}{c^2}\frac{\partial p}{\partial t}\right.$$
$$\left. + \left(1 - \frac{2m}{r}\right)^{\frac{1}{2}}\frac{1}{c}\left\{F_{(\phi)(i)}J^{(i)} + \frac{V^{(\phi)}}{c}F_{(t)(\alpha)}J^{(\alpha)}\right\}\right], \qquad (2.2.22)$$

the continuity equation

$$\left(\rho + \frac{p}{c^2}\right) \left[\left(1 - \frac{2m}{r}\right)^{\frac{1}{2}}\left\{\left(1 - \frac{2m}{r}\right)^{\frac{1}{2}}\frac{1}{r^2}\frac{\partial}{\partial r}\left(r^2 V^{(r)}\right)\right.\right.$$

$$+ \quad \frac{1}{r\sin\theta}\left(\frac{\partial}{\partial\theta}\left(\sin\theta V^{(\theta)}\right)+\frac{\partial V^{(\phi)}}{\partial\phi}\right)\Bigg\}\Bigg] + \frac{D}{Dt}\left(\rho-\frac{p}{c^2}\right)$$

$$+ \quad \left(1-\frac{V^2}{c^2}\right)\frac{1}{c^2}\frac{\partial p}{\partial t} + \frac{1}{c^2}\left(1-\frac{V^2}{c^2}\right)\left(1-\frac{2m}{r}\right)^{\frac{1}{2}} F_{(t)(\alpha)}J^{(\alpha)}$$

$$- \quad \frac{2}{c^2}\left(1-\frac{2m}{r}\right)^{\frac{1}{2}}\left[F_{(t)(\alpha)}J^{(\alpha)}+\frac{V^{(\alpha)}}{c}F_{(\alpha)(i)}J^{(i)}\right]=0, \qquad (2.2.23)$$

Maxwell's equations

$$\frac{1}{c}\frac{\partial}{\partial t}\left(F_{(\theta)(\phi)}\right) + \frac{1}{r^2\sin\theta}\left[\frac{\partial}{\partial\theta}\left\{r\sin\theta\left(1-\frac{2m}{r}\right)^{\frac{1}{2}}F_{(\phi)(t)}\right\}\right.$$

$$\left. - \quad \frac{\partial}{\partial\phi}\left\{r\left(1-\frac{2m}{r}\right)^{\frac{1}{2}}F_{(\theta)(t)}\right\}\right]=0, \qquad (2.2.24)$$

$$\frac{1}{c}\frac{\partial}{\partial t}\left(F_{(\phi)(r)}\right) + \frac{1}{r sin\theta}\left(1-\frac{2m}{r}\right)^{\frac{1}{2}}\left[\frac{\partial}{\partial\phi}F_{(r)(t)}\right.$$

$$\left. - \quad \frac{\partial}{\partial r}\left\{r\sin\theta\left(1-\frac{2m}{r}\right)^{\frac{1}{2}}F_{(\phi)(t)}\right\}\right]=0, \qquad (2.2.25)$$

$$\frac{1}{c}\frac{\partial}{\partial t}\left(F_{(r)(\theta)}\right) + \frac{1}{r}\left(1-\frac{2m}{r}\right)^{\frac{1}{2}}\left[\frac{\partial}{\partial r}\left\{r\left(1-\frac{2m}{r}\right)^{\frac{1}{2}}F_{(\theta)(t)}\right\}\right.$$

$$\left. - \quad \frac{\partial}{\partial\theta}F_{(r)(t)}\right]=0, \qquad (2.2.26)$$

$$\frac{\partial}{\partial r}\left(r^2\sin\theta F_{(\theta)(\phi)}\right) + \frac{\partial}{\partial\theta}\left\{r\sin\theta\left(1-\frac{2m}{r}\right)^{-\frac{1}{2}}F_{(\phi)(r)}\right\}$$

$$+ \quad \frac{\partial}{\partial\phi}\left\{r\left(1-\frac{2m}{r}\right)^{-\frac{1}{2}}F_{(r)(\theta)}\right\}=0, \qquad (2.2.27)$$

$$\frac{1}{c}\frac{\partial}{\partial t}\left(F_{(r)(t)}\right) - \left(1-\frac{2m}{r}\right)^{\frac{1}{2}}\frac{1}{r\sin\theta}\frac{\partial}{\partial\theta}\left(\sin\theta F_{(r)(\theta)}\right)$$

$$- \quad \left(1-\frac{2m}{r}\right)^{\frac{1}{2}}\frac{1}{r\sin\theta}\frac{\partial}{\partial\phi}\left(F_{(r)(\phi)}\right)$$

$$= -\frac{4\pi}{c}\left(1-\frac{2m}{r}\right)^{\frac{1}{2}} J^{(r)}, \tag{2.2.28}$$

$$\begin{aligned}\frac{1}{c}\frac{\partial}{\partial t}\left(F_{(\theta)(t)}\right) &- \left(1-\frac{2m}{r}\right)^{\frac{1}{2}}\frac{\partial}{\partial r}\left[r\left(1-\frac{2m}{r}\right)^{\frac{1}{2}} F_{(\theta)(r)}\right] \\ &- \frac{1}{r\sin\theta}\left(1-\frac{2m}{r}\right)^{\frac{1}{2}}\frac{\partial}{\partial\phi}\left(F_{(\theta)(\phi)}\right) \\ &= -\frac{4\pi}{c}\left(1-\frac{2m}{r}\right)^{\frac{1}{2}} J^{(\theta)}, \end{aligned} \tag{2.2.29}$$

$$\begin{aligned}\frac{1}{c}\frac{\partial}{\partial t}\left(F_{(\phi)(t)}\right) &- \frac{1}{r}\left(1-\frac{2m}{r}\right)^{\frac{1}{2}}\frac{\partial}{\partial r}\left[r\left(1-\frac{2m}{r}\right)^{\frac{1}{2}} F_{(\phi)(r)}\right] \\ &- \frac{1}{r}\left(1-\frac{2m}{r}\right)^{\frac{1}{2}}\frac{\partial}{\partial\theta}\left[F_{(\phi)(\theta)}\right] \\ &= -\frac{4\pi}{c}\left(1-\frac{2m}{r}\right)^{\frac{1}{2}} J^{(\phi)}, \end{aligned} \tag{2.2.30}$$

$$\begin{aligned}\frac{1}{r}\frac{\partial}{\partial r}\left(r^2 F_{(t)(r)}\right) &+ \left(1-\frac{2m}{r}\right)^{-\frac{1}{2}}\frac{1}{\sin\theta}\frac{\partial}{\partial\theta}\left[\sin\theta F_{(t)(\theta)}\right] \\ &+ \left(1-\frac{2m}{r}\right)^{-\frac{1}{2}}\frac{1}{\sin\theta}\frac{\partial}{\partial\phi}\left[F_{(t)(\phi)}\right] \\ &= \frac{4\pi r}{c}\left(1-\frac{2m}{r}\right)^{-\frac{1}{2}} J^{(t)}, \end{aligned} \tag{2.2.31}$$

and Ohm's law

$$J^{(r)} = -\frac{\sigma}{c}\left(1-\frac{V^2}{c^2}\right)^{-\frac{1}{2}}\left[cF_{(r)(t)} + F_{(r)(\theta)}V^{(\theta)} + F_{(r)(\phi)}V^{(\phi)}\right], \tag{2.2.32}$$

$$J^{(\theta)} = -\frac{\sigma}{c}\left(1-\frac{V^2}{c^2}\right)^{-\frac{1}{2}}\left[cF_{(\theta)(t)} + F_{(\theta)(r)}V^{(r)} + F_{(\theta)(\phi)}V^{(\phi)}\right], \tag{2.2.33}$$

$$J^{(\phi)} = -\frac{\sigma}{c}\left(1-\frac{V^2}{c^2}\right)^{-\frac{1}{2}}\left[cF_{(\phi)(t)} + F_{(\phi)(r)}V^{(r)} + F_{(\phi)(\theta)}V^{(\theta)}\right], \tag{2.2.34}$$

$$J^{(t)} = -\frac{\sigma}{c}\left(1-\frac{V^2}{c^2}\right)^{-\frac{1}{2}}\left[F_{(r)(t)}V^{(r)}+F_{(\theta)(t)}V^{(\theta)}+F_{(\phi)(t)}V^{(\phi)}\right], \quad (2.2.35)$$

where, we have defined

$$V^2 = V^{(r)^2}+V^{(\theta)^2}+V^{(\phi)^2}, \quad (2.2.36)$$

and

$$\frac{D}{Dt} = \frac{\partial}{\partial t}+\left(1-\frac{2m}{r}\right)^{\frac{1}{2}}\left[\left(1-\frac{2m}{r}\right)^{\frac{1}{2}}V^{(r)}\frac{\partial}{\partial r}+\frac{V^{(\theta)}}{r}\frac{\partial}{\partial\theta}+\frac{V^{(\phi)}}{r\sin\theta}\frac{\partial}{\partial\phi}\right]. \quad (2.2.37)$$

Thus, we have a closed system of 12 equations in 12 variables (B_r, B_θ, B_ϕ, E_r, E_θ, E_ϕ, V^r, V^θ, V^ϕ, p, ρ and charge density J^t).

2.3 Equations governing general perturbation

In order to consider the stability of the plasma flow around the compact object, we consider small perturbations of the physical variables Ψ as $\Psi_0+\delta\Psi$, where Ψ_0 is the equilibrium part and $\delta\Psi$ is the generic perturbation. We restrict the analysis to the theory of linear perturabtion only *i.e.* we assume $\frac{\delta\Psi}{\Psi_0} \ll 1$. Introducing these notations into the general equations (2.2.20 - 2.2.35) and retaining only the linear terms in the perturbations, the following linearised set of equations governing the perturbations are obtained.

The linearised perturbed momentum equations are given by

$$\left(\rho_0+\frac{p_0}{c^2}\right)\left[\frac{D}{Dx}\left(\delta V^{(r)}\right)+\frac{\delta D}{Dx}(V_0^{(r)})-\frac{2m}{r^2}V_0^{(r)}\delta V^{(r)}\right.$$
$$\left.-\frac{2}{r}\left(1-\frac{2m}{r}\right)\left(V_0^{(\theta)}\delta V^{(\theta)}+V_0^{(\phi)}\delta V^{(\phi)}\right)\right]$$

$$
\begin{aligned}
&+ \left(\delta\rho + \frac{\delta p}{c^2}\right)\left[\frac{D}{Dt}(V_0^{(r)}) + \frac{mc^2}{r^2}\left(1 - \frac{{V_0^{(r)}}^2}{c^2}\right)\right. \\
&- \left.\frac{1}{r}\left(1 - \frac{2m}{r}\right)\left({V_0^{(\theta)}}^2 + {V_0^{(\phi)}}^2\right)\right] \\
&= -\left(1 - \frac{V_0^2}{c^2}\right)\left[\left(1 - \frac{2m}{r}\right)\frac{\partial}{\partial r}(\delta p) + \frac{V_0^{(r)}}{c^2}\frac{\partial}{\partial t}(\delta p) + \frac{\delta V^{(r)}}{c^2}\frac{\partial p_0}{\partial t}\right. \\
&+ \left(1 - \frac{2m}{r}\right)^{\frac{1}{2}}\frac{1}{c}\left\{\left(F_{0(r)(i)}\delta J^{(i)} + \delta F_{(r)(i)}J_0^{(i)}\right)\right. \\
&+ \left.\left.\frac{\delta V^{(r)}}{c}\left(F_{0(t)(\alpha)}J_0^{(\alpha)}\right) + \frac{V_0^{(r)}}{c}\left(\delta F_{(t)(\alpha)}J_0^{(\alpha)}\right)\right\}\right] \\
&+ \frac{2V_0\delta V}{c^2}\left[\left(1 - \frac{2m}{r}\right)\frac{\partial p_0}{\partial r} + \frac{V_0^{(r)}}{c^2}\frac{\partial p_0}{\partial t}\right. \\
&+ \left.\left(1 - \frac{2m}{r}\right)^{\frac{1}{2}}\frac{1}{c}\left\{F_{0(r)(i)}J_0^{(i)} + \frac{V_0^{(r)}}{c}\left(F_{0(t)(\alpha)}J_0^{(\alpha)}\right)\right\}\right], \qquad (2.3.1)
\end{aligned}
$$

$$
\begin{aligned}
\left(\rho_0 + \frac{p_0}{c^2}\right) &\left[\frac{D}{Dx}\left(\delta V^{(\theta)}\right) + \left(1 - \frac{3m}{r}\right)\frac{1}{r}\left(V_0^{(\theta)}\delta V^{(r)} + V_0^{(r)}\delta V^{(\theta)}\right)\right. \\
&- \left.\left(1 - \frac{2m}{r}\right)^{\frac{1}{2}}\frac{\cot\theta}{r}2V_0^{(\phi)}\delta V^{(\phi)} + \frac{\delta D}{Dx}(V_0^{(\theta)})\right] \\
&+ \left(\delta\rho + \frac{\delta p}{c^2}\right)\left[\frac{D}{Dt}(V_0^{(\theta)}) + \left(1 - \frac{3m}{r}\right)\frac{V_0^{(r)}V_0^{(\theta)}}{r} - \left(1 - \frac{2m}{r}\right)^{\frac{1}{2}}\frac{\cot\theta}{r}{V_0^{(\phi)}}^2\right] \\
&= -\left(1 - \frac{V_0^2}{c^2}\right)\left[\left(1 - \frac{2m}{r}\right)^{\frac{1}{2}}\frac{1}{r}\frac{\partial}{\partial\theta}(\delta p) + \frac{V_0^{(\theta)}}{c^2}\frac{\partial}{\partial t}(\delta p) + \frac{\delta V^{(\theta)}}{c^2}\frac{\partial p_0}{\partial t}\right. \\
&+ \left(1 - \frac{2m}{r}\right)^{\frac{1}{2}}\frac{1}{c}\left\{\left(F_{0(\theta)(i)}\delta J^{(i)} + \delta F_{(\theta)(i)}J_0^{(i)}\right)\right. \\
&+ \left.\left.\frac{\delta V^{(\theta)}}{c}\left(F_{0(t)(\alpha)}J_0^{(\alpha)}\right) + \frac{V_0^{(\theta)}}{c}\left(\delta F_{(t)(\alpha)}J_0^{(\alpha)}\right)\right\}\right]
\end{aligned}
$$

$$+ \quad \frac{2V_0\delta V}{c^2}\left[\left(1-\frac{2m}{r}\right)^{\frac{1}{2}}\frac{1}{r}\frac{\partial p_0}{\partial\theta}+\frac{V_0^{(\theta)}}{c^2}\frac{\partial p_0}{\partial t}\right.$$

$$\left.+ \quad \left(1-\frac{2m}{r}\right)^{\frac{1}{2}}\frac{1}{c}\left\{F_{0(\theta)(i)}J_0^{(i)}+\frac{V_0^{(\theta)}}{c}\left(F_{0(t)(\alpha)}J_0^{(\alpha)}\right)\right\}\right], \tag{2.3.2}$$

$$\left(\rho_0+\frac{p_0}{c^2}\right) \quad \left[\frac{D}{Dx}\left(\delta V^{(\phi)}\right)+\left(1-\frac{3m}{r}\right)\frac{1}{r}\left(V_0^{(r)}\delta V^{(\phi)}+V_0^{(\phi)}\delta V^{(r)}\right)\right.$$

$$- \quad \left.\left(1-\frac{2m}{r}\right)^{\frac{1}{2}}\frac{\cot\theta}{r}\left(V_0^{(\theta)}\delta V^{(\phi)}+\delta V^{(\theta)}V_0^{(\phi)}\right)+\frac{\delta D}{Dx}(V_0^{(\phi)})\right] *$$

$$+ \quad \left(\delta\rho+\frac{\delta p}{c^2}\right)\left[\frac{D}{Dt}(V_0^{(\phi)})+\left(1-\frac{3m}{r}\right)\frac{V_0^{(r)}V_0^{(\phi)}}{r}\right.$$

$$\left.- \quad \left(1-\frac{2m}{r}\right)^{\frac{1}{2}}\frac{\cot\theta}{r}V_0^{(\theta)}V_0^{(\phi)}\right]$$

$$= \quad -\left(1-\frac{V_0^2}{c^2}\right)\left[\left(1-\frac{2m}{r}\right)^{\frac{1}{2}}\frac{1}{r\sin\theta}\frac{\partial}{\partial\phi}(\delta p)+\frac{V_0^{(\phi)}}{c^2}\frac{\partial}{\partial t}(\delta p)+\frac{\delta V^{(\phi)}}{c^2}\frac{\partial p_0}{\partial t}\right.$$

$$+ \quad \left(1-\frac{2m}{r}\right)^{\frac{1}{2}}\frac{1}{c}\left\{\left(F_{0(\phi)(i)}\delta J^{(i)}+\delta F_{(\phi)(i)}J_0^{(i)}\right)\right.$$

$$\left.\left.+ \quad \frac{\delta V^{(\phi)}}{c}\left(F_{0(t)(\alpha)}J_0^{(\alpha)}\right)+\frac{V_0^{(\phi)}}{c}\left(\delta F_{(t)(\alpha)}J_0^{(\alpha)}\right)\right\}\right]$$

$$+ \quad \frac{2V_0\delta V}{c^2}\left[\left(1-\frac{2m}{r}\right)^{\frac{1}{2}}\frac{1}{r\sin\theta}\frac{\partial p_0}{\partial\phi}+\frac{V_0^{(\phi)}}{c^2}\frac{\partial p_0}{\partial t}\right.$$

$$\left.+ \quad \left(1-\frac{2m}{r}\right)^{\frac{1}{2}}\frac{1}{c}\left\{F_{0(\phi)(i)}J_0^{(i)}+\frac{V_0^{(\phi)}}{c}\left(F_{0(t)(\alpha)}J_0^{(\alpha)}\right)\right\}\right]. \tag{2.3.3}$$

The linearised perturbed continuity equation is given by

$$\left(\rho_0+\frac{p_0}{c^2}\right) \quad \left[\left(1-\frac{2m}{r}\right)^{\frac{1}{2}}\left\{\frac{1}{r^2}\left(1-\frac{2m}{r}\right)^{\frac{1}{2}}\frac{\partial}{\partial r}\left(r^2\delta V^{(r)}\right)\right.\right.$$

$$\left.\left.+ \quad \frac{1}{r\sin\theta}\left(\frac{\partial}{\partial\theta}\left(\sin\theta\delta V^{(\theta)}\right)+\frac{\partial}{\partial\phi}\left(\delta V^{(\phi)}\right)\right)\right\}\right]$$

$$
\begin{aligned}
&+ \left(\delta\rho + \frac{\delta p}{c^2}\right)\left[\left(1-\frac{2m}{r}\right)^{\frac{1}{2}}\left\{\frac{1}{r^2}\left(1-\frac{2m}{r}\right)^{\frac{1}{2}}\frac{\partial}{\partial r}\left(r^2 V_0^{(r)}\right)\right.\right.\\
&+ \left.\left.\frac{1}{r\sin\theta}\left(\frac{\partial}{\partial\theta}\left(\sin\theta V_0^{(\theta)}\right)+\frac{\partial V_0^{(\phi)}}{\partial\phi}\right)\right\}\right]\\
&+ \frac{D}{Dx}\left(\delta\rho-\frac{\delta p}{c^2}\right)+\frac{\delta D}{Dx}\left(\rho_0-\frac{p_0}{c^2}\right)+\frac{1}{c^2}\left(1-\frac{V_0^2}{c^2}\right)\frac{\partial}{\partial t}(\delta p)\\
&- \frac{2V_0\delta V}{c^4}\frac{\partial p_0}{\partial t}+\frac{1}{c^2}\left(1-\frac{V_0^2}{c^2}\right)\left(1-\frac{2m}{r}\right)^{\frac{1}{2}}\\
&\times \left(\delta F_{(t)(\alpha)}J_0^{(\alpha)}+F_{0(t)(\alpha)}\delta J^{(\alpha)}\right)\\
&= \frac{2V_0\delta V}{c^4}\left(1-\frac{2m}{r}\right)^{\frac{1}{2}}\left(F_{0(t)(\alpha)}J^{(\alpha)}\right)\\
&+ \frac{2}{c^2}\left(1-\frac{2m}{r}\right)^{\frac{1}{2}}\left[\left\{F_{0(t)(\alpha)}\delta J^{(\alpha)}+\delta F_{(t)(\alpha)}J_0^{(\alpha)}\right\}\right.\\
&+ \left.\frac{\delta V^{(\alpha)}}{c}F_{0(\alpha)(i)}J_0^{(i)}+\frac{V_0^{(\alpha)}}{c}\left\{F_{0(\alpha)(i)}\delta J^{(i)}+\delta F_{(\alpha)(i)}J_0^{(i)}\right\}\right], \qquad (2.3.4)
\end{aligned}
$$

The linearised perturbed Maxwell's equations are written as

$$
\begin{aligned}
&\frac{1}{c}\frac{\partial}{\partial t}\left(\delta F_{(\theta)(\phi)}\right) + \frac{1}{r^2\sin\theta}\left[\frac{\partial}{\partial\theta}\left\{r\sin\theta\left(1-\frac{2m}{r}\right)^{\frac{1}{2}}\delta F_{(\phi)(t)}\right\}\right.\\
&\qquad - \left.\frac{\partial}{\partial\phi}\left\{r\left(1-\frac{2m}{r}\right)^{\frac{1}{2}}\delta F_{(\theta)(t)}\right\}\right]=0, \qquad (2.3.5)
\end{aligned}
$$

$$
\begin{aligned}
&\frac{1}{c}\frac{\partial}{\partial t}\left(\delta F_{(\phi)(r)}\right) + \frac{1}{r\sin\theta}\left(1-\frac{2m}{r}\right)^{\frac{1}{2}}\left[\frac{\partial}{\partial\phi}\left(\delta F_{(r)(t)}\right)\right.\\
&\qquad - \left.\frac{\partial}{\partial r}\left\{r\sin\theta\left(1-\frac{2m}{r}\right)^{\frac{1}{2}}\delta F_{(\phi)(t)}\right\}\right]=0, \qquad (2.3.6)
\end{aligned}
$$

$$
\frac{1}{c}\frac{\partial}{\partial t}\left(\delta F_{(r)(\theta)}\right) + \frac{1}{r}\left(1-\frac{2m}{r}\right)^{\frac{1}{2}}\left[\frac{\partial}{\partial r}\left\{r\left(1-\frac{2m}{r}\right)^{\frac{1}{2}}\delta F_{(\theta)(t)}\right\}\right.
$$

$$- \frac{\partial}{\partial\theta}\left(\delta F_{(r)(t)}\right)\Big] = 0, \tag{2.3.7}$$

$$\frac{\partial}{\partial r}\left(r^2\sin\theta\ \delta F_{(\theta)(\phi)}\right) + \frac{\partial}{\partial\theta}\left\{r\sin\theta\left(1-\frac{2m}{r}\right)^{-\frac{1}{2}}\delta F_{(\phi)(r)}\right\} + \frac{\partial}{\partial\phi}\left\{r\left(1-\frac{2m}{r}\right)^{-\frac{1}{2}}\delta F_{(r)(\theta)}\right\} = 0, \tag{2.3.8}$$

$$\begin{aligned}\frac{1}{c}\frac{\partial}{\partial t}\left(\delta F_{(r)(t)}\right) &- \left(1-\frac{2m}{r}\right)^{\frac{1}{2}}\frac{1}{r\sin\theta}\frac{\partial}{\partial\theta}\left(\sin\theta\ \delta F_{(r)(\theta)}\right)\\ &- \left(1-\frac{2m}{r}\right)^{\frac{1}{2}}\frac{1}{r\sin\theta}\frac{\partial}{\partial\phi}\left(\delta F_{(r)(\phi)}\right)\\ &= -\frac{4\pi}{c}\left(1-\frac{2m}{r}\right)^{\frac{1}{2}}\delta J^{(r)},\end{aligned} \tag{2.3.9}$$

$$\begin{aligned}\frac{1}{c}\frac{\partial}{\partial t}\left(\delta F_{(\theta)(t)}\right) &- \left(1-\frac{2m}{r}\right)^{\frac{1}{2}}\frac{\partial}{\partial r}\left[r\left(1-\frac{2m}{r}\right)^{\frac{1}{2}}\delta F_{(\theta)(r)}\right]\\ &- \frac{1}{r\sin\theta}\left(1-\frac{2m}{r}\right)^{\frac{1}{2}}\frac{\partial}{\partial\phi}\left(\delta F_{(\theta)(\phi)}\right)\\ &= -\frac{4\pi}{c}\left(1-\frac{2m}{r}\right)^{\frac{1}{2}}\delta J^{(\theta)},\end{aligned} \tag{2.3.10}$$

$$\begin{aligned}\frac{1}{c}\frac{\partial}{\partial t}\left(\delta F_{(\phi)(t)}\right) &- \frac{1}{r}\left(1-\frac{2m}{r}\right)^{\frac{1}{2}}\frac{\partial}{\partial r}\left[r\left(1-\frac{2m}{r}\right)^{\frac{1}{2}}\delta F_{(\phi)(r)}\right]\\ &- \frac{1}{r}\left(1-\frac{2m}{r}\right)^{\frac{1}{2}}\frac{\partial}{\partial\theta}\left[\delta F_{(\phi)(\theta)}\right]\\ &= -\frac{4\pi}{c}\left(1-\frac{2m}{r}\right)^{\frac{1}{2}}\delta J^{(\phi)},\end{aligned} \tag{2.3.11}$$

$$\frac{1}{r}\frac{\partial}{\partial r}\left(r^2\delta F_{(t)(r)}\right) + \left(1-\frac{2m}{r}\right)^{-\frac{1}{2}}\frac{1}{\sin\theta}\frac{\partial}{\partial\theta}\left[\sin\theta\delta F_{(t)(\theta)}\right]$$

$$+ \quad \left(1-\frac{2m}{r}\right)^{-\frac{1}{2}} \frac{1}{\sin\theta}\frac{\partial}{\partial\phi}\left[\delta F_{(t)(\phi)}\right]$$

$$= \quad \frac{4\pi r}{c}\left(1-\frac{2m}{r}\right)^{-\frac{1}{2}} \delta J^{(t)}. \tag{2.3.12}$$

Finally, the linearised perturbed Ohm's law in components form are written as

$$\begin{aligned}
\delta J^{(r)} &= -\frac{\sigma}{c}\left(1-\frac{V_0^2}{c^2}\right)^{-\frac{1}{2}} \left[c\delta F_{(r)(t)} + \delta F_{(r)(\theta)}V^{(\theta)} + \delta F_{(r)(\phi)}V^{(\phi)}\right. \\
&+ \left. F_{(r)(\theta)}\delta V^{(\theta)} + F_{(r)(\phi)}\delta V^{(\phi)}\right] \\
&+ \frac{2\sigma}{c^3}V_0\delta V\left[cF_{(r)(t)} + F_{(r)(\theta)}V^{(\theta)} + F_{(r)(\phi)}V^{(\phi)}\right],
\end{aligned} \tag{2.3.13}$$

$$\begin{aligned}
\delta J^{(\theta)} &= -\frac{\sigma}{c}\left(1-\frac{V_0^2}{c^2}\right)^{-\frac{1}{2}} \left[c\delta F_{(\theta)(t)} + \delta F_{(\theta)(r)}V^{(r)} + \delta F_{(\theta)(\phi)}V^{(\phi)}\right. \\
&+ \left. F_{(\theta)(r)}\delta V^{(r)} + F_{(\theta)(\phi)}\delta V^{(\phi)}\right] \\
&+ \frac{2\sigma}{c^3}V_0\delta V\left[cF_{(\theta)(t)} + F_{(\theta)(r)}V^{(r)} + F_{(\theta)(\phi)}V^{(\phi)}\right],
\end{aligned} \tag{2.3.14}$$

$$\begin{aligned}
\delta J^{(\phi)} &= -\frac{\sigma}{c}\left(1-\frac{V_0^2}{c^2}\right)^{-\frac{1}{2}} \left[c\delta F_{(\phi)(t)} + \delta F_{(\phi)(r)}V^{(r)} + \delta F_{(\phi)(\theta)}V^{(\theta)}\right. \\
&+ \left. F_{(\phi)(r)}\delta V^{(r)} + F_{(\phi)(\theta)(r)}\delta V^{(\theta)}\right] \\
&+ \frac{2\sigma}{c^3}V_0\delta V\left[cF_{(\phi)(t)} + F_{(\phi)(r)}V^{(r)} + F_{(\phi)(\theta)}V^{(\theta)}\right],
\end{aligned} \tag{2.3.15}$$

$$\begin{aligned}
\delta J^{(t)} &= -\frac{\sigma}{c}\left(1-\frac{V_0^2}{c^2}\right)^{-\frac{1}{2}} \left[F_{0(\alpha)(t)}\delta V^{(\alpha)} + c\delta F_{(\alpha)(t)}V^{(\alpha)}\right]. \\
&+ \frac{2\sigma}{c^3}V_0\delta V\left[F_{(r)(t)}V^{(r)} + F_{(\theta)(t)}V^{(\theta)} + F_{(\phi)(t)}V^{(\phi)}\right].
\end{aligned} \tag{2.3.16}$$

In deriving the above set of equations (2.3.1-2.3.16), we have used the following notations.

$$V_0^2 = {V_0^{(r)}}^2 + {V_0^{(\theta)}}^2 + {V_0^{(\phi)}}^2, \tag{2.3.17}$$

$$V_0\delta V = V_0^{(r)}\delta V^{(r)} + V_0^{(\theta)}\delta V^{(\theta)} + V_0^{(\phi)}\delta V^{(\phi)}, \tag{2.3.18}$$

$$\frac{D}{Dx} = \left(1-\frac{2m}{r}\right)^{\frac{1}{2}}\left[\left(1-\frac{2m}{r}\right)^{\frac{1}{2}}V_0^{(r)}\frac{\partial}{\partial r} + \frac{V_0^{(\theta)}}{r}\frac{\partial}{\partial\theta} + \frac{V_0^{(\phi)}}{r\sin\theta}\frac{\partial}{\partial\phi}\right]. \tag{2.3.19}$$

To discuss the stability as governed by the above set of equations, we follow two different approaches depending on the different physical situations. If the scale length over which the disturbances grow is quite large in comparison with the wavelength of the perturbation, then a local stability analysis is performed and following the standard normal mode analysis (Chandrasekhar [95]), the general time dependent perturbations are written as:

$$\delta\Psi(r,\theta,\phi,t) = \Psi_1 exp[i(\omega t + \mathrm{kr} + \mathrm{n}\theta + \mathrm{m}\phi)] \tag{2.3.20}$$

where k, n and m are real wave numbers in radial, meridional and azimuthal direction respectively and ω, the frequency, could be complex. For illustration, let us consider the case of radial perturbation only where the scale length is defined as the pressure scale length L_p, with $L_p^{-1} = \frac{1}{p_0}\frac{dp_0}{dr}$. If $\mathrm{k}L_p \gg 1$, then the criterion for the local analysis is satisfied and a wave like solution, as shown above, is assumed. As a result of these assumptions, the differential equations governing the flow and fields are reduced to algebraic equations and a dispersion relation could be obtained after considerable algebra. The roots of the dispersion relation (*i.e.* $\omega's$) are in general complex. The real component of ω (ω_r) gives the propagation characteristic of the mode while negative imaginary component (ω_i) indicates an instability and determines its growth rate. It is to be noted that in a local stability analysis, the spatial variation of the amplitude (Ψ_1) is assumed to be constant over the entire scale length.

If, on the other hand, the approximation of scale length is not valid, then the generic time dependent perturbations, for an axisymmetric system, are written

as

$$\delta\Psi(r,\theta,\phi,t) = \Psi_1(r,\theta)exp\,[i(\omega t + m\phi)] \qquad (2.3.21)$$

where the amplitude Ψ_1 no longer remains a constant but becomes a function of r and θ. This procedure is generally followed, when the steady state solutions are inhomogeneous in spatial directions. The appropriate partial differential equations are then solved through the standard method of *eigenvalue techniques*. This approach involves transformation of the system of linearised differential equations into the form of an algebraic matrix eigenvalue equation $(\mathrm{A} - \omega \mathrm{B})\ \mathrm{X} = 0$. A non-trivial solution of this homogeneous system requires a zero value for the determinant of the associated matrix of the coefficients ($\mid A\ -\ \omega B \mid = 0$). Therefore, given a set of equilibrium parameters $\Psi_0(r,\theta)$ and the corresponding wave numbers, we have to make a search for the zeros of the determinant in the plane (ω_r, ω_i); the corresponding values of the complex parameter ω are the required eigenvalues. By using numerical methods, one can obtain solution of this system of equations. We have adopted one of the better known programs accronymed EISPACK [96,97] which is a systematised collection of subroutines to compute the eigenvalues and eigenvectors.

In this chapter, we have developed a general set of equations, in relativistic formalism, for the study of structure and stability of plasma flows around magnetosphere of compact objects. In subsequent chapters, we use this formalism to study equilibrium configurations and their stability properties.

Chapter 3

EQUILIBRIUM STRUCTURE FOR A PLASMA MAGNETOSPHERE AROUND COMPACT OBJECTS

3.1 Introduction

In the last chapter, considering the background geometry to be the Schwarzschild geometry, the dynamical equations for the analysis of the magnetospheric plasma flow around compact objects were developed. Here, we apply these equations to the study of the equilibrium structures around a spherical compact source, which could be either a neutron star or a black hole. The study in its entirety is quite involved. As a first step, towards the solutions of the problem, a fairly simple but an analytical equilibrium configuration is presented here. For a steady and axisymmetric electromagnetic field and matter distribution, the investigation is carried out for an incompressible fluid with toroidal flow supported by poloidal magnetic field and radial gravitational field.

As mentioned in Chap. 1, though there have been numerous discussions of

the magnetospheric theory with considerable progress, only a few of them attempts to obtain self- consistent configurations of the global magnetic field structures. For a neutron star, the calculations invariably neglect the major changes in the external dipole magnetic field that are expected to result from diamagnetic currents induced in the accreting plasma. A global magnetic field is important because it provides the stage for various physical processes and may even affect the physical interpretation of the observed phenomena. This problem, in the Newtonian formalism, was studied by Low and Uchida [98], where they confined their study to the discussion of the axisymmetric non-rotating magnetosphere in equilibrium with the magnetized mass accreted by the central gravitating star. Their analysis indicated that the mass slides down along the field lines to the point closest to the star and is stratified in hydrostatic equilibrium to form a disc in the equatorial plane. The picture obtained was encouraging enough to look for detailed analysis wherein one could also consider the relativistic equations through curved space formalism.

In a completely different approach, Lovelace and coworkers [60,61] have considered the flow of an ideal (infinite conductivity) relativistic MHD fluid around a compact object. The analysis was centered in solving the second order Grad-Shafranov equation for the magnetic flux function through numerical techniques. As a particular application, Lovelace et. al [60] analyse, numerically, magnetic thin discs with no poloidal flow and no toroidal field. This theory was later generalised to curved space time [61] where a virial equation was derived from the basic MHD equations in Schwarzschild geometry. This equation was used to show that the ratio of the total electromagnetic energy to the gravitational binding energy between the black hole and the matter outside it, is less than unity. However, no equilibrium solution was reported in the paper. Under an identical approximation of infinite

conductivity, the fully general relativistic formulation of Bhaskaran & Prasanna [64,65] demonstrates the possible existence of equilibrium configurations.

For a long time, these and many more (Frank *et al.* [34]) theoretical descriptions of plasma flow around the compact objects were based on the approximation of thin discs which assumed (*i*) very small vertical thickness of the disc, (*ii*) hydrostatic equilibrium along the vertical direction and (*iii*) no significant pressure gradient forces in the radial direction. This in turn leads to a Keplerian velocity distribution in the azimuthal direction. In the light of growing observational evidences [68], it appears that some of the above assumptions may not be valid for accreting systems. It is probable that there are accretion discs which are geometrically thick in the vertical direction and hence the assumption of hydrostatic equilibrium would be inappropriate for the dynamics of such discs. In addition, the inclusion of magnetic fields in the dynamics suggests the break down of the assumption of Keplerian distribution. In the limit of thin disc, this conjecture is supported by the computation of Lovalace [60] and Kaburaki [56] which are based entirely on two different approaches. Lovelace *et. al.* contemplates the azimuthal velocity of the disc matter to be much less than Keplerian value while the analytical calculations of Kaburaki show that the velocity reduces by a factor of $\sqrt{6}$. Such a situation is different from the standard model of viscous accretion discs (without magnetic fields) where one could justify the omission of pressure gradients and definitely assume the azimuthal velocity to be Keplerian.

Keeping this dilemma of Keplerian velocity distribution in the dynamics of accretion discs, in mind, a simple analysis in the relativistic framework including the effects of magnetic fields is carried out in this chapter. The objective of this analysis is two fold:

(*i*) to carry out a rigorous calculation of the equilibrium structure around a non-rotating compact object including the effects of general relativity through the analysis of fluid as well as Maxwell's equations self consistently, and

(*ii*) to study the flow pattern in the azimuthal direction that could sustain equilibrium disc configurations.

The outline of this chapter is as follows. In Section 2, we describe the dynamical equations that are most suitable for such studies. Possible equilibrium solutions in the limit of thin and thick discs are derived in Section 3. Conclusions and discussions are presented in Section 4.

3.2 Dynamical equations

In this section, we derive the necessary equations from the most general set of equations given in Chap. 2 for our particular assumptions which are described below.

3.2.1 Geometry

The plasma flow and the electromagnetic fields are assumed to be stationary and axially symmetric i.e. the properties of the flow are independent of t and ϕ. Also, it is easy to verify that the toroidal component of the electric field (E_ϕ) is zero due to the symmetry assumed. With this symmetry, the governing equations of (2.2.20-2.2.31) are given as

the equations of momentum balance

$$\left(\rho+\frac{p}{c^2}\right)\left[\left(1-\frac{2m}{r}\right)^{\frac{1}{2}}\left\{\left(1-\frac{2m}{r}\right)^{\frac{1}{2}}V^{(r)}\frac{\partial V^{(r)}}{\partial r}+\frac{V^{(\theta)}}{r}\frac{\partial V^{(r)}}{\partial\theta}\right\}\right.$$
$$\left.+\frac{mc^2}{r^2}\left(1-\frac{V^{(r)^2}}{c^2}\right)-\left(1-\frac{2m}{r}\right)\frac{1}{r}\left(V^{(\theta)^2}+V^{(\phi)^2}\right)\right]$$
$$+\left(1-\frac{V^2}{c^2}\right)\left[\left(1-\frac{2m}{r}\right)\frac{\partial p}{\partial r}\right.$$
$$+\left(1-\frac{2m}{r}\right)^{\frac{1}{2}}\frac{1}{c}\left\{E_{(r)}J^{(t)}+B_{(\phi)}J^{(\theta)}-B_{(\theta)}J^{(\phi)}\right\}$$
$$\left.-\left(1-\frac{2m}{r}\right)^{\frac{1}{2}}\frac{V^{(r)}}{c^2}\left(E_{(\alpha)}J^{(\alpha)}\right)\right]=0, \qquad (3.2.1)$$

$$\left(\rho+\frac{p}{c^2}\right)\left[\left(1-\frac{2m}{r}\right)^{\frac{1}{2}}\left\{\left(1-\frac{2m}{r}\right)^{\frac{1}{2}}V^{(r)}\frac{\partial V^{(\theta)}}{\partial r}+\frac{V^{(\theta)}}{r}\frac{\partial V^{(\theta)}}{\partial\theta}\right\}\right.$$
$$\left.\left(1-\frac{3m}{r}\right)\frac{V^{(r)}V^{(\theta)}}{r}-\left(1-\frac{2m}{r}\right)^{\frac{1}{2}}\frac{cot\theta}{r}V^{(\phi)^2}\right]$$
$$+\left(1-\frac{V^2}{c^2}\right)\left(\frac{1-2m}{r}\right)^{\frac{1}{2}}\left[\frac{1}{r}\frac{\partial p}{\partial\theta}+\frac{1}{c}\left(E_{(\theta)}J^{(t)}+B_{(r)}J^{(\phi)}\right.\right.$$
$$\left.\left.-B_{(\phi)}J^{(r)}\right\}-\frac{V^{(\theta)}}{c^2}\left\{E_{(r)}J^{(r)}+E_{(\theta)}J^{(\theta)}\right\}\right]=0, \qquad (3.2.2)$$

$$\left(\rho+\frac{p}{c^2}\right)\left[\left(1-\frac{2m}{r}\right)^{\frac{1}{2}}\left\{\left(1-\frac{2m}{r}\right)^{\frac{1}{2}}V^{(r)}\frac{\partial V^{(\phi)}}{\partial r}+\frac{V^{(\theta)}}{r}\frac{\partial V^{(\phi)}}{\partial\theta}\right\}\right.$$
$$\left.+\left(1-\frac{3m}{r}\right)\frac{V^{(r)}V^{(\phi)}}{r}+\left(1-\frac{2m}{r}\right)^{\frac{1}{2}}\frac{cot\theta}{r}V^{(\phi)}V^{(\theta)}\right]+\left(1-\frac{V^2}{c^2}\right)$$
$$\times\left(1-\frac{2m}{r}\right)^{\frac{1}{2}}\frac{1}{c}\left[\left\{B_{(\theta)}J^{(r)}-B_{(r)}J^{(\theta)}\right\}-\frac{V^{(\phi)}}{c}\left(E_{(\alpha)}J^{(\alpha)}\right)\right]=0, \qquad (3.2.3)$$

the continuity equation

$$\left(\rho+\frac{p}{c^2}\right)\left[\left(1-\frac{2m}{r}\right)^{\frac{1}{2}}\left\{\left(1-\frac{2m}{r}\right)^{\frac{1}{2}}\frac{\partial V^{(r)}}{\partial r}+\frac{1}{r}\frac{\partial V^{(\theta)}}{\partial\theta}+\frac{cot\theta}{r}V^{(\theta)}\right.\right.$$

$$\left.\left.+\left(1-\frac{2m}{r}\right)^{\frac{1}{2}}\frac{2}{r}V^{(r)}\right\}\right]+\left(1-\frac{2m}{r}\right)^{\frac{1}{2}}\left\{V^{(r)}\left(1-\frac{2m}{r}\right)^{\frac{1}{2}}\frac{\partial\rho}{\partial r}+\frac{V^{(\theta)}}{r}\frac{\partial\rho}{\partial\theta}\right\}$$

$$-\frac{1}{c^2}\left(1-\frac{2m}{r}\right)^{\frac{1}{2}}\left\{\left(1-\frac{2m}{r}\right)^{\frac{1}{2}}V^{(r)}\frac{\partial p}{\partial r}+\frac{V^{(\theta)}}{r}\frac{\partial p}{\partial\theta}\right\}$$

$$+\frac{1}{c^2}\left(1-\frac{V^2}{c^2}\right)\left(1-\frac{2m}{r}\right)^{\frac{1}{2}}\left(E_{(\alpha)}J^{(\alpha)}\right)$$

$$-\frac{2}{c^2}\left(1-\frac{2m}{r}\right)^{\frac{1}{2}}\left[E_{(\alpha)}J^{(\alpha)}+\frac{V^{(r)}}{c}\left\{B_{(\phi)}J^{(r)}-B_{(\theta)}J^{(\phi)}\right\}\right.$$

$$\left.+\frac{V^{(\theta)}}{c}\left\{B_{(r)}J^{(\phi)}-B_{(\phi)}J^{(r)}\right\}+\frac{V^{(\phi)}}{c}\left\{B_{(\theta)}J^{(r)}-B_{(r)}J^{(\theta)}\right\}\right]=0, \quad (3.2.4)$$

and the Maxwell's equations

$$\frac{\partial}{\partial\theta}\left(\sin\theta B_{(\phi)}\right)=-\frac{4\pi r}{c}\sin\theta J^{(r)}, \quad (3.2.5)$$

$$\frac{\partial}{\partial r}\left[r\left(1-\frac{2m}{r}\right)^{\frac{1}{2}}B_{(\phi)}\right]=\frac{4\pi r}{c}J^{(\theta)}, \quad (3.2.6)$$

$$\frac{\partial}{\partial r}\left[r\left(1-\frac{2m}{r}\right)^{\frac{1}{2}}B_{(\theta)}\right]-\frac{\partial B_{(r)}}{\partial\theta}=-\frac{4\pi r}{c}J^{(\phi)}, \quad (3.2.7)$$

$$\left(1-\frac{2m}{r}\right)^{\frac{1}{2}}\frac{\partial}{\partial r}\left[r^2\sin\theta E_{(r)}\right]+\frac{\partial}{\partial\theta}\left[r\sin\theta E_{(\theta)}\right]=-\frac{4\pi}{c}r^2\sin\theta J^{(t)}, \quad (3.2.8)$$

$$\frac{\partial}{\partial r}\left[r^2\sin\theta B_{(r)}\right]+\frac{\partial}{\partial\theta}\left[r\left(1-\frac{2m}{r}\right)^{-\frac{1}{2}}\sin\theta B_{(\theta)}\right]=0, \quad (3.2.9)$$

$$\frac{\partial}{\partial r}\left[r\left(1-\frac{2m}{r}\right)^{\frac{1}{2}}E_{(\theta)}\right]-\frac{\partial E_{(r)}}{\partial\theta}=0. \quad (3.2.10)$$

3.3 Possible solutions

One admissible solution of the Maxwell's equations (3.2.9-3.2.10 & 3.2.5-3.2.6)

$$\begin{aligned} E_{(r)} &= E_0 \left(\frac{R}{r}\right)^3 \cos\theta, \\ E_{(\theta)} &= \frac{E_0}{2} \left(\frac{R}{r}\right)^3 \left(1 - \frac{2m}{r}\right)^{-\frac{1}{2}} \sin\theta \end{aligned} \tag{3.3.1}$$

$$\begin{aligned} B_{(r)} &= B_0 \left(\frac{R}{r}\right)^3 \cos\theta, \\ B_{(\theta)} &= \frac{B_0}{2} \left(\frac{R}{r}\right)^3 \left(1 - \frac{2m}{r}\right)^{\frac{1}{2}} \sin\theta, \\ B_{(\phi)} &= \frac{k_1}{r \sin\theta} \left(1 - \frac{2m}{r}\right)^{-\frac{1}{2}}. \end{aligned} \tag{3.3.2}$$

gives rise to the currents

$$\begin{aligned} J^{(r)} &= 0, \\ J^{(\theta)} &= 0, \\ J^{(\phi)} &= -\frac{3mc}{4\pi} \frac{B_0}{r^2} \left(\frac{R}{r}\right)^3 \sin\theta, \\ J^{(t)} &= -\frac{2mc}{4\pi} \frac{E_0}{r^2} \left(\frac{R}{r}\right)^3 \left(1 - \frac{2m}{r}\right)^{-\frac{1}{2}} \cos\theta, \end{aligned} \tag{3.3.3}$$

where R, B_0, and E_0 denote the radius, magnetic and electric field strengths on the surface of the compact object respectively and k_1 is an arbitrary constant. As the currents in the radial and meridional directions are zero, one can look for a self-consistent solution of the fluid equations for a purely rotating fluid having only the azimuthal component of $V^{(\alpha)}$ to be nonzero. It is also to be noted that as a result of $J^{(r)}$ and $J^{(\theta)}$ being zero, $B_{(\phi)}$ does not enter into the calculations and hence the arbitrary constant k_1 is assumed to be zero ($B_{(\phi)} = 0$). With these simplifying

assumptions, equations (3.2.3 and 3.2.4) get satisfied while the other two momentum equations (3.2.1 & 3.2.2) take the form

$$\left(\rho+\frac{p}{c^2}\right)\left(1-\frac{V^{(\phi)^2}}{c^2}\right)^{-1}\left[\frac{MG}{r^2}-\left(1-\frac{2m}{r}\right)\frac{V^{(\phi)^2}}{r}\right]$$
$$+\left(1-\frac{2m}{r}\right)\frac{\partial p}{\partial r}+\frac{m}{4\pi r^2}\left(\frac{R}{r}\right)^6\left(1-\frac{2m}{r}\right)$$
$$\times\left[\frac{3}{2}B_0^2\sin^2\theta-2E_0^2\left(1-\frac{2m}{r}\right)^{-1}\cos^2\theta\right]=0, \qquad (3.3.4)$$

$$\left(\rho+\frac{p}{c^2}\right)\left(1-\frac{V^{(\phi)^2}}{c^2}\right)^{-1}V^{(\phi)^2}cot\theta-\frac{\partial p}{\partial\theta}$$
$$+\frac{m}{4\pi r}\left(\frac{R}{r}\right)^6\left[3B_0^2+E_0^2\left(1-\frac{2m}{r}\right)^{-1}\right]\sin\theta\cos\theta=0. \qquad (3.3.5)$$

As there are three variables (V^{ϕ}, ρ & p) to be determined and only two equations, we would require an equation of state to close the system. Our aim is now to solve this restricted problem for different physical systems.

3.4 Thin disc

As a test case, if one restricts the discussion to the matter confined to the equatorial plane ($\theta=\frac{\pi}{2}$) of the disc, then equation (3.3.5) gets satisfied identically while (3.3.4) yields

$$\left(\rho+\frac{p}{c^2}\right)\left(1-\frac{V^{(\phi)^2}}{c^2}\right)^{-1}\left[\frac{MG}{r^2}\left(1-\frac{2m}{r}\right)^{-1}-\frac{V^{(\phi)^2}}{r}\right]$$
$$+\frac{\partial p}{\partial r}+\frac{3m}{8\pi}\frac{B_0^2R^6}{r^8}=0. \qquad (3.4.1)$$

To solve this equation, we assume, as a first approximation, the magneotfluid, to be incompressible and further specify the nature of the velocity distribution and

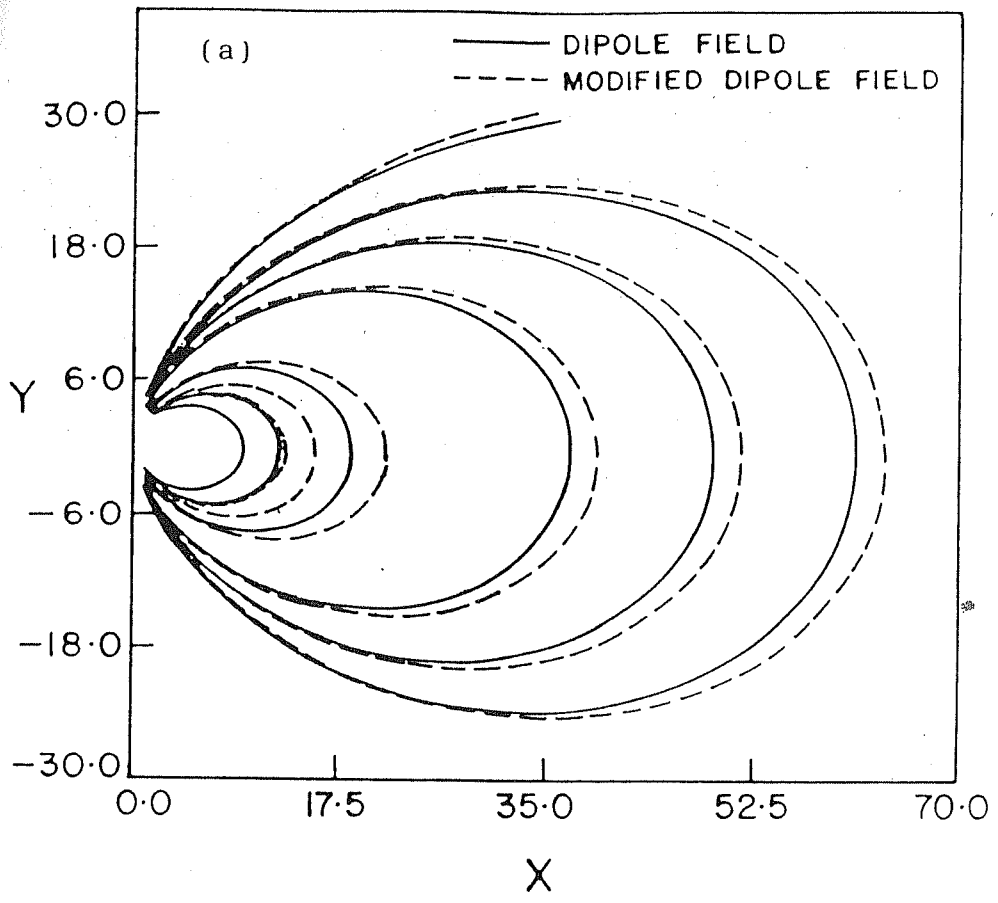

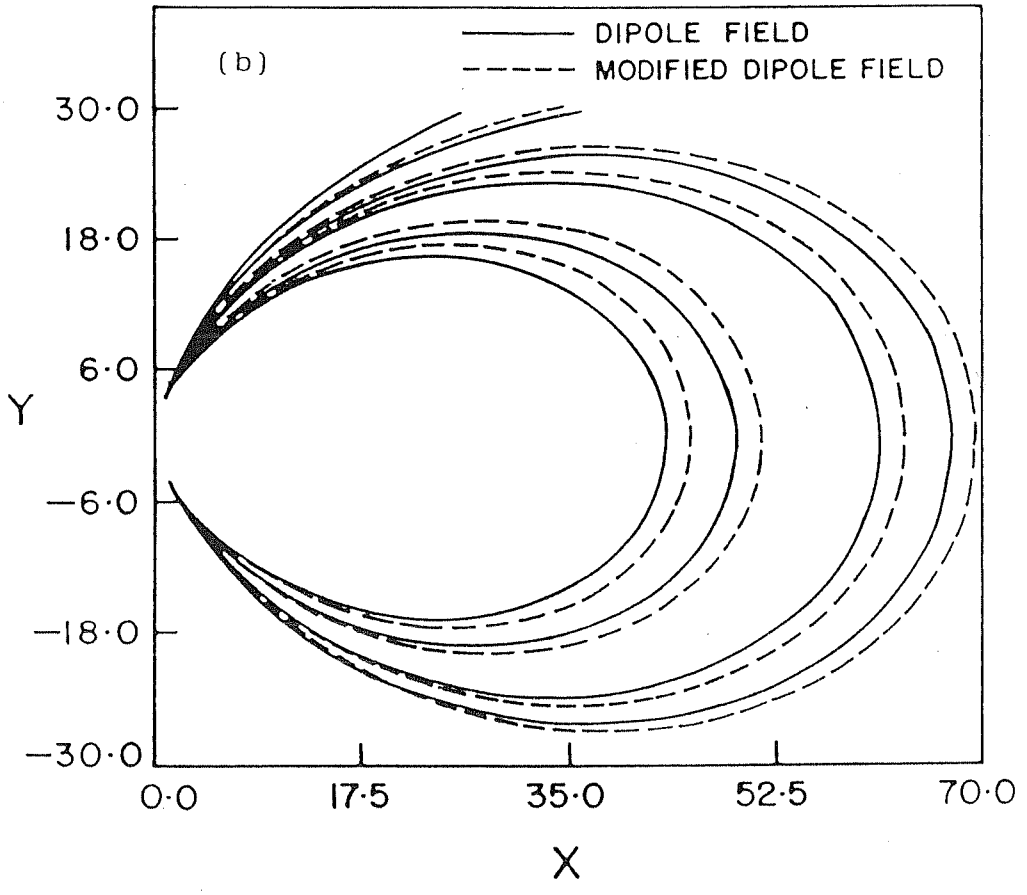

Figure 3.1. Magnetic field configuration in the meridional plane for a compact object having radius (a) R = 3m (b) R = 12m for relativistic (broken line) and Newtonian case (solid line).

analyse the effects on the disc configurations.

3.4.1 Free fall velocity

Considering the motion of the magnetofluid to be governed by the free fall velocity

$$V^{(\phi)} = \sqrt{\frac{2GM}{r}},$$

equation (3.4.1) reduces to

$$\frac{dp}{dr} - \frac{mc^2}{r^2}\left(1 - \frac{2m}{r}\right)^{-2}\left(1 - \frac{4m}{r}\right)\left(\rho + \frac{p}{c^2}\right) + \frac{3m}{8\pi}\frac{B_0^2 R^6}{r^8} = 0. \tag{3.4.2}$$

In order to look for an exact analytic solution in closed form, one takes the Newtonian limit of this equation and obtains

$$\frac{dp}{dr} - \frac{m}{r^2}\left(\rho c^2 + p\right) + \frac{3m}{8\pi}\frac{B_0^2 R^6}{r^8} = 0, \tag{3.4.3}$$

whose solution for an incompressible fluid (ρ = constant = ρ_0) is given by

$$\begin{aligned}\left(\rho_0 + \frac{p}{c^2}\right) &= De^{-m/r} + \frac{3B_0^2 R^6}{8\pi m^6}\left[\left(\frac{m}{r} - 6\right)\left(\frac{m}{r}\right)^5\right. \\ &\left. + 30\left(\frac{m}{r} - 4\right)\left(\frac{m}{r}\right)^3 + \frac{360m}{r}\left(\frac{m}{r} - 2\right) + 720\right].\end{aligned} \tag{3.4.4}$$

For a steady and stable disc configuration, the constant of integration D is obtained from the boundary condition that at the inner edge $r = r_a$, the hydrostatic pressure p equals the pressure due to stellar magnetic field *i.e.*

$$p = P_m = \frac{B^2}{8\pi}. \tag{3.4.5}$$

If one uses accretion disc model of Pringle & Rees [38], this occurs at the radius

$$r_p = 0.89\left[\frac{rV_r}{hV_{ff}}\right]^{\frac{2}{7}} l_o, \tag{3.4.6}$$

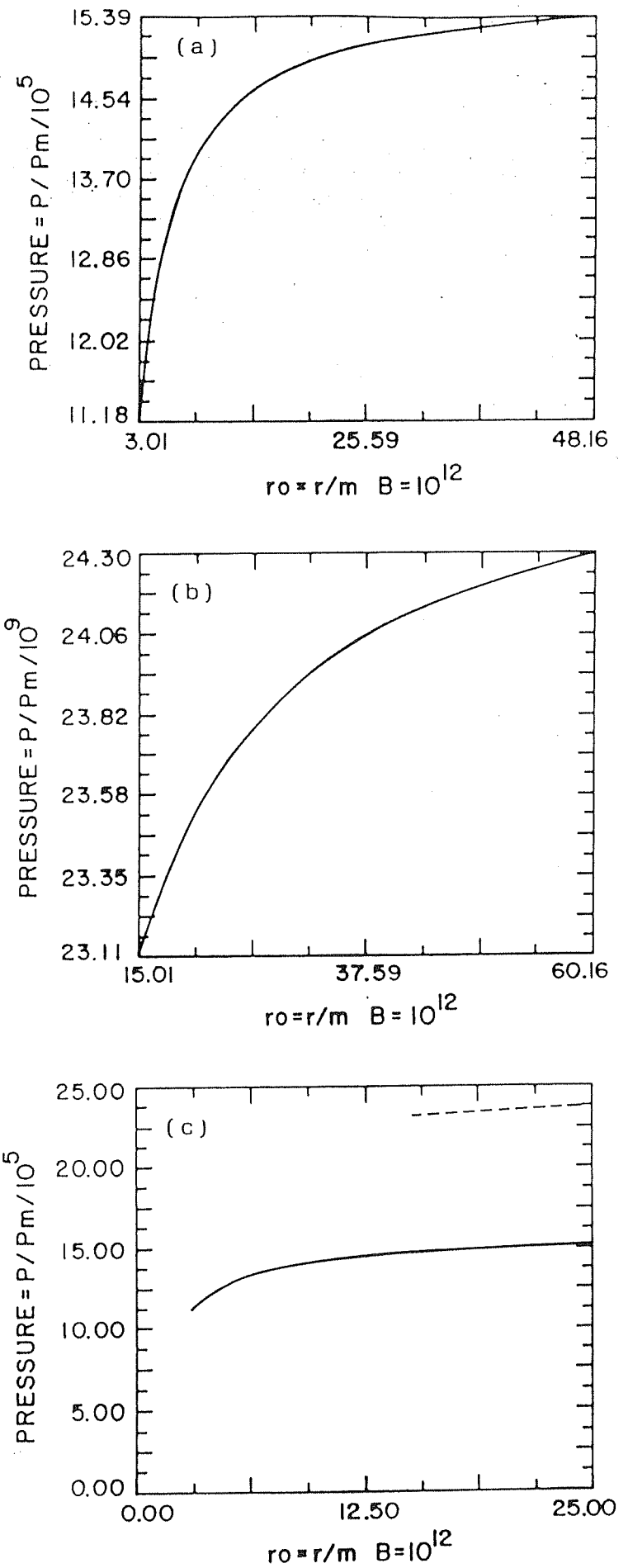

Figure 3.2. Pressure profiles in the Newtonian limit for thin disc with $V^{(\phi)} = \sqrt{2GM/r}$ for a compact object with (a) R=3m, (b) R=15m; comparison of the two pressure profiles is shown in (c) by solid (R=3m), and broken (R=15m) lines.

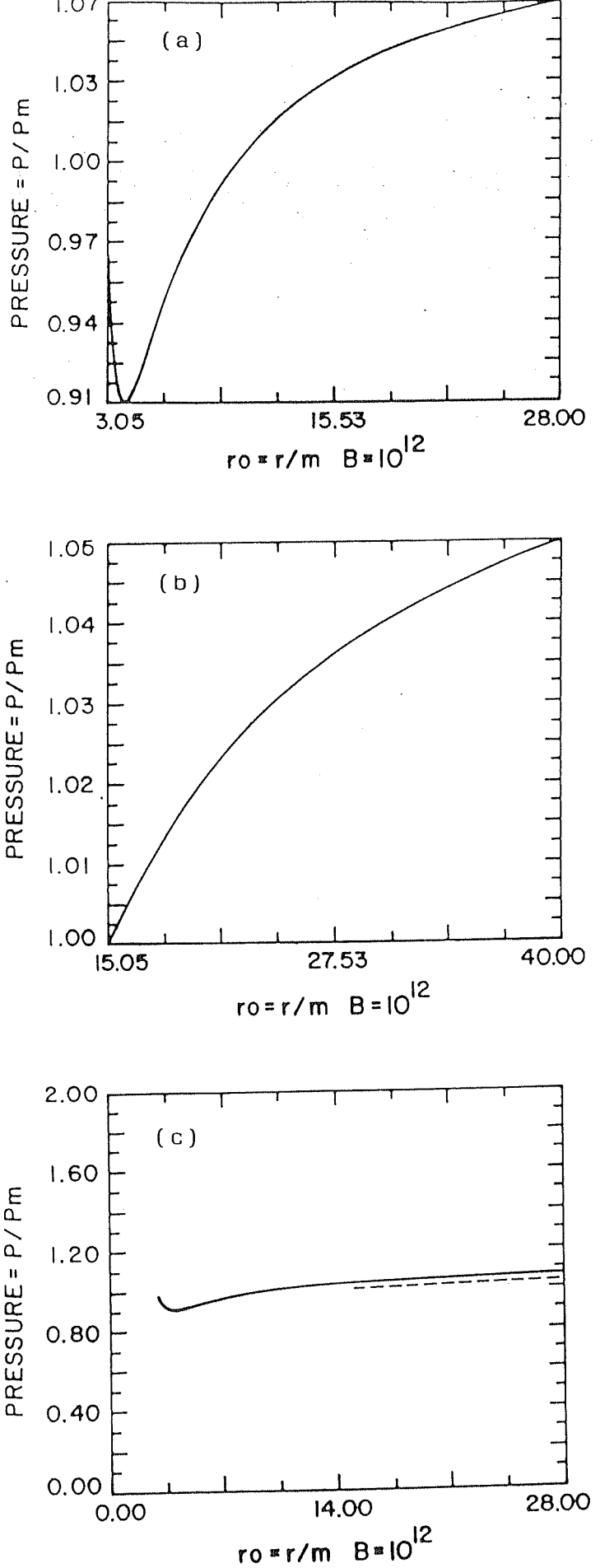

Figure 3.3. Pressure profiles for thin disc with $V^{(\phi)} = \sqrt{2GM/r}$ for a compact object with (a) R=3m, and (b) R=15m with no approximation; comparison of the two pressure profiles is (c) by solid (R=3m), and broken (R=15m) lines.

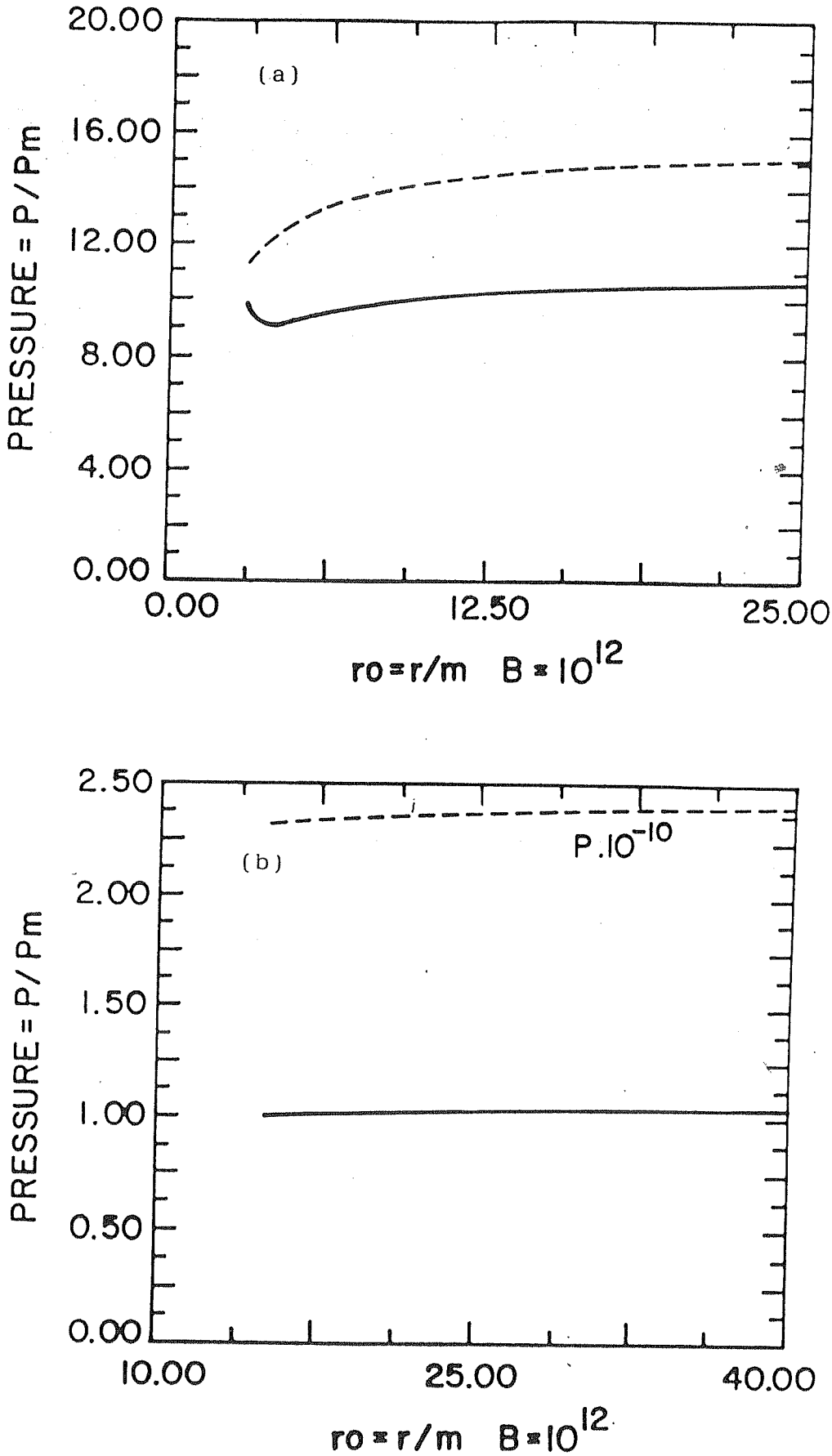

Figure 3.4. Comparison of pressure profiles for $V^{(\phi)} = \sqrt{2GM/r}$ with (broken line) and without (solid line) approximation for (a) R=3m, (b) R=15m.

where V_r is the inward radial drift velocity in the disc, h is the disc semi-thickness, $V_{ff} = (2GM/r)^{\frac{1}{2}}$, and

$$l_0 = \left[\frac{\mu^4 MG}{L^2 R^2}\right]^{\frac{1}{7}} = 3.88 \times 10^8 L_{37}^{-\frac{2}{7}} \mu_{30}^{\frac{4}{7}} (\frac{M}{M_\theta})^{\frac{1}{7}} R_6^{-\frac{2}{7}} \text{cm}, \tag{3.4.7}$$

is a characteristic length which appears in nearly all estimates of the size of accreting neutron star magnetospheres. Here, L is the accretion luminosity in units of 10^{37}ergs-s^{-1}, μ is the magnetic moment in units of 10^{30} gauss and R is the stellar radius in units of 10^6 cm. On the other hand, if we specify the inner edge distance x_a, the unknown integration constant D can be easily evaluated from the boundary condition mentioned above and by doing so, we obtain

$$D = 10^3\rho + 3n^6\left[\frac{1}{x_a^5} - \frac{5}{x_a^4} + \frac{20}{x_a^3} - \frac{60}{x_a^2} + \frac{120}{x_a} - 120\right], \tag{3.4.8}$$

where $n = R/m$ and $x_a = r_a/m$. Fig. 3.2 gives the profiles of pressure in terms of the magnetic pressure (P_m) for two different compact objects having radii R = 3m and R = 15m corresponding to a black hole and a neutron star respectively. The solution of the complete equation (3.4.2) is obtained numerically and the pressure profiles are shown in Figs. 3.3 & 3.4. It is to be noted that for obtaining the plots, we have taken $\mu_{30} = 1$ ($B_0 = 10^{12}$ gauss), and $(\rho_0) = 10$ gm/cm^3.

3.4.2 Relativistic Keplerian distribution

If we assume the velocity distribution to be relativistic Keplerian

$$V^{(\phi)} = \sqrt{\left(1 - \frac{2m}{r}\right)^{-1} \frac{MG}{r}},$$

equation (3.4.1) yields

$$\frac{dp}{dr} = -\frac{3m}{8\pi} \frac{B_0^2 R^6}{r^8} . \tag{3.4.9}$$

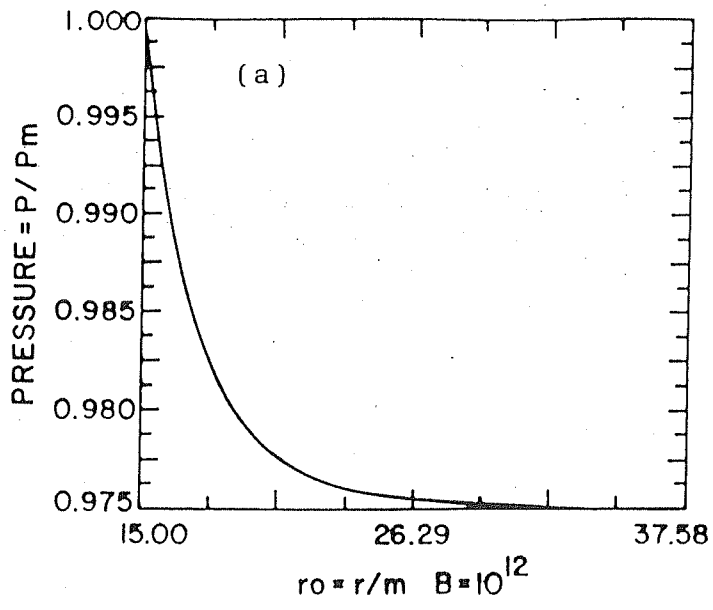

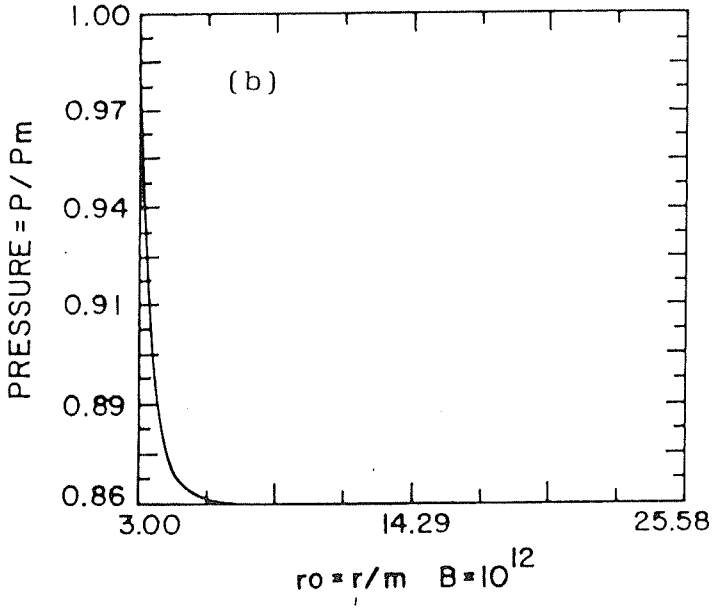

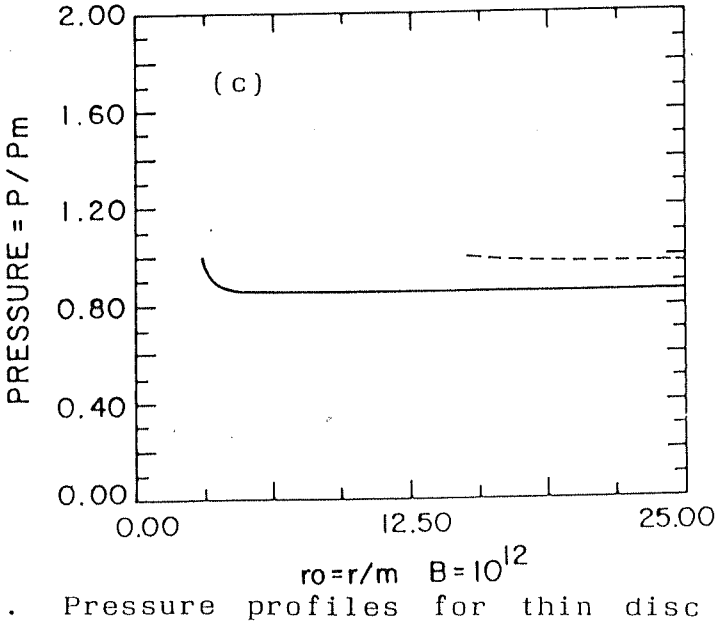

Figure 3.5. Pressure profiles for thin disc with $V^{(\phi)} = \sqrt{(1-2m/r)GM/r}$ for a compact object with (a) R=3m, (b) R=15m; comparison of the two pressure profiles is made in (c) by solid (R=3m), and broken (R=15m) lines.

whose solution is

$$p = D + \frac{3m}{56\pi}\frac{B_0^2 R^6}{r^7}. \tag{3.4.10}$$

Using the previously mentioned boundary condition (3.4.5), one evaluates D and finally obtains the pressure to be:

$$p = \frac{B_0^2 R^6}{8\pi r_a^6}\left[1 - \frac{3m}{7r_a}\left\{1 - \left(\frac{r_a}{r}\right)^7\right\}\right]. \tag{3.4.11}$$

The pressure profile as a function of x (x = r/m) is illustrated in Fig. 3.5. It is evident that for a relativistic Keplerian velocity distribution there exists a perfect balance between the centrifugal and gravitational forces. This leaves the magnetic stress to balance the pressure gradient force. Now, if we assume that the contribution from the magnetic field is negligible, then integration of equation (3.4.9) would yield pressure to be constant all over the disc surface, which would be an idealistic picture. Instead of relativistic formalism , if one uses the Newtonian equations, Keplerian velocity distribution would generate the same expression (equation 3.4.9). It is also apparent that in the absence of magnetic field for a self-consistent calculation, the pressure gradient force in the radial direction has to be neglected unless other forces (like radiation pressure) are involved. However, we emphasize that in most of the calculations of thin disc including magnetic fields (Kaburaki, [50]), the radial momentum balance equation is neglected and the meridional component is integrated to obtain the pressure, which in our opinion is inconsistent.

3.4.3 Keplerian distribution

Assuming the azimuthal velocity to be Keplerian,

$$V^{(\phi)} = \sqrt{\frac{GM}{r}},$$

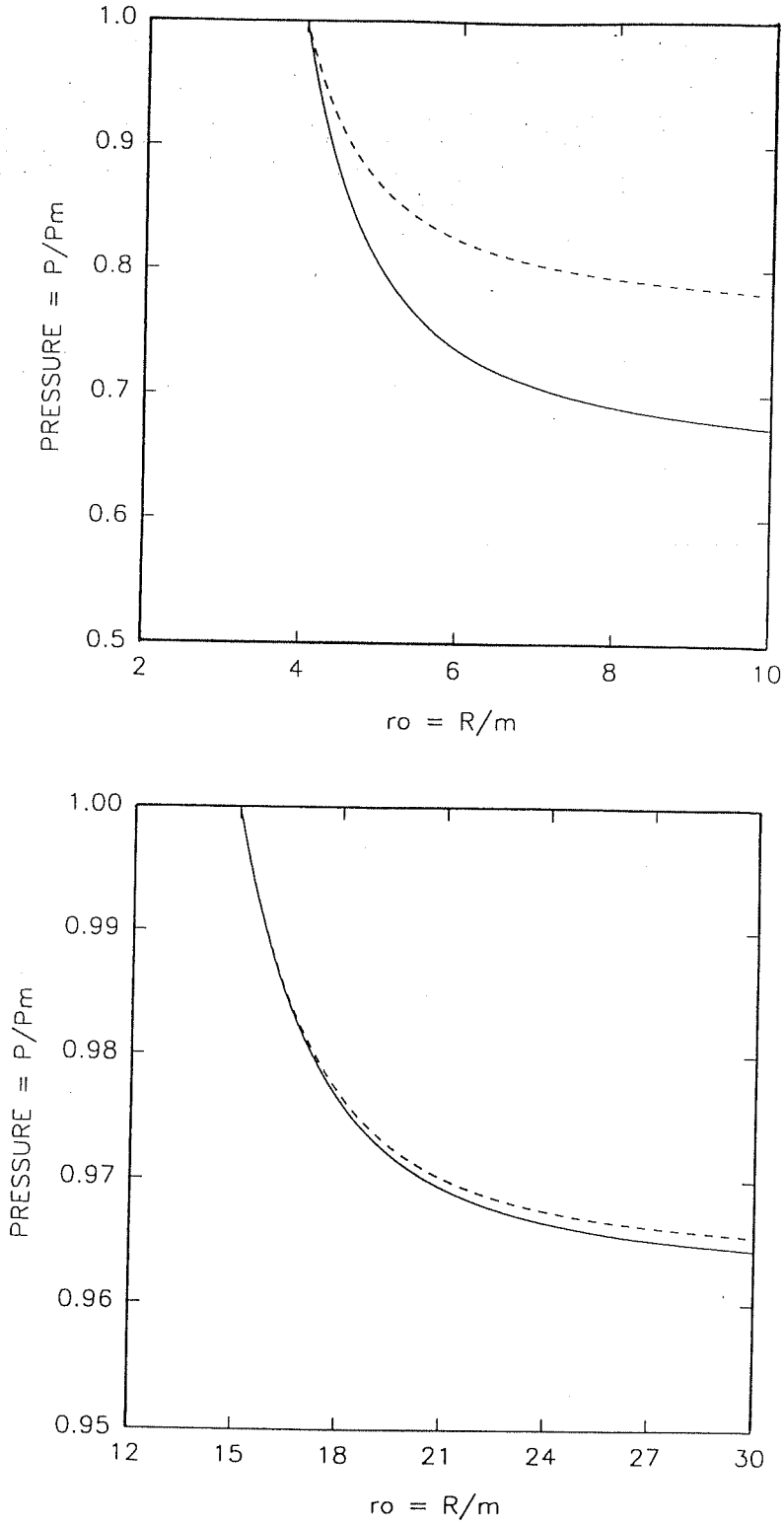

Figure 3.6. Pressure profiles for thin disc with $V^{(\Phi)}=\sqrt{GM/r}$ for a compact object with (broken line) and without (solid line) approximation for (a) R=3m, (b) R=15m.

equation (3.4.1) gives,

$$\frac{dp}{dr} + (\rho c^2 + p)\left(1 - \frac{3m}{r} + \frac{2m^2}{r^2}\right)^{-1} \frac{2m^2}{r^3} = -\frac{3m}{8\pi}\frac{B_0^2 R^6}{r^8}. \tag{3.4.12}$$

Retaining terms of order m^2 only, we get

$$\frac{dp}{dr} + (\rho c^2 + p)\frac{2m^2}{r^3} = -\frac{3m}{8\pi}\frac{B_0^2 R^6}{r^8}. \tag{3.4.13}$$

Using the boundary condition mentioned in equation (3.4.5), the above two equations are integrated numerically and the corresponding presure profiles are depicted in Fig. 3.6.

3.5 Thick Disc

The physics of thick discs is more complex than that of thin discs. In the case of thick discs, one has to solve coupled partial differential equations (see below) as compared to thin discs where one solves ordinary differential equations due to the assumption of separation of vertical and radial disc structures. In order to understand the dynamics of thick discs, we restrict, as in the case of thin discs, the magnetofluid to be incompressible and study the effect of velocity patterns on the disc dynamics for the angular momentum distributions illustrated in case of thin discs.

3.5.1 Free fall velocity

With free fall velocity distributions,

$$V^{(\phi)} = \sqrt{\frac{2GM}{r}},$$

the momentum equations (3.3.4 & 3.3.5) are rewritten in the following form:

$$\frac{\partial p}{\partial r} = (\rho c^2 + p)\frac{m}{r^2}\left(1-\frac{2m}{r}\right)^{-2}\left(1-\frac{4m}{r}\right) - \frac{mR^6}{4\pi r^8}\left[\frac{3}{2}B_0^2\sin^2\theta - 2E_0^2\left(1-\frac{2m}{r}\right)^{-1}\cos^2\theta\right], \quad (3.5.1)$$

$$\frac{\partial p}{\partial \theta} = (\rho c^2 + p)\frac{2m}{r}\left(1-\frac{2m}{r}\right)^{-1} cot\ \theta + \frac{mR^6}{4\pi r^7}\left[3B_0^2 + E_0^2\left(1-\frac{2m}{r}\right)^{-1}\right]\sin\theta\cos\theta. \quad (3.5.2)$$

Assuming a separable form for $(\rho c^2 + p)$, in the form $(\rho c^2 + p) = f(r)\sin^2\theta$, the integrability condition for an incompressible fluid ($\rho = \rho_0$) yields the equation

$$\frac{df}{dr} - \frac{2f}{r} - \frac{R^6}{8\pi r^7}\left[18B_0^2\left(1-\frac{2m}{r}\right) + 3E_0^2\left(1-\frac{2m}{r}\right)^{-1}\left(1-\frac{4m}{3r}\right)\right] = 0, \quad (3.5.3)$$

whose exact solution is

$$f = Dr^2 + \frac{R^6r^2}{8\pi}\left[B_0^2\left(\frac{4m}{r^9}-\frac{9}{4r^8}\right) + E_0^2\left\{-\frac{1}{4r^8} + \frac{1}{14mr^7} + \frac{1}{24m^2r^6} + \frac{1}{40m^3r^5} + \frac{1}{64m^4r^4} + \frac{1}{96m^5r^3} + \frac{1}{128m^6r^2} + \frac{1}{128m^7r} + \frac{1}{256m^8}ln\left(1-\frac{2m}{r}\right)\right\}\right]. \quad (3.5.4)$$

The constant of integration D can be evaluated using the boundary condition mentioned earlier in case of the thin disc (equation 3.4.5). The pressure profile for a given set of parameters is then obtained and is shown in Fig. 3.7a.

3.5.2 Relativistic Keplerian distribution

Considering the velocity distribution to be relativistic Keplerian,

$$V^{(\phi)} = \sqrt{\left(1-\frac{2m}{r}\right)^{-1}\frac{MG}{r}},$$

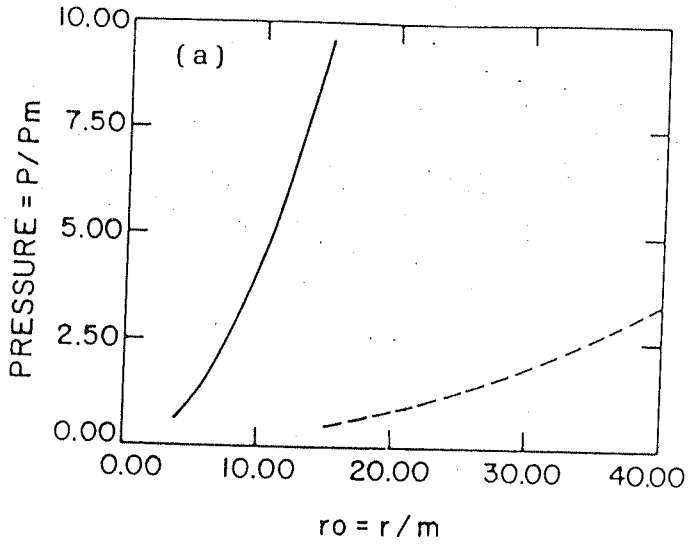

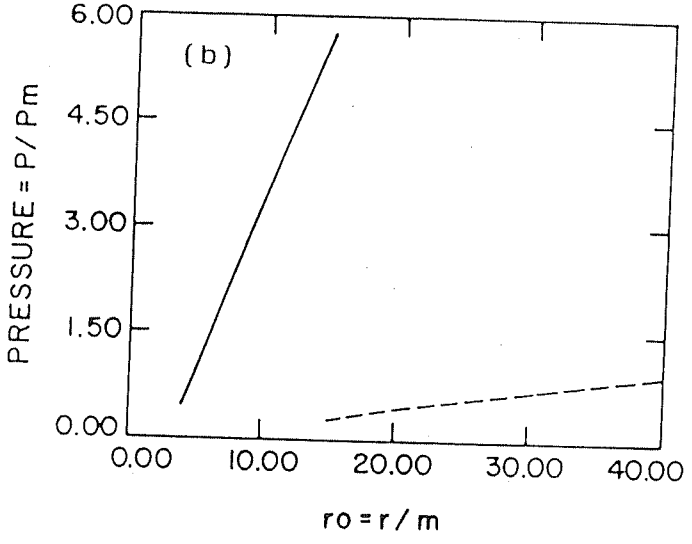

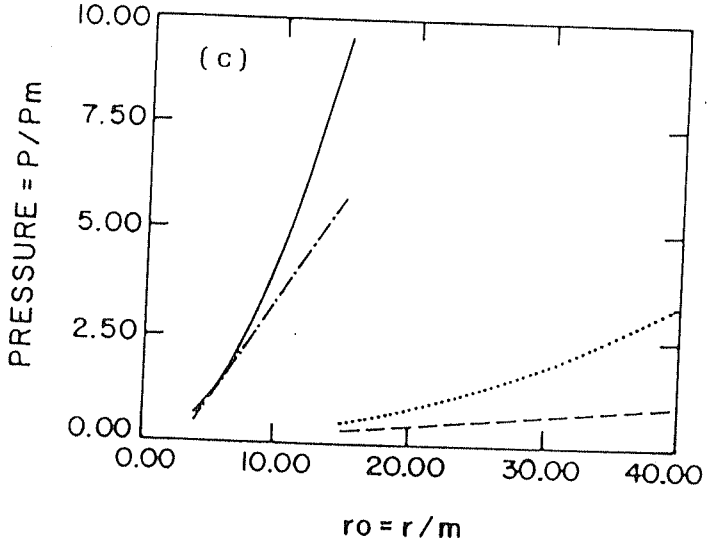

Figure 3.7. Pressure profile for thick disc with (a) $V^{(\phi)}=\sqrt{2GM/r}$, and (b) $V^{(\phi)}=\sqrt{(1-2m/r)GM/r}$ for a compact object with R=3.5m (solid line) and R=12m (broken line); comparison of profiles is made in (c) for the two cases: (a) R=3.5m (——), and R=12m (.....), (b) R=3.5m (-·-·-·), and R=12m (----).

equations (3.3.4 & 3.3.5) reduce to the pair of equations,

$$\frac{\partial p}{\partial r} = -\frac{m}{4\pi r^2}\left(\frac{R}{r}\right)^6\left[\frac{3}{2}B_0^2\sin^2\theta - 2E_0^2\left(1-\frac{2m}{r}\right)^{-1}\cos^2\theta\right], \qquad (3.5.5)$$

$$\frac{\partial p}{\partial \theta} = (\rho c^2+p)\left(1-\frac{2m}{r}\right)^{-1}\frac{m}{r}cot\ \theta + \frac{m}{4\pi r}\left(\frac{R}{r}\right)^6\left[3B_0^2+E_0^2\left(1-\frac{2m}{r}\right)^{-1}\right]\sin\theta\cos\theta. \qquad (3.5.6)$$

As before, with $(\rho c^2+p) = f(r)\sin^2\theta$, the integrability condition requires

$$\frac{d}{dr}\left(\frac{f}{r-3m}\right) = \frac{r^6}{4\pi}\left[\frac{18B_0^2}{r^8}+\frac{3E_0^2}{r^8}\left(1-\frac{2m}{r}\right)^{-2}\left(1-\frac{4m}{r}\right)\right], \qquad (3.5.7)$$

whose solution is

$$(\rho c^2+p) = \left[D(r-3m)-(r-3m)\left\{\frac{18b_0^2R^6}{28\pi r^7}\right\} - (r-3m)\frac{E_0^2R^6}{60\pi}\left(-\frac{5}{2mr^6}-\frac{3}{4m^2r^5}+\frac{5}{16m^4r^3}+\frac{15}{32m^5r^2}+\frac{45}{64m^6r} + \frac{15}{128m^7}\left(1-\frac{2m}{r}\right)^{-1}+\frac{60}{128m^7}ln\left(1-\frac{2m}{r}\right)\right)\right]\sin^2\theta. \qquad (3.5.8)$$

The pressure profile in the meridional plane of the thick disc for this case is depicted in Fig. 3.7b. Fig. 3.7c shows the comparison of the pressure profiles for the thick disc configurations presented in Sect. 3.5.1 and Sect. 3.5.2.

3.5.3 Keplerian distribution

With the assumption of Keplerian velocity distribution,

$$V^{(\phi)} = \sqrt{\frac{GM}{r}},$$

equations (3.3.4 & 3.3.5) give

$$\frac{\partial p}{\partial r} + (\rho c^2+p)\left(1-\frac{2m}{r}\right)^{-1}\left[\left(1-\frac{2m}{r}\right)^{-1}\frac{m}{r^2}-\frac{m}{r^2}\right]$$

$$+\frac{m}{4\pi r^2}\left(\frac{R}{r}\right)^6\left[\frac{3}{2}B_0^2\sin^2\theta - 2E_0^2\left(1-\frac{2m}{r}\right)^{-1}\cos^2\theta\right] = 0, \qquad (3.5.9)$$

$$\frac{\partial p}{\partial\theta} + (\rho c^2 + p)\left(1-\frac{2m}{r}\right)^{-1}\frac{Gm}{r}cot\ \theta$$
$$-\frac{m}{4\pi r}\left(\frac{R}{r}\right)^6\left[\frac{3}{2}B_0^2 + 2E_0^2\left(1-\frac{2m}{r}\right)^{-1}\right]\sin\theta\cos\theta = 0. \qquad (3.5.10)$$

As before, the integrability condition requires,

$$\begin{aligned}\frac{df}{dr} &= f(r)\left[\frac{1}{r}+\frac{m}{r^2}\left(1-\frac{m}{r}\right)^{-1} - \frac{4m}{r^2}\left(1-\frac{2m}{r}\right)^{-1}\right] \\ &+ \frac{1}{4\pi r}\left(\frac{R}{r}\right)^6\left[18B_0^2 + 3E_0^2\left(1-\frac{2m}{r}\right)^{-1}\left(1-\frac{m}{r}\right)\right] \\ &- \frac{2m}{4\pi r^2}\left(\frac{R}{r}\right)^6 E_0^2\left(1-\frac{2m}{r}\right)^{-2}\left(1-\frac{m}{r}\right). \qquad (3.5.11)\end{aligned}$$

Using the pressure balance condition (3.4.5) at the inner edge, the pressure profile for a given set of values is evaluated numerically and is shown in Fig. 3.8.

3.6 Discussions and conclusions

The structure of the magnetic field lines (Fig. 3.1) highlights the importance of general relativity in the study of disc configurations. Due to the presence of the gravitational field of the compact object, we find that the field structure is modified to the effect that the field strength at every point enhances. In addition, it is noticed that the enhancement is more prominent in the case of the black hole (R = 2m) than in case of the Neutron star (R = 12m). This emphasizes the fact that the effects are stronger for a more compact object.

The results for pressure distribution in the meridional plane ($\theta = \pi/2$; thin disc limit) of the disc clearly shows the difference that could arise due to varied

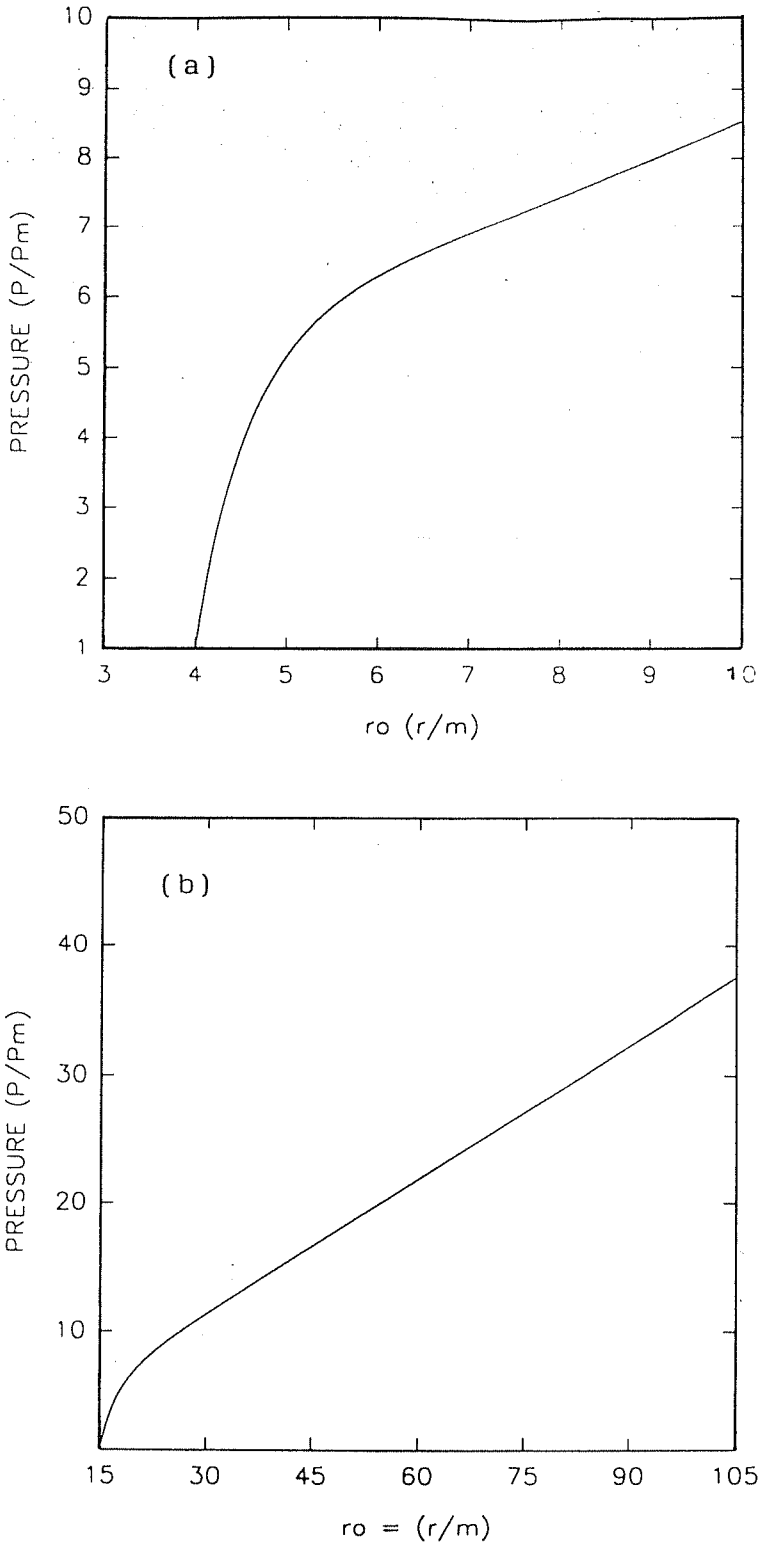

Figure 3.8. Pressure profile for thick disc with $V^{(\phi)} = \sqrt{GM/r}$ for (a) R=3m, and (b) R=12m.

velocity distributions. Particularly, if the velocity distribution is higher than Keplerian, the difference between the Newtonian and the general relativistic treatment is very interesting. In the Newtonian limit, the solution presents a pressure distribution (Fig. 3.2) which is increasing from the inner edge outwards for a short distance and then stays almost constant. On the other hand, in the case when no approximation was made (Fig. 3.3), the pressure first decreases to reach a minimum and then increases outward just as in the earlier case. The minimum occurs at r = 4m which could be mainly due to the general relativistic term $(1 - \frac{4m}{r})$ in the equation (3.4.1). In contrast, when we consider the velocity distribution to be relativistic Keplerian or Keplerian, the pressure profiles (Figs. 3.4 & 3.5) are more physical decreasing outwards as one would normally expect. For a thin disc, it can be concluded that for an equilibrium configuration of plasma flow around a compact object having an intrinsic magnetic field, a velocity greater than the Keplerian velocity is inconsistent with the fully relativistic equations.

In case of thick discs, since the integration constant gets multiplied by r^2, r and (r-3m) for Keplerian, relativistic Keplerian and a velocity higher than Keplerian respectively, the pressure profiles (Figs. 3.7 & 3.8) increase outward monotonically. The increasing pressure distribution indicates an unstable configuration. Thus, we conclude that for the type of electromagnetic field configuration that we have considered, no physically meaningful solution exists for a prescribed velocity distribution as chosen above.

Despite the reasonable equilibrium configuration in the fully relativistic treatment of the thin discs, there may still be an unsatisfactory element as far as Ohm's law is considered, since we have not specifically made use of it. It is worth noting

that if one were to consider Ohm's law

$$J^i = \sigma F^i{}_k U^k, \tag{3.6.1}$$

along with the dynamical equations (3.2.1) to (3.2.10), then it is clear that the electric and magnetic fields are coupled through the velocity field and it would not be consistent to choose certain components of V^α to be zero *apriori*. This would mean a more complex set of coupled nonlinear equations for which the existence of an equilibrium solution may not be always guaranteed.

In conclusion, we find that for a situation wherein the current contribution of the plasma on the existing electromagnetic field of the compact object is neglected, Keplerian or relativistic Keplerian velocity configuration in equilibrium with the electromagnetic field does admit a reasonable pressure profile.

Chapter 4

ACCRETING MAGNETOFLUID AROUND A COMPACT OBJECT: A NEWTONIAN ANALYSIS

4.1 Introduction

The structure of magnetospheres around accreting neutron stars is central to the understanding of a wide variety of high energy cosmic sources. The study of magnetospheres of accreting neutron stars began with the discovery of bright pulsating X-ray sources (Schreier [2], Tananbaum [3]) in the early 1970's and the interpretation of these as rotating neutron stars (Pringle [38], Davidson & Ostriker [39], Lamb [40]). Most of the energy emitted by these objects is in the form of X-rays with energies in the range of 0.1 - 0.3 keV and is supplied by accretion of matter onto the star's surface. As the accreting matter approaches the rotating neutron star, it is more and more influenced by its magnetic field until eventually the motion is completely determined by the field and the plasma ends up on the surface of the star either by flowing along the field lines or across it due to diffusion or instabilities

at the inner edge. Although the details of the accretion process in the region where the magnetic field dominates the dynamics have been studied by a number of investigators (see Prasanna [11]and references therein), the general description of the plasma flow from the disc midplane to the stellar surface is complex and a satisfactory theoretical description is not yet found (Anzer & Börner [55]). The angular momentum transport mechanisms in the disc and the rotating magnetosphere are just two examples for which only simplified model versions have been discussed.

On the other hand, the large scale structure of the magnetospheres of these stars is important since many of the observational properties including pulse shapes, spin up rates and intensity fluctuations depend on it. There have been considerable progress in the understanding of the dynamics of thin discs with external magnetic fields. In this context, there exists two different types of models. The first kind of models assume that the stellar magnetic field is presumed to thread a broad region of the disc as a consequence of turbulent diffusion, magnetic field reconnection and Kelvin-Helmholtz instabilities (Ghosh & Lamb [47]). In contrast, the second kind of models are based upon the assumption that the disc material is characterized by infinite conductivity such that the stellar field is completely screened from the disc. It seems promising to develop a general theory for steady, axisymmetric magnetohydrodynamic (MHD) flows around a magnetized star or a compact object. In ideal MHD limit, Lovelace and co workers [60,61] have considered a general theory in both Newtonian and relativistic limits. The theory leads to a basic second order Grad-Shafranov equation which was then solved numerically. The first analytical equilibrium solution including the finite conductivity of the fluid for the case of a non-rotating magnetized star in the thin disc limit was obtained by Kaburaki

[50,56] but as mentioned in Chap. 1 these equilibrium solutions are not self consistent. First, the system yields two solutions for the radial velocity and secondly the electric vector does not satisfy the Faraday's law.

In order to understand the dynamics of finite resistive thick discs in a better perspective, we elucidate in this chapter, the importance of magnetic field on the accretion flow process by developing a general theory in the Newtonian framework. This theory is similar to the theory developed by Abramowicz et. al. [72] for thick accretion discs. The difference lies in the consideration of magnetic fields and finite conductivity of the plasma. Thus, our theory is more appropriate for hydromagnetic flows around compact objects. The plan of this chapter is as follows. In Section 4.2 we give the basic Newtonian equations which are derived from the corresponding relativistic equations given in Chap. 2. The possible equilibrium structure is described in Section 4.3. Special cases of thin and thick disc solutions are illustrated in Section 4.4. Global properties of the thick disc configuration is highlighted in section 4.5. Conclusions are drawn in Section 4.6.

4.2 Formalism

In this section, we derive the Newtonian limit of the dynamical equations of Chap. 2 (equations 2.2.20-2.2.31) for the stationary and axisymmetric magnetofluid around a compact object of mass M. In the Newtonian limit, the momentum and mass conservation equations are written as

the momentum equations

$$\rho\left[V^r\frac{\partial V^r}{\partial r} + \frac{V^\theta}{r}\frac{\partial V^r}{\partial \theta} + \frac{MG}{r^2} - \frac{1}{r}\left(V^{\theta 2} + V^{\phi 2}\right)\right] + \frac{\partial p}{\partial r} + \left(E_r J^t + B_\theta J^\phi - B_\phi J^\theta\right) = 0, \tag{4.2.1}$$

$$\rho\left[V^r\frac{\partial V^\theta}{\partial r} + \frac{V^\theta}{r}\frac{\partial V^\theta}{\partial\theta} + \frac{1}{r}\left(V^rV^\theta + V^{\phi^2}cot\theta\right)\right] + \frac{1}{r}\frac{\partial p}{\partial\theta} + \left(E_\theta J^t + B_r J^\phi - B_\phi J^r\right) = 0, \tag{4.2.2}$$

$$\rho\left[V^r\frac{\partial V^\phi}{\partial r} + \frac{V^\theta}{r}\frac{\partial V^\phi}{\partial\theta} + \frac{1}{r}\left(V^rV^\phi + V^\theta V^\phi cot\theta\right)\right] + \left(B_\theta J^r - B_r J^\theta\right) = 0, \tag{4.2.3}$$

the continuity equation

$$\rho\left[\frac{\partial V^r}{\partial r} + \frac{1}{r}\frac{V^\theta}{\theta} + \frac{1}{r}\left(2V^r + cot\theta V^\theta\right)\right] + V^r\frac{\partial\rho}{\partial r} + \frac{V^\theta}{r}\frac{\partial\rho}{\partial\theta} = 0. \tag{4.2.4}$$

The Maxwell's equations are given by

$$\frac{\sin\theta}{r}\frac{\partial}{\partial\theta}\left(\sin\theta B_\phi\right) = -\frac{4\pi}{c}J^r, \tag{4.2.5}$$

$$\frac{1}{r}\frac{\partial}{\partial r}\left(rB_\phi\right) = \frac{4\pi}{c}J^\theta, \tag{4.2.6}$$

$$\frac{\partial}{\partial r}\left(rB_\theta\right) - \frac{\partial}{\partial\theta}\left(B_r\right) = -\frac{4\pi}{c}rJ^\phi, \tag{4.2.7}$$

$$\frac{\partial}{\partial r}\left(r^2E_r\right) + \frac{r}{\sin\theta}\frac{\partial}{\partial\theta}\left(\sin\theta E_\theta\right) = -\frac{4\pi}{c}r^2J^t, \tag{4.2.8}$$

$$\frac{\partial}{\partial r}\left(rE_\theta\right) - \frac{\partial}{\partial\theta}\left(E_r\right) = 0, \tag{4.2.9}$$

$$\frac{\partial}{\partial r}\left(r^2B_r\right) + \frac{r}{\sin\theta}\frac{\partial}{\partial\theta}\left(\sin\theta B_\theta\right) = 0. \tag{4.2.10}$$

where ρ, p and G denote the density, pressure and the gravitational constant, $\left(V^r, V^\theta, V^\phi\right)$ indicate the spatial components of fluid four velocity U^i and electric and magnetic fields are represented by $\mathbf{E}$ and $\mathbf{B}$ respectively. J^i is the current density defined through the covariant Ohm's law which for a quasi-neutral plasma

$(\epsilon = 0)$ reduces to

$$J^i = \frac{\sigma}{c} F^i{}_k U^k. \tag{4.2.11}$$

Here ϵ is the charge density measured locally, and σ is the electrical conductivity of the fluid which, for simplicity, has been assumed to be constant throughout the disc. One of the admissible solutions of equations (4.2.5-4.2.6) is

$$B_\phi = \frac{1}{r \sin\theta}, \tag{4.2.12}$$

which yields $J^r = J^\theta = 0$. As a consequence, Ohm's law (4.2.11) yields

$$E_r = \frac{B_\theta V^\phi}{c}, \tag{4.2.13}$$

$$E_\theta = -\frac{B_r V^\phi}{c}, \tag{4.2.14}$$

$$J^\phi = -\frac{\sigma}{c}\left(B_\theta V^r - B_r V^\theta\right), \tag{4.2.15}$$

$$J^t = -\frac{\sigma}{c}\left(E_r V^r + E_\theta V^\theta\right) = \frac{J^\phi V^\phi}{c} \tag{4.2.16}$$

Using equation (4.2.8) in (4.2.16), we obtain

$$\frac{\partial}{\partial r}\left(r^2 E_r\right) + \frac{r}{\sin\theta}\frac{\partial}{\partial\theta}\left(\sin\theta E_\theta\right) = \frac{4\pi\sigma r}{c^2}(E.V) \tag{4.2.17}$$

which is not in the standard form of the Poisson's equation $\bigtriangledown \cdot \mathbf{E} = 4\pi q$. This apparent ambiguity in definition is due to the fact that $\mathbf{E}$ and ϵ are measured in different coordinate systems. As mentioned earlier, ϵ is measured locally while J^t is determined *w.r.t* the global Cartesian coordinate system. In fact, this relation gives the transformation law for q and ϵ (Greenberg [100])

$$q = \epsilon + \frac{\sigma}{c^2}(E.V), \tag{4.2.18}$$

where q is the charge density as measured *w.r.t.* the global Cartesian coordinate system.

We define, for a stationary and axisymmetric case, the total derivative

$$d = V^r \frac{\partial}{\partial r} + \frac{V^\theta}{r} \frac{\partial}{\partial \theta}, \tag{4.2.19}$$

and cite the final equations that govern the flow of the magnetofluid,

$$\rho \left[d(V^r) + \frac{MG}{r^2} - \frac{1}{r} \left(V^{\theta 2} + V^{\phi 2} \right) \right] + \frac{\partial p}{\partial r} = \frac{B_\theta J^\phi}{c}, \tag{4.2.20}$$

$$\rho \left[d\left(V^\theta\right) + \frac{1}{r} \left(V^r V^\theta - V^{\phi 2} cot\theta \right) \right] + \frac{1}{r} \frac{\partial p}{\partial \theta} = -\frac{B_r J^\phi}{c}, \tag{4.2.21}$$

$$d\left(r \sin\theta V^\phi\right) = 0, \tag{4.2.22}$$

$$\frac{\partial}{\partial r} \left(r^2 \rho \sin\theta V^r \right) + \frac{\partial}{\partial \theta} \left(r \rho \sin\theta V^\theta \right) = 0. \tag{4.2.23}$$

In deriving equations (4.2.20) and (4.2.21), (4.2.16) has been used and terms of order V^2/c^2 has been neglected. Finally, we rewrite the remaining Maxwell's equations (4.2.7 - 4.2.10) in a more useful format.

$$J^\phi = -\frac{c}{4\pi r} \left[\frac{\partial}{\partial r} \left(r B_\theta \right) - \frac{\partial}{\partial \theta} \left(B_r \right) \right], \tag{4.2.24}$$

$$J^t = -\frac{1}{4\pi r^2} \left[\frac{\partial}{\partial r} \left(r^2 B_\theta V^\phi \right) - \frac{r}{\sin\theta} \frac{\partial}{\partial \theta} \left(\sin\theta B_r V^\phi \right) \right], \tag{4.2.25}$$

$$\frac{\partial}{\partial r} \left(r B_r V^\phi \right) + \frac{\partial}{\partial \theta} \left(B_\theta V^\phi \right) = 0, \tag{4.2.26}$$

$$\frac{\partial}{\partial r} \left(r^2 B_r \right) + \frac{r}{\sin\theta} \frac{\partial}{\partial \theta} \left(\sin\theta B_\theta \right) = 0. \tag{4.2.27}$$

A closer look at expressions (4.2.15) and (4.2.24) reveal that there are two different

definitions of the current components J^{ϕ} and the consistency demands the condition

$$\sigma\left(B_{\theta}V^{r}-B_{r}V^{\theta}\right)-\frac{c^{2}}{4\pi r}\left[\frac{\partial}{\partial r}\left(rB_{\theta}\right)-\frac{\partial}{\partial\theta}\left(B_{r}\right)\right]=0. \tag{4.2.28}$$

To summarize, the basic equations that govern the flow of a stationary and axisymmetric magnetofluid are represented by equations (4.2.20-4.2.26) and (4.2.28). Also, the self-consistent electric field components can be obtained from (4.2.13 & 4.2.14).

4.3 Possible structure

Integrating equation (4.2.22), one has the azimuthal velocity

$$V^{\phi}=\frac{L}{r\sin\theta}, \tag{4.3.1}$$

where L is the constant of integration. As has been considered previously (Fishbone & Moncrief [69]), we choose $L^{2}=nGMR_{in}$ such that the range of values of n signifies various possible bounded discs. Using this, after some algebra, we obtain a class of solutions for the magnetic field components:

$$B_{r} = -B_{1}r^{k-1}\sin^{k-1}\theta\cos\theta, \tag{4.3.2}$$

$$B_{\theta} = B_{1}r^{k-1}\sin^{k}\theta, \tag{4.3.3}$$

where k and B_1 are the constants of integration. The derivations of the electric field components and the current components are now straight forward and the results are

$$E_{r} = \frac{L}{c}B_{1}r^{k-2}\sin^{k-1}\theta, \tag{4.3.4}$$

$$E_{\theta} = \frac{L}{c}B_{1}r^{k-2}\sin^{k-1}\theta\cos\theta, \tag{4.3.5}$$

$$J^{\phi} = (1-k)\frac{c}{4\pi}B_1(r\sin\theta)^{k-2}, \tag{4.3.6}$$

$$J^{t} = (1-k)\frac{L}{4\pi}B_1(r\sin\theta)^{k-3}. \tag{4.3.7}$$

Substituting the functional form of the magnetic field and the current components, the consistency relation (4.2.28) reduces to

$$V^r + V^\theta \cot\theta = \frac{(k-1)c^2}{4\pi\sigma r\sin^2\theta}. \tag{4.3.8}$$

Multiplying (4.2.20) by V^r and (4.2.21) by V^θ and adding, we obtain the Bernoulli's equation

$$d\overline{p} + \rho\left[d\left\{\left(\frac{V^2}{2}\right) - \left(\frac{MG}{r}\right)\right\}\right] = 0, \tag{4.3.9}$$

where we have used the following notations:

$$B^2 = B_r^2 + B_\theta^2 = \left[B_1(r\sin\theta)^{k-1}\right]^2,$$

$$\overline{p} = p + \frac{B^2}{8\pi},$$

$$V^2 = \left[V^{r2} + V^{\theta 2} + V^{\phi 2}\right].$$

The system of dynamical equations are now given by the the equation of continuity (4.2.23), the Bernoulli's equation (4.3.9) and the consistency relation (4.3.8). Since there are four variables to be determined *viz.* p, ρ, V^r and V^θ, one needs an equation of state to close the system.

4.4 Special cases

4.4.1 Thin disc

For the case of a thin disc ($\theta = \pi/2$ and $V^\theta = 0$), equation (4.3.8) yields

$$V^r = \frac{(k-1)c^2}{4\pi\sigma r} \tag{4.4.1}$$

The condition that $V^r/c \ll 1$ sets a lower limit on the value of the conductivity of the fluid as given by

$$\sigma \gg \frac{(1-k)c}{4\pi r}. \tag{4.4.2}$$

The accretion rate $\dot{M}$ is obtained by integrating the mass conservation law (4.2.23)

$$\dot{M} = \int_{\theta_{min}}^{\theta_{max}} \rho r^2 V^r d\theta \ . \tag{4.4.3}$$

This relation yields the density

$$\rho = \frac{4\pi\sigma\dot{M}}{(1-k)rc^2} = 10^{-4}\dot{M}_{18}\,\sigma_6\,r_7 \ \mathrm{gm\,cm^{-3}}, \tag{4.4.4}$$

where the subscript implies the units in which the parameters are measured *e.g.* $\dot{M}_{18}$ implies that the accretion rate is measured in units of 10^{18}. Knowing the mass conservation rate and the conductivity of the fluid, we can calculate the density distribution. More appropriately, one can specify the density at the outer boundary (ρ_{out}) and find out the accretion rate of the magnetofluid. Finally, integration of Bernoulli's equation (4.3.9) yields

$$p = \mathcal{P}_0 + \frac{4\pi GM\dot{M}\sigma}{(1-k)c^2r^2} - \frac{1}{3r^3}\left(\frac{(1-k)\dot{M}c^2}{4\pi\sigma} + \frac{4\pi\dot{M}\sigma L^2}{(1-k)c^2}\right) - \frac{B^2}{8\pi}, \tag{4.4.5}$$

where $\mathcal{P}_0$ is the integration constant.

4.4.1.1 Boundary conditions

The solutions obtained above for a thin disc contains two arbitrary integration constants B_1 and $\mathcal{P}_0$. The magnetic moment of the disc (B_1) is determined through the requirement of total pressure equilibrium across the boundary. We consider the external magnetic field to be dipolar, which could match for a modeling of accretion discs around neutron stars, and further we set, without the loss of generality, $\mathcal{P}_0 = 0$.

As described above, equating the energy density of the dipole magnetic field to that of the accreting plasma, we obtain

$$B_{\rm i}^2 = \left(\frac{x_{in}}{n}\right)^{2-2k}\left(\frac{2\pi\sigma\dot{M}}{(1-k)mx_{in}^2}\right) + \left[1-\frac{2n}{3}-\frac{1}{24x_{in}}\left\{\frac{(1-k)c}{4\pi\sigma}\right\}^2\right] - B_0^2\left(\frac{N}{x}\right)^{4+2k}, \qquad (4.4.6)$$

where B_0 is the surface magnetic field of the compact object and we have also introduced the dimensionless parameters N (N = R/m) and x_{in} ($= r_{in}$/m) respectively.

As the left-hand-side of equation (4.4.6) is a quadratic term, the right-hand-side should be positive definite. This implies that the sum of the first two terms in the above expression should be larger than the third. This puts an upper limit on the value of B_0 which we denote by B_c and find

$$B_{\rm c}^2 = \left(\frac{x_{in}}{n}\right)^{2-2k}\left(\frac{2\pi\sigma\dot{M}}{(1-k)mx_{in}^2}\right) + \left[1-\frac{2n}{3}-\frac{1}{24x_{in}}\left\{\frac{(1-k)c}{4\pi\sigma}\right\}^2\right], \qquad (4.4.7)$$

The same argument of positiveness also requires that the second term itself should be positive. This demands

$$n < \frac{3}{2}\left[1-\frac{1}{24x_{in}}\left\{\frac{(1-k)}{4\pi\sigma}\right\}^2\right]. \qquad (4.4.8)$$

Accordingly, the disc is bounded by 0 < n < 1.5 which differs slightly from the result of Fishbone & Moncrief [69], where the disc is bounded by 1< n <2. The difference could be attributed to the presence of the magnetic field.

The effect of different parameters on the pressure is investigated by plotting pressure as a function of r for different values of n and k. For k = 0 and n = 1, the pressure distribution (Fig. 4.1a) decreases smoothly with distance but as n increases and reaches a critical value, the profiles show turning point behaviour indicating the presence of large pressure gradients around that point. This region being nearer to

the inner boundary indicates the presence of plasma instabilities near this edge. The same effects can also be seen by keeping n constant and varying k (Fig. 4.1a). The effect of compactness (role of gravity) can be visualized by comparing the Figs. 4.1b and 4.1c. For the same values of k and n, Fig. 4.1b is plotted for an object with R = 12m and R_{in} = 15m whereas Fig. 4.1c corresponds to R = 6m and R_{in} = 9m. But as a result of this change, the smoothly decreasing pressure profile (Fig. 4.1b) started showing the turning point behaviour (Fig. 4.1c). This clearly illustrates the importance of gravity for compact objects.

4.4.2 Thick disk

Despite its enormous promises (central engine in active galactic nuclei, origin of jets, etc.), the theory of thick accretion discs is still in its infancy. In case of thin discs, the horizontal and vertical structures separate out and the model is described by ordinary differential equations. Consequently, one has an explicit analytic solution in the deep interior of the thin disc *i.e.* on the equatorial plane. On the contrary, the deep interior of a thick disc is an extended region. Its structure is described by rather complicated partial differential equations and in most of the cases, these equations are to be solved by sophisticated computer codes.

In order to comprehend the dynamics of thick discs analytically including the effects of magnetic fields we assume, as a first approximation, the magnetofluid to be incompressible ($\rho = \rho_0$). With this simplification, the continuity equation (4.2.23) can be expressed as $\nabla \cdot \mathbf{V} = 0$, which implies $\mathrm{V} = \nabla \times \mathbf{F}$, where $\mathbf{F}$ is any arbitrary vector function. The components of the velocity vector can be written as

$$V^r = \frac{1}{r \sin\theta} \frac{\partial}{\partial \theta} (F_\phi \sin\theta), \tag{4.4.9}$$

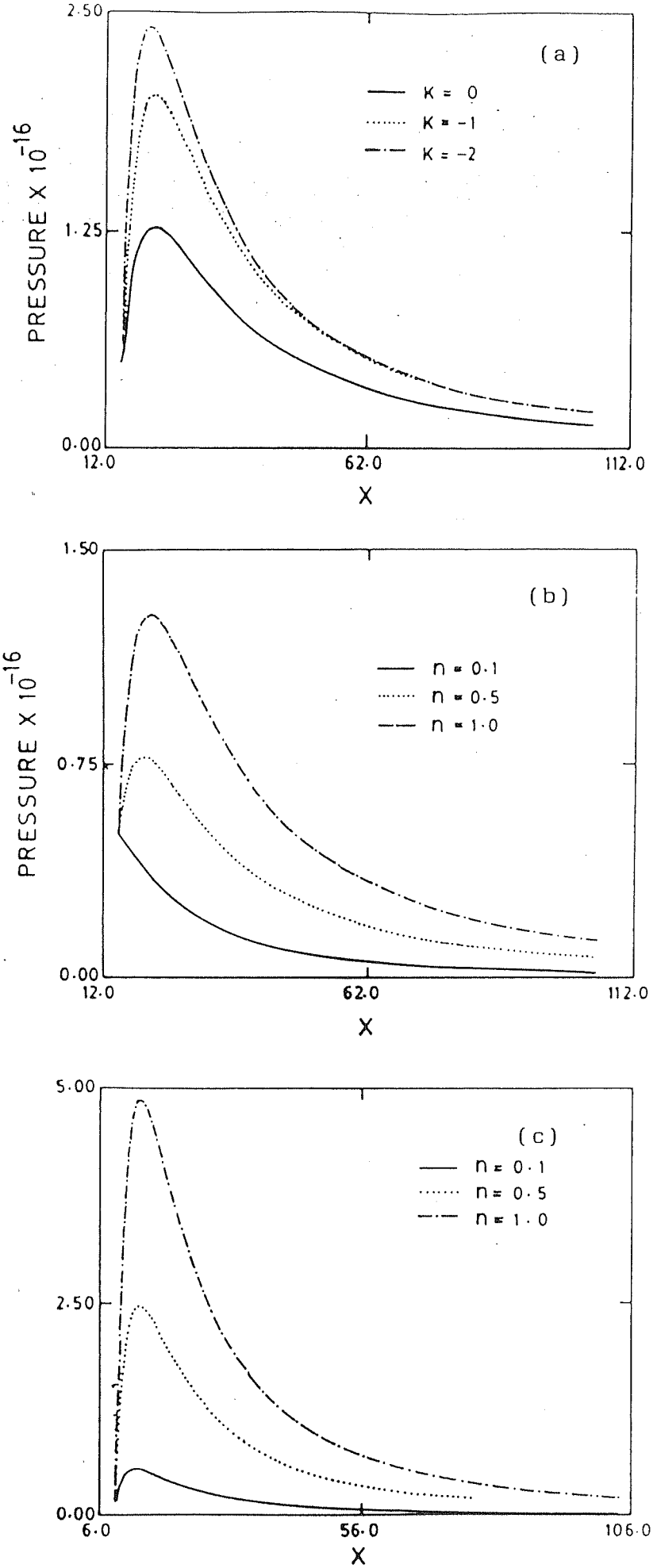

Figure 4.1. Pressure profile for the thin disc for a compact object with (a) R=12m and n = 1, (b) R=12m and k = 0 and (c) R=6m and k = 0.

$$V^{\theta} = -\frac{1}{r}\frac{\partial}{\partial r}(rF_{\phi}), \tag{4.4.10}$$

$$V^{\phi} = \frac{L}{r\sin\theta} = -\frac{1}{r}\frac{\partial}{\partial r}(rF_{\theta}) - \frac{1}{r}\frac{\partial}{\partial\theta}(F_r). \tag{4.4.11}$$

Using equations (4.4.9) and (4.4.10) in the consistency relation (4.3.8), the expression for F_{ϕ} is found to be

$$F_{\phi} = f(Ar\sin\theta) + \frac{(1-k)c^2}{4\pi\sigma}\cot\theta, \tag{4.4.12}$$

where f is any arbitrary function of r and θ and A is a constant. We use a power-law distribution for f such that

$$F_{\phi} = f(Ar\sin\theta)^s + \frac{(1-k)c^2}{4\pi\sigma}\cot\theta. \tag{4.4.13}$$

From the symmetry consideration, we know that V^{θ} must change sign across the equatorial plane. We use this fact as the boundary condition to evaluate the integration constant A and find that A = 0. This yields

$$V^{r} = -\frac{(1-k)c^2}{4\pi\sigma r}, \tag{4.4.14}$$

$$V^{\theta} = -\frac{(1-k)c^2}{4\pi\sigma r}\cot\theta. \tag{4.4.15}$$

In the limit of thin disc, V^{θ} vanishes and V^{r} goes over to (4.4.1) which ensures the consistency of our calculation. As in case of thin disc, the condition that $V^{r}/c \ll 1$ sets a lower limit on the value of the conductivity of the fluid as given by

$$\sigma \gg \frac{(1-k)c}{4\pi r}. \tag{4.4.16}$$

Finally, the integration of Bernoulli's equation (4.3.9), for an incompressible fluid ($\rho = \rho_0$) yields pressure to be

$$p = \rho_0\left(\mathcal{P}_0 + \frac{MG}{r} - \frac{V^2}{2}\right) - \frac{B^2}{8\pi}. \tag{4.4.17}$$

A similar calculation in the limit of zero angular momentum ($V^{\phi} = 0$) in two dimensions was carried out by Bisnovatyi-Kogan & Blinnikkov [101]. The analysis shows that during accretion the matter accumulates in the plane $\theta = \pi/2$ and subsequently forms a thin disc. However, our investigation of thick disc structure is more physical due to the inclusion of angular momentum.

4.5 Global properties of the thick disc

In this section, we focus our attention on the global properties *viz.* self-consistent magnetic field structure, pressure distribution, angular momentum transfer and energetics of the thick disc configuration.

4.5.1 Magnetic field structure

In the presence of the magnetofluid with finite resistivity, magnetic lines of force can penetrate the accretion disc (Ghosh & Lamb [47]) and hence the magnetic field lines should be continuous at the edge of the disc. Equating the disc field with the external field at the inner boundary, we obtain

$$B_1 = B_0 \left(\frac{R}{r}\right)^{2+k}, \tag{4.5.1}$$

where the external magnetic field is assumed to be a dipolar which for k $<$ -2 decreases with distance more rapidly than the disc field. The total magnetic field is given by the sum of the external and disc fields and the components are written in a non-dimensional form for k $=-2$ as

$$\frac{R^3 B_r}{\mu} = 2x^{-3}\cos\theta + x^{k-1}\sin^k\theta, \tag{4.5.2}$$

$$\frac{R^3 B_\theta}{\mu} = x^{-3}\sin\theta + x^{k-1}\sin^{k-1}\theta\cos\theta. \tag{4.5.3}$$

We plot the field lines with and without the disc field in Fig. 4.3. It is evident that inside the disc dipolar field lines are pushed in by the plasma accreted in the disc. Also, it is apparent that the field lines are connected with the distorted dipolar field lines at the surface of the disc and are continuous at the inner boundary as postulated earlier.

4.5.2 Pressure distribution

In order to obtain the constant of integration $\mathcal{P}_0$ (4.4.17), we use the definition of the inner boundary between the disc and the magnetosphere as outlined in the case of the thin disc. Thus, equating the pressure on either side of the the boundary, $\mathcal{P}_0$ is found to be

$$\mathcal{P}_0 = \frac{\left[(B_{total})^2\right]_{in}}{8\pi\rho_0} + \frac{V^2}{2} - \frac{c^2}{x_{in}} \tag{4.5.4}$$

where

$$(B_{total})^2 = (B_{star})^2 + (B_{disc})^2 .$$

As before,we choose $L^2 = nGMr_{in}$ and obtain the pressure profiles (Figs. 4.4 & 4.5) for different values of n and k (with k $<$ 1 which guarantees the flow). Figs. 4.4a& 4.4b show the effect of B_0 on the pressure distribution and on comparison, we find the existence of a critical value of the surface magnetic field for a prescribed value of k and n. Above this critical value, the pressure profile increases with distance. Furthermore, Table 1 demonstrates the presence of a lower bound on the value of B_0. Below this value, pressure becomes negative which indicates an unphysical situation. These observations point to the fact that a disc can exist in equilibrium configurations only for a certain range of B_0 values which, in turn, depend on other physical parameters like σ, ρ_{out} and $\dot{M}$. The thick disc pressure p

n	k	$\rho.10^4$ (gm cc^{-1})	$\sigma.10^8$ (s^{-1})	$B_0.10^{-8}$ (gauss)	Pressure p. 10^{-16} (dyne cm^{-2})	
					at x_{in}	at x_{out}
0.1	0	1	1	1.953	0.010	-0.47
				19.53	1.043	0.58
				976.562	2607.595	2652.63
0.1	-1	1	1	1.953	0.010	-0.47
				19.53	1.043	0.56
				976.562	26.595	2617.97

Table 4.1: Comparison of pressure values for a thick disc for different magnetic field strengths B_0 for n = 0.1 and k = 0 and -1.

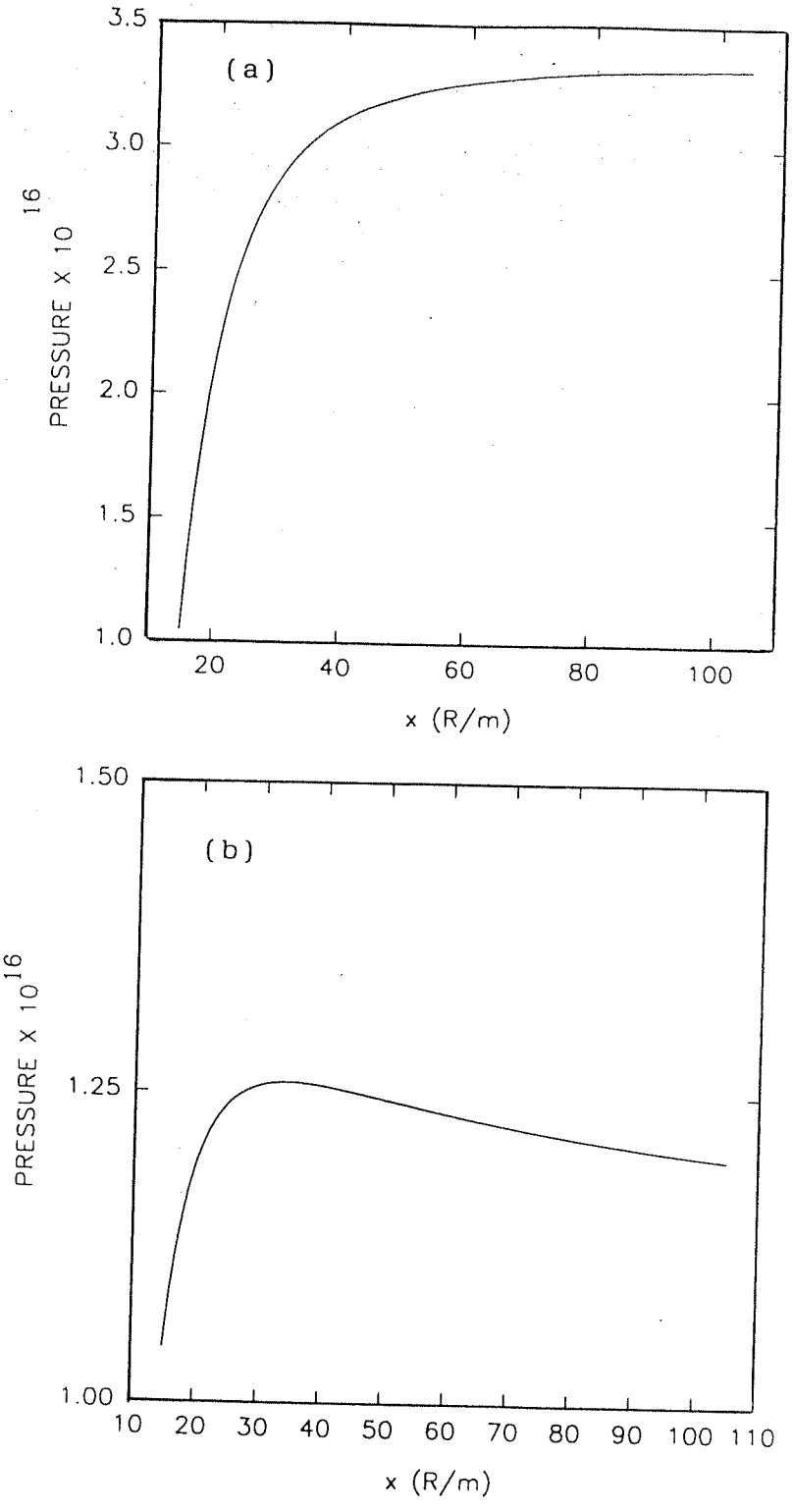

Figure 4.2. Pressure profile for a thick disc for a compact object with R=12m, n = 1.5, k = 0 and (a)$\sigma = 10^3$ (b) σ = 5 X 10^3.

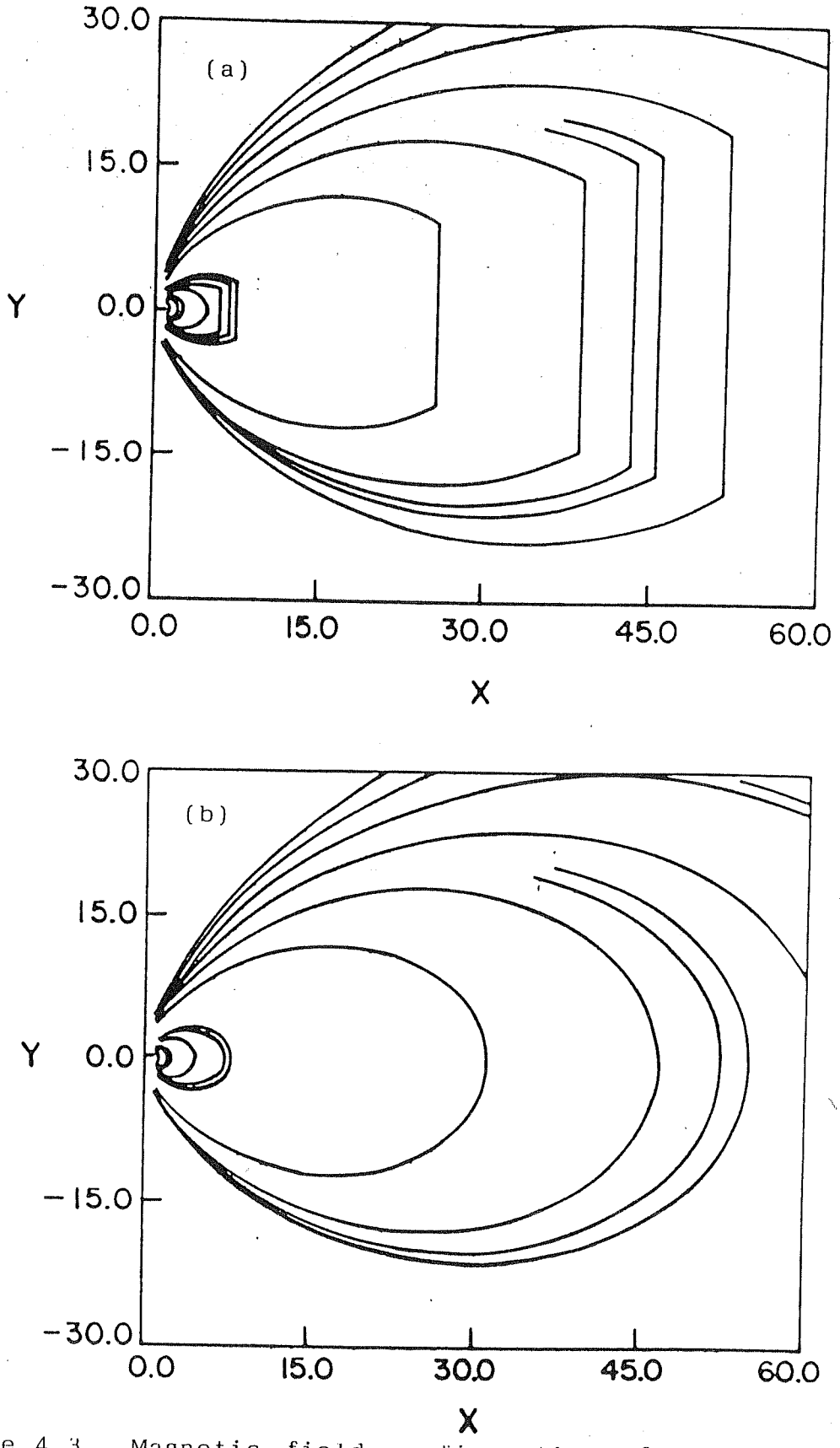

Figure 4.3. Magnetic field configuration of the central star having a dipole field for (a) with the disc field (k = -2), and (b) without the disc field.

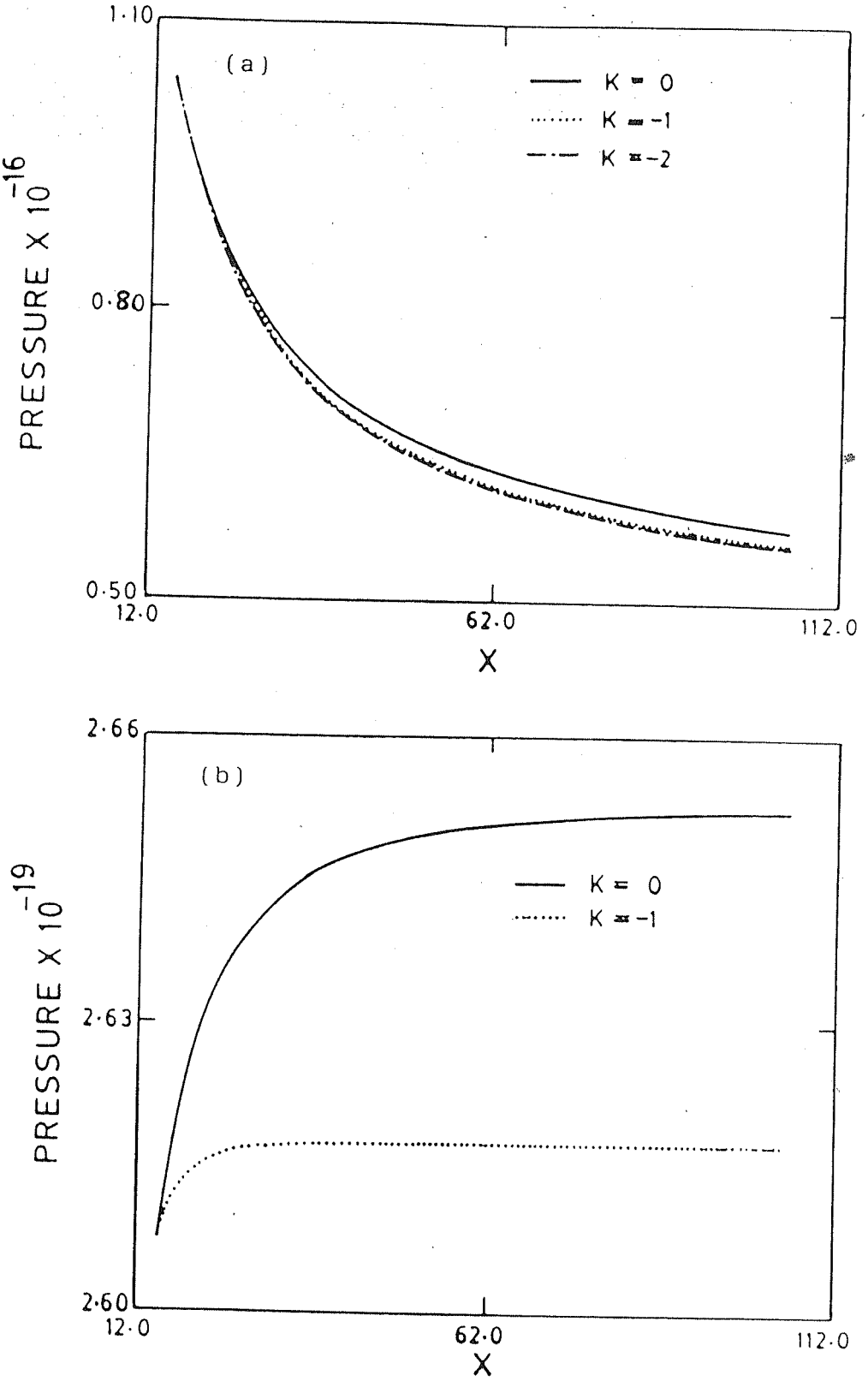

Figure 4.4. Pressure profile for a thick disc for a compact object with R=12m, n=0.1 and (a) $B_0=10^8$ gauss (b) $B_0 = 5 \times 10^8$ gauss.

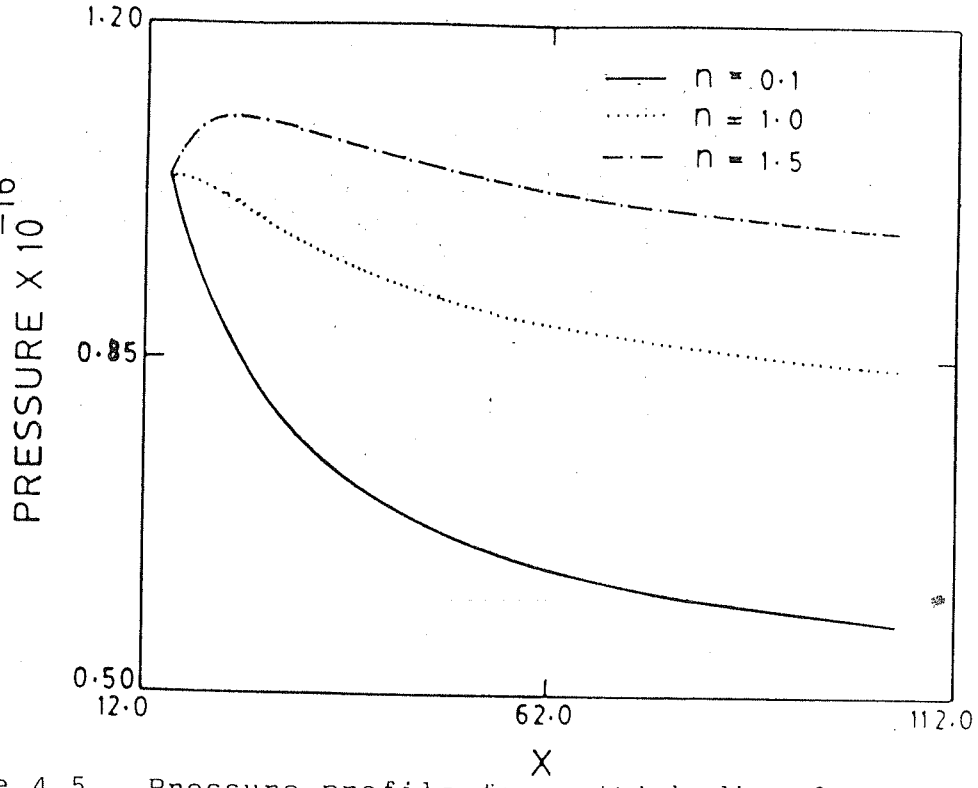

Figure 4.5. Pressure profile for a thick disc for $B_0 = 10^8$, k = 0 and for different values of n.

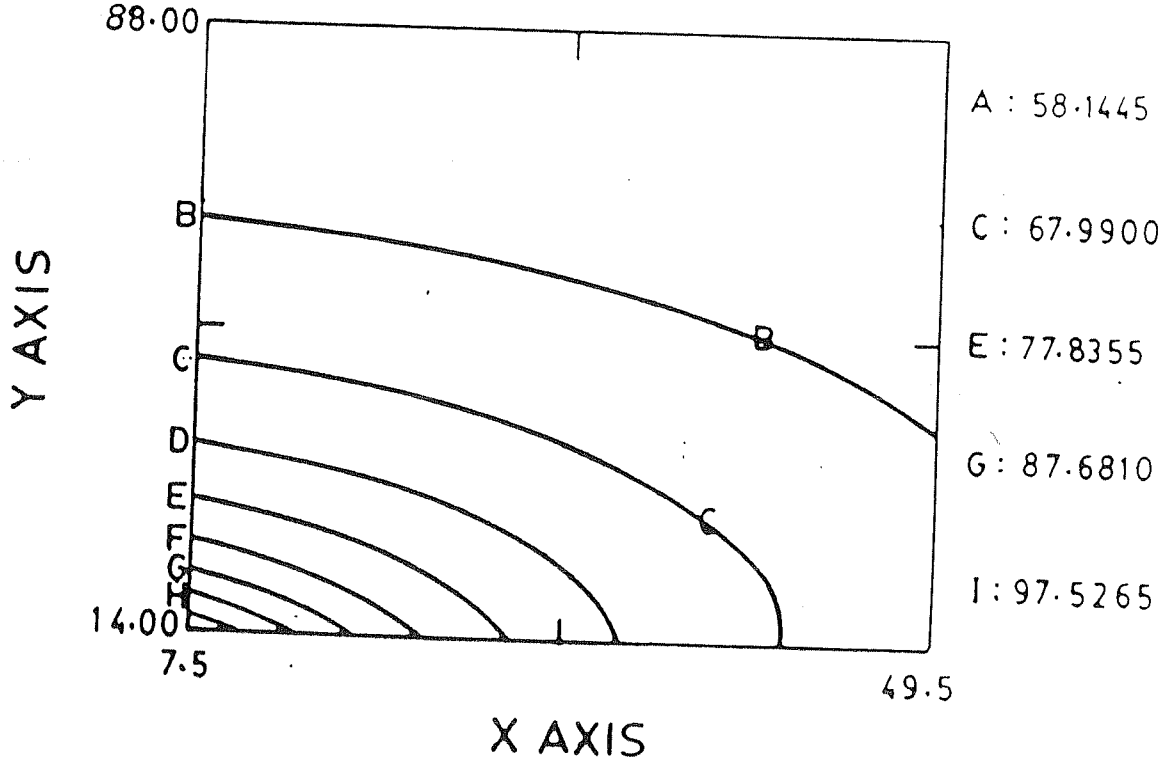

Figure 4.6. Pressure contours for a thick disc for k = 0 and n = 0.1.

for different n values is depicted in Fig. 4.5. Similar to the thin disc case, one can notice the turning point behaviour of the pressure distribution. However, the thick disc configuration can exist in stable states for higher angular momentum values. For example, for k = 0, in the case of thin disc (Fig. 4.1b), the pressure profile exhibits turning point behaviour for n = 0.5 whereas in the case of the thick disc (Fig. 4.5), this happens for n $\geq$ 1. Thus, for a given set of values of k, B_0, σ and ρ_{out} a thick disc with Keplerian velocity remains in equilibrium while a thin disc does not remain in steady configuration. A plot of pressure (Fig. 4.2) for different values of conductivity also illustrates that there exists a critical value of the conductivity below which the pressure profile shows unphysical behaviour. This threshold value agrees with the expression derived in equation (4.4.16).

4.5.3 Accretion rate and angular momentum

Once the physical quantities of the disc are known, we can calculate the accretion rate. Since, the accreting matter converges towards the central plane of the disc from both sides, the total mass accretion rate in the disc becomes a function of r (Kaburaki [56]). As the disc is in a steady state, we integrate the mass flux over the entire surface to obtain

$$\dot{M} = -2\pi \int_{\pi-\theta_{min}}^{\pi+\theta_{min}} \left(r^2 \rho V^r \sin\theta\right) d\theta = \frac{(1-k)\rho c^2 r}{\sigma} \sin\theta_{min}, \qquad (4.5.5)$$

which is indeed a function of r and θ_{min}, where θ_{min} is the polar angle beyond which no radial flow exists. The accretion rate at the inner boundary is

$$\dot{M}_{in} = \frac{(1-k)\rho c^2 r_{in}}{\sigma} \sin\theta_{min}. \qquad (4.5.6)$$

Henceforth, the accretion rate will be expressed in terms of $\dot{M}_{in}$.

We calculate the rate at which the angular momentum is transported by the matter inward past the point r = r_{in} within the disc. Through a vertical stripe encircling the origin with an arbitrary r, the angular momentum is carried by the fluid at a rate

$$M(r)V^{\phi}r = (\sqrt{2})^{-1}\dot{M}_{in}\sqrt{nGMr_{in}}. \tag{4.5.7}$$

Consequently, the amount of matter that enters into the disc through the outer edge leaves the inner edge exerting no net torque on the disc. The transfer rate due to the convergent flow of matter is

$$2\int_{r_{in}}^{r_{out}} \rho V^{\theta}(r,\theta_{min})\, V^{\phi}(r) 2\pi r^2 dr = 0. \tag{4.5.8}$$

Therefore, there is no momentum transfer through the vertical flow of the matter. As a result, there is no net torque acting on the disc and this guarantees the existence of a steady and stable thick accretion disc. However, one can not expect to balance the angular momentum inflow in the meridional direction as there are no magnetic stress across radial and meridional surfaces due to the non-existence of the toroidal component of the magnetic field ($B_{\phi} = 0$). This angular momentum imbalance would perhaps produce a non-zero torque and it may be possible that this torque is responsible for the absence of the pinching of the magnetic field structure within the disc.

4.5.4 Energetics

The energy radiated (F) from the unit surface is supplied by the gravitational contraction of the matter. The energy flux is computed from the definition

$$2\pi r 2F = \frac{GM}{r^2}\left[-2\pi r^2 \rho V^{r}(r,\pi/2)\right] \tag{4.5.9}$$

from which:

$$F_{in} = \frac{GM\dot{M}_{in}}{8\pi r_{in}^3} \tag{4.5.10}$$

and the total disc luminosity in the steady state is

$$L_{disc} = \frac{GM\dot{M}_{in}}{2r_{in}} = \frac{1}{2}L_{acc}. \tag{4.5.11}$$

The other half of the gravitational energy being carried away by the plasma across the inner edge has to be released very close to the compact object, where it is believed that the instability would play a major role. If the disc is not transparent to the radiation, then the heat produced is transported to its surface. Approximately, we have

$$\sigma_T T^4 = F_{in} \tag{4.5.12}$$

where σ_T is the Stefan-Boltzmann constant.

4.6 Conclusion

Considering the plasma to be resistive and including all the three fluid velocity components, we have derived, in the Newtonian limit, a self-consistent equilibrium solution for a plasma disc having only a poloidal magnetic field. The accreting plasma in the presence of a dipole magnetic field gives rise to a current in the azimuthal direction and a charge density J^t as determined from the Global Cartesian coordinate system. This current generates the disc field which is continuous across the disc boundary due to the presence of the finite resistivity of the plasma. The calculation of angular momentum reveals that there is no net flow of angular momentum and hence an axisymmetric thick disc configuration can exist in a steady state. Calculation of pressure profiles for different magnetic field strengths

show that there exist minimum as well as maximum bounds for the magnetic field strength of the compact object for which the disc equilibria are meaningful. However, the presence of large pressure gradients indicates the occurrence of plasma instabilities in the inner edge which we will pursue in the next chapter.

A similar calculation without the magnetic fields but including all the components of flow velocity around Schwarzschild black holes was carried out by Kuwahara [75]. Our results qualitatively agrees with his results, *viz.*

- The radial and the meridional velocities play a minor role in the structure of the disc but assume a dominant role in determining the accretion rate and angular momentum transfer.

- The radial velocity of the flow is subsonic at the inner boundary.

To summarize, one finds that self-consistent equilibrium solutions in the Newtonian framework do exist for a non-rotating compact object with a purely poloidal magnetic field accreting matter from a disc having all the three non zero components of the velocity vector.

Chapter 5

PLASMA INSTABILITY AT THE INNER EDGE OF THE ACCRETION DISC

5.1 Introduction

Recent developments in the study of accretion discs around compact objects has stressed the inclusion of self generated electromagnetic fields and pressure gradient forces in the dynamical equations governing the structure and stability of accretion discs (Prasanna [11]). Addition of electromagnetic forces brings the inner edge of the disc closer to the central object, thus enhancing the efficiency of the energy release. The presence of strong magnetic field defines the magnetosphere where the accretion flow is dominated by magnetic pressure. The radial distance where the magnetic pressure equals the fluid pressure of the accreting matter is defined as the magnetopause or the inner boundary. In Chap. 1 (page 14), we observed that the disc luminosity is just half of the accretion luminosity and the other half is to be released at the inner boundary or at the stellar surface. In either case, the boundary layer plays a dominant role in the accretion process. If the energy

is radiated at the boundary layer, then one has to understand the different plasma processes that convert the gravitational energy into X-rays. On the other hand, if the energy has to be released at the stellar surface, then the boundary layer plays an important role in pushing the matter inside. For a theoretical interpretation of X-rays from binary sources, attention has been focused on the various physical processes and MHD instabilities that could arise as a result of the interaction between the magnetic field of a NS and matter in a thin Keplerian disc. Recently, this interaction has attracted considerable attention with regard to the formation of binary radio pulsars, the origin of quasi- periodic oscillations from low mass X-Ray binaries (Taam *et al.* [102]) and observed time variation of the pulse periods of X-ray sources. This interaction which regulates the spin of the central object by transferring material and angular momentum from the disc could also be a possible mechanism for spinning the old pulsars to milli-second regime. Also, in the case of AGN's, Wiita [9] pointed out that instabilities in the accretion discs could lead to multiple ways of inducing variabilities, for example release of large amounts of magnetic energy on the surface of the disc (Shields [103]). In this context, it is necessary to understand the different modes of instabilities that could arise in discs supported by the gas and magnetic pressure around compact objects under radial and axisymmetric perturbations. The other important reason for extending the study to time dependent behaviour is to check whether the steady state models are stable against small perturbations. If not, it is possible that some assumptions made in the course of obtaining the equilibrium solutions are not compatible with the further assumption of steadiness of the disc. Further, the observable properties of a steady optically thick disc are largely independent of viscosity and does not provide much information about it. However, the size of the viscosity controls the

rate of plasma flow. Thus, it is believed that observations of time dependant disc behaviour may provide quantitative information about the disc viscosity. In the absence of a better model involving the physical processes, such a semi empirical approach to the problem seems to be most reasonable (Frank *et al.* [34]).

Most of the earlier studies on the disc instabilities were confined to the analysis of α-disc models which elucidated the existence of two kinds of instabilities *viz.* secular and thermal modes. In general, it has been found that these two instabilities would significantly affect almost any thin accretion disc models. It was also conjectured that the instability could explain the variation of the luminosity in AGN if the growth rate of the modes are limited by non-linear terms (Wiita [9]) and such studies are yet to be considered. However, the local stability analysis of Abramowicz *et al.* [104] showed that some of the unstable modes driven by viscosity could be stabilized only for barotropic or radially in-flowing fluids.

The interaction between a thin accretion Keplerian disc with the magnetosphere of a rotating neutron star has been investigated by several workers. The existence of the velocity jump between the disc material and the magnetosphere invariably indicates the presence of K-H instabilities. The linear K-H instability of non-magnetized shear layer is well known for flows with a subsonic velocity change (Chandrasekhar, [95]). Other important instabilities that can occur are the hydromagnetic, and Rayleigh-Taylor (RT) instabilities. Although these instabilities have been widely discussed in plasma physics, they have not been exhaustively studied in the context of astrophysical plasmas, in general and in magnetospheres around compact objects, in particular.

Many authors (Choudhury & Lovelace [105], Pietrini & Toricelli-Ciamponi

[106], and Corbelli & Torricelli-Ciamponi [107]) have analyzed K-H and hydromagnetic instabilities to model extragalactic radio jets using ideal MHD equations. A general study of K-H instability (KHI) in a compressible plasma has been carried out by Miura & Pritchett [108]. This analysis shows that the shorter wavelengths of K-H mode are stabilized by finite width of the shear layer. It was further observed that the compressibility increases the growth rate of pure ideal magnetic modes (Pietrini & Toricelli-Ciamponi [106]) whereas it lowers those of KHI (Miura & Pritchet [108]). KHI was invoked in context of field penetration into the magnetic disc by Ghosh & Lamb [47] and by Schralemann [44]. The important effect of KHI is to mix the turbulent magnetic field and plasma on spatial scales small enough to permit diffusion of plasma onto field lines. Thus, it is useful to consider KHI in order to understand the above time and spatial scales. In the context of disc accretion, Anzer & Börner [85,86] have explored some further aspects of the KHI. Restricting the analysis to a purely hydrodynamic treatment and assuming equal sound speeds on both side of the boundary layer, they [85] found that the instability can grow to large amplitudes only within a narrow ring around the co rotation radius. Subsequently, the analysis was extended to incorporate the magnetic field and to allow for different sound speeds in the disc and in the magnetosphere (Anzer & Börner [86]). However, this study was still restricted to a simplified planar geometry with constant density and constant magnetic field.

In order to elucidate the importance of inhomogeneous magnetic field and finite conductivity of the plasma on different instabilities, we attempt in this Chapter, a study of the linear stability analysis of plasma discs around compact objects whose equilibrium configuration under the influence of gravitational, electromagnetic and centrifugal forces was considered in Chap. 4. The importance of the

stability analysis lies in our equilibrium configuration which is more realistic as compared to other models to understand plasma processes in accretion discs. Our configuration involves smooth profiles for all equilibrium quantities whereas other models consider discontinuous profile either in the magnetic field or in the velocity flow. If one considers a plasma (disc) with finite resistivity, some analysis (not necessarily in astrophysical context) seems to indicate that the finite resistivity of the plasma leads to the existence of a new mode (Shivamoggi [109]).

The outline of this Chapter is as follows. In Section 5.2, we write down the perturbation equations explicitly. The relevant equations for performing a radial-azimuthal stability analysis in the domain of global approximation is presented in Section 5.3. The results of local radial perturbations in the frame work of an analytical description are presented in Section 5.4. Section 5.5 deals with an alternate method to carry out the stability analysis. This is used to perform the radial-azimuthal analysis in Section 5.6. Conclusions are drawn in Section 5.7.

5.2 Linearised equations

Here, we present the linearised Newtonian perturbation equations which are derived from the generalized relativistic equations (2.3.1-2.3.16) presented in Chap. 2.

The linearised Maxwell's equations are given by,

$$\begin{aligned}
\frac{1}{c}\frac{\partial E_1}{\partial t} &- \frac{1}{r}\frac{\partial B_3}{\partial \theta} - \frac{\cot\theta}{r}B_3 + \frac{1}{r\sin\theta}\frac{\partial B_2}{\partial \phi} \\
&+ 4\pi\sigma c^{-2}\left[cE_1 + B_3V^{\theta} - B_2V^{\phi} - B_{\theta}V_3\right] = 0, \qquad (5.2.1) \\
\frac{1}{c}\frac{\partial E_2}{\partial t} &+ \frac{1}{r}\frac{\partial B_3}{\partial r} + \frac{B_3}{r} - \frac{1}{r\sin\theta}\frac{\partial B_1}{\partial \phi}
\end{aligned}$$

$$+ \quad 4\pi\sigma c^{-2}\left[cE_2 + B_1V^\phi - B_3V^r + B_rV_3\right] = 0, \tag{5.2.2}$$

$$\frac{1}{c}\frac{\partial E_3}{\partial t} + \frac{1}{r}\frac{\partial B_1}{\partial \theta} - \frac{B_2}{r} - \frac{\partial B_2}{\partial r}$$
$$+ \quad 4\pi\sigma c^{-2}\left[cE_3 - B_1V^\theta + B_2V^r + B_\theta V_1 - B_rV_2\right] = 0, \tag{5.2.3}$$

$$\frac{1}{c}\frac{\partial B_1}{\partial t} + \frac{1}{r}\left(\frac{\partial E_3}{\partial \theta} + \cot\theta E_3\right) - \frac{1}{r\sin\theta}\frac{\partial E_2}{\partial \phi} = 0, \tag{5.2.4}$$

$$\frac{1}{c}\frac{\partial B_2}{\partial t} - \frac{E_3}{r} - \frac{\partial E_3}{\partial r} + \frac{1}{r\sin\theta}\frac{\partial E_1}{\partial \phi} = 0, \tag{5.2.5}$$

$$\frac{1}{c}\frac{\partial B_3}{\partial t} + \frac{E_2}{r} + \frac{\partial E_2}{\partial r} - \frac{1}{r}\frac{\partial E_1}{\partial \theta} = 0. \tag{5.2.6}$$

The linearised momentum equations are given by

$$\frac{\partial V_1}{\partial t} + V^r\frac{\partial V_1}{\partial r} + V_1\frac{\partial V^r}{\partial r} + \frac{V^\theta}{r}\frac{\partial V_1}{\partial \theta} + \frac{V_2}{r}\frac{\partial V^r}{\partial \theta} + \frac{V^\phi}{r\sin\theta}\frac{\partial V_3}{\partial \phi} + \frac{V_3}{r\sin\theta}\frac{\partial V^\phi}{\partial \phi}$$
$$- \frac{2}{r}\left(V^\theta V_2 + V^\phi V_3\right) + \frac{1}{\rho_0}\frac{\partial p_1}{\partial r} - \frac{\rho_1}{\rho_0^2}\frac{\partial P}{\partial r}$$
$$+ \frac{1}{c\rho_0}\left[B_\phi J_2 + B_3J^\theta - B_\theta J_3 - B_2J^\phi + E_rJ_4 + E_1J^t\right]$$
$$- \frac{\rho_1}{c\rho_0^2}\left[E_rJ^t + B_\phi J^\theta - B_\theta J^\phi\right] = 0, \tag{5.2.7}$$

$$\frac{\partial V_2}{\partial t} + V^r\frac{\partial V_2}{\partial r} + V_1\frac{\partial V^\theta}{\partial r} + \frac{V^\theta}{r}\frac{\partial V_2}{\partial \theta} + \frac{V_2}{r}\frac{\partial V^\theta}{\partial \theta} + \frac{V^\phi}{r\sin\theta}\frac{\partial V_2}{\partial \phi} + \frac{V_3}{r\sin\theta}\frac{\partial V^\theta}{\partial \phi}$$
$$+ \frac{1}{r}\left(V^rV_2 + V^\theta V_1 - 2\cot\theta V^\phi V_3\right) + \frac{1}{r\rho_0}\frac{\partial P_1}{\partial \theta} - \frac{\rho_1}{r\rho_0^2}\frac{\partial P_0}{\partial \theta}$$
$$+ \frac{1}{c\rho_0}\left[B_rJ_3 + B_1J^\phi - B_\phi J_1 - B_3J^r + E_\theta J_4 + E_2J^t\right]$$
$$- \frac{\rho_1}{c\rho_0^2}\left[E_\theta J^t + B_rJ^\phi - B_\phi J^r\right] = 0, \tag{5.2.8}$$

$$\frac{\partial V_3}{\partial t} + V^r\frac{\partial V_3}{\partial r} + V_1\frac{\partial V^\phi}{\partial r} + \frac{V^\theta}{r}\frac{\partial V_3}{\partial \theta} + \frac{V_2}{r}\frac{\partial V^\phi}{\partial \theta} + \frac{V^\phi}{r\sin\theta}\frac{\partial V_3}{\partial \phi} + \frac{V_3}{r\sin\theta}\frac{\partial V^\phi}{\partial \phi}$$

$$+ \quad \frac{1}{r}\left[\left(V^r V_3 + V^\phi V_1\right)\right] + \cot\theta\left(V^\theta V_3 + V^\phi V_2\right) + \frac{1}{r\sin\theta\rho_0}\left(\frac{\partial P_1}{\partial\phi} - \frac{\rho_1}{r\rho_0}\frac{\partial P_0}{\partial\phi}\right)$$

$$+ \quad \frac{1}{c\rho_0}\left[B_\theta J_1 + B_2 J^r - B_r J_2 - B_1 J^\theta + E_\phi J_4 + E_3 J^t\right]$$

$$- \quad \frac{\rho_1}{c\rho_0^2}\left[E_\phi J^t + B_\theta J^r - B_r J^\theta\right] = 0. \tag{5.2.9}$$

The linearised perturbed continuity equation is given by

$$\frac{\partial\rho_1}{\partial t} + \rho_0\left[\frac{\partial V_1}{\partial r} + \frac{1}{r}\frac{\partial V_2}{\partial\theta} + \frac{1}{r\sin\theta}\frac{\partial V_3}{\partial\phi} + \frac{2V_1}{r} + \cot\theta\frac{V_2}{r}\right]$$

$$+ \quad \rho_1\left(\frac{\partial V^r}{\partial r} + \frac{1}{r}\frac{\partial V^\theta}{\partial\theta} + \frac{1}{r\sin\theta}\frac{\partial V^\phi}{\partial\phi} + \frac{2V^r}{r} + \cot\theta\frac{V^\theta}{r}\right)$$

$$+ \quad V^r\frac{\partial\rho_1}{\partial r} + \frac{V^\theta}{r}\frac{\partial\rho_1}{\partial\theta} + \frac{V^\phi}{r\sin\theta}\frac{\partial\rho_1}{\partial\phi}$$

$$+ \quad V_1\frac{\partial\rho_0}{\partial r} + \frac{V_2}{r}\frac{\partial\rho_0}{\partial\theta} + \frac{V_3}{r\sin\theta}\frac{\partial\rho_0}{\partial\phi} = 0. \tag{5.2.10}$$

The four components of the linearised Ohm's law are given by

$$J_1 = -\frac{\sigma}{c}\left[cE_1 + B_\phi V_2 + B_3 V^\theta - B_2 V^\phi - B_\theta V_3\right] \tag{5.2.11}$$

$$J_2 = -\frac{\sigma}{c}\left[cE_2 + B_r V_3 + B_1 V^\phi - B_\phi V_1 - B_3 V^r\right] \tag{5.2.12}$$

$$J_3 = -\frac{\sigma}{c}\left[cE_3 + B_\theta V_1 + B_2 V^r - B_1 V^\theta - B_r V_2\right] \tag{5.2.13}$$

$$J_4 = -\frac{\sigma}{c}[E.V], \tag{5.2.14}$$

where

$$E.V = E_1 V^r + E_r V_1 + E_2 V^\theta + E_\theta V_2 + E_\phi V_3 + E_3 V^\phi. \tag{5.2.15}$$

Physical quantities with numeral subscripts denote perturbed variables. As for the energy equation, we use the adiabatic law

$$\frac{d}{dt}\left[P\rho^{-\gamma}\right] = 0, \tag{5.2.16}$$

i.e we consider the plasma to be an ideal fluid with no heat exchange with its surroundings. Note that, the equilibrium solutions were derived for an incompressible plasma and this equation is necessary only to perform the stability analysis (see Corbelli & Ciamponi [107]).

5.3 A general formulation for stability analysis

In this section, we carry out the detailed stability analysis of the equilibrium configuration given in Chap. 4 where the existence of instability near the inner edge of the accretion disc was conjectured. The complete set of linearised perturbation equations are given in the previous section.

Following the standard normal mode analysis, the general time dependant perturbations are written in the following form

$$\Psi_1(r,\phi,t) = \psi(r)\ exp\ [i(\nu t + m\phi)] \tag{5.3.1}$$

where m is the azimuthal mode number signifying the number of azimuthal crests around a circumference of radius r, ν is the frequency which may be complex and $\psi(r)$ is the amplitude of the perturbation which is also complex. Further, for the sake of simplicity and for an analytical understanding of the nature of the instabilities, we assume the flow to be along the azimuthal direction only ($V^\phi \neq 0$; $V^r, V^\theta = 0$). This could be justified from the analysis of Chap. 4, where it was concluded that the azimuthal component of the fluid flow dominates the motion of the plasma at the inner edge while the other two velocity components play a minor role in the structure of the disc. Upon substituting the radial-azimuthal perturbations into the disc equations (5.2.1 - 5.2.10, 5.2.16), the linearised perturbation equations in

dimensionless form are written as

$$(i\omega+\hat{\sigma})\,\hat{E}_1+\frac{im}{\alpha}\hat{B}_2-\hat{\sigma}\hat{V}_3-\hat{\sigma}\hat{V}^{\phi}\hat{B}_2=0, \tag{5.3.2}$$

$$(i\omega+\hat{\sigma})\,\hat{E}_2+\frac{d\hat{B}_3}{d\alpha}+\frac{\hat{B}_3}{\alpha}+\left(\hat{\sigma}\hat{V}^{\phi}-\frac{im}{\alpha}\right)\hat{B}_1=0, \tag{5.3.3}$$

$$(i\omega+\hat{\sigma})\,\hat{E}_3-\frac{d\hat{B}_2}{d\alpha}-\frac{\hat{B}_2}{\alpha}+\hat{\sigma}\hat{V}_1=0, \tag{5.3.4}$$

$$i\omega\hat{B}_1-\frac{im}{\alpha}\hat{E}_2=0, \tag{5.3.5}$$

$$i\omega\hat{B}_2-\frac{im}{\alpha}\hat{E}_1-\frac{\hat{E}_3}{\alpha}-\frac{d\hat{E}_3}{d\alpha}=0, \tag{5.3.6}$$

$$i\omega\hat{B}_3+\frac{\hat{E}_2}{\alpha}+\frac{d\hat{E}_2}{d\alpha}=0, \tag{5.3.7}$$

$$i\omega\hat{V}_1+\frac{im\hat{V}^{\phi}}{\alpha}V_3+\hat{\sigma}\hat{V}_A^2\hat{V}_1-\frac{2\hat{V}^{\phi}}{\alpha}\hat{V}_3+\hat{\sigma}\hat{V}_A^2\hat{E}_3$$
$$+\left(\frac{(\gamma-1)}{\rho_0 c^2}\frac{dP_0}{d\alpha}\right)\rho_1+C_s^2\frac{d\rho_1}{d\alpha}=0, \tag{5.3.8}$$

$$\left(i\omega+\frac{im}{\alpha}\hat{V}^{\phi}\right)\hat{V}_2=0, \tag{5.3.9}$$

$$i\omega\hat{V}_3+\left(\frac{im\hat{V}^{\phi}}{\alpha}+\hat{\sigma}\hat{V}_A^2\right)\hat{V}_3-\hat{\sigma}\hat{V}_A^2\left(\hat{E}_1-\hat{B}_2\hat{V}^{\phi}\right)+C_s^2\frac{im}{\alpha}\rho_1=0, \tag{5.3.10}$$

$$\left(i\omega+\frac{im\hat{V}^{\phi}}{\alpha}\right)\rho_1+\left(\frac{2}{\alpha}+\frac{d}{d\alpha}\right)\hat{V}_1+\frac{im}{\alpha}\hat{V}_3=0. \tag{5.3.11}$$

where the hat over the quantities represent the dimensionless variables with $\hat{E}$ $= E\ /B_\theta$, and $\hat{B}\ =\ \mathrm{B}/B_\theta$. In addition, we have defined the other normalized quantities as below.

$$\hat{V}^{\phi}=V^{\phi}/c,\quad \alpha=r/R$$

$$\hat{\sigma}=4\pi\sigma R/c,\quad \omega=\nu R/c$$

$$\hat{V}_a^2 = \frac{B_\theta^2}{4\pi\rho_0 c^2}, \quad C_s^2 = \frac{\gamma P}{\rho_0 c^2}. \tag{5.3.12}$$

In subsequent analysis the hat over the quantities will be dropped.

5.4 One dimensional perturbation analysis

5.4.1 Local analysis

In order to give a basis for a physical understanding of the nature of the instabilities, we perform here, a local analysis. The approach of local analysis is a well established procedure in plasma physics which assumes the wavelength (λ) of the perturbation to be small compared to the scale size of the inhomogeneity in the system. For example, if one assumes the scale size to be the pressure scale length ($L_p = \frac{1}{p_0}\frac{dP}{dr}$), then the condition can be written as $kL_p \gg 1$, where k is the wave number and, if satisfied, implies that the space variation of the amplitude of the perturbation over its scale length can be neglected. In addition, a local analysis allows one to Fourier transform the perturbed variables even in the direction of inhomogeneity (Rognlien & Weinstock [110]). Thus, the differential equations are transformed into the algebraic equations whose solutions are not very difficult to find.

5.4.2 Analytical results

We first consider a special case of one dimensional perturbation in the radial direction (m = 0). Under, the local approximation, we Fourier transform all the perturbed quantities in the radial direction. With this simplification, a look at the set of equations with m = 0, (5.3.2-5.3.11) discloses that the perturbed meridional velocity (*i.e.* V_2) enters into the dynamics only through equation (5.3.9) and it

is not required for the description of mode characteristics. Also equation (5.3.5) leads to $\omega B_1 = 0$. For consistency V_2 and B_1 are assumed to be zero for non-zero eigenvalue ω. It is now straight forward to eliminate the perturbed magnetic fields from equations (5.3.6-5.3.7) and finally, a somewhat lengthy calculation produces the simple result

$$Q_1 E_2 = 0, \tag{5.4.1}$$

$$Q_2 E_1 - Q_3 E_3 = 0, \tag{5.4.2}$$

$$Q_5 E_3 - Q_4 E_1 = 0, \tag{5.4.3}$$

where the complex coefficients Q_1 to Q_5 are defined in the Appendix B. Setting the determinant of the above set of equations to zero, for a non-trivial solution, we obtain the dispersion relation (DR) in the form,

$$Q_1 (Q_2 Q_5 - Q_3 Q_4) = 0. \tag{5.4.4}$$

It is apparent that there exists two distinct dispersion relations corresponding to $Q_1 = 0$ and $(Q_2 Q_5 - Q_3 Q_4) = 0$ and both are algebraic relations. The roots to the above DR are in general complex. The real component of ω gives an oscillatory nature to the wave while the negative imaginary component characterizes the instability and determines the growth rate of the unstable modes.

Case 1: Resistive electromagnetic mode

The dispersion relation $Q_1 = 0$ can be explicitly written as,

$$\omega^2 - i\omega\sigma - (k^2 - \alpha^{-2} - 2ik\alpha^{-1}) = 0. \tag{5.4.5}$$

Separating ω into real and imaginary components, the solution is found to be,

$$\omega_r = \frac{2k}{\alpha\sigma}, \tag{5.4.6}$$

$$\omega_i = 0.5\sigma \left[1 \pm \left\{1 + \frac{4}{\sigma^2}\left(k^2 + \frac{4k^2}{\alpha^2\sigma^2} - \frac{1}{\alpha^2}\right)\right\}^{\frac{1}{2}}\right]. \qquad (5.4.7)$$

It is evident that the root with the negative sign gives the growth rate of the instability. Since, the second term inside the curly bracket is less than 1, it can be expanded binomially which for $k\alpha \gg 1$ gives the growth rate as

$$\omega_i = -\frac{k^2}{\sigma}. \qquad (5.4.8)$$

In dimensional form the real component of ω,

$$\nu_r = kc\left(\frac{2c}{4\pi r\sigma}\right), \qquad (5.4.9)$$

suggests that this mode which is propagating in the radially inward direction is electromagnetic in nature but its form is different from that of an electromagnetic wave in vacuum due to the presence of the finite conductivity. We conjecture that this mode is a consequence of the finite conductivity of the fluid as mentioned by Shivamoggi [109] and would not arise if one assumes the perturbed electric field in the meridional direction to be zero. It may be argued that the relative motion between the magnetofluid and the magnetic field causes this instability since finite conductivity prevents the magnetic field to follow the plasma flow or vice-versa. The variation of growth rate versus the wave number and the dispersion curve are depicted in Fig. 5.1.

Case 2. $(Q_2Q_5 - Q_3Q_4) = 0.$

The dispersion relation corresponding to $(Q_2Q_5 - Q_3Q_4) = 0$ in a compact form is written as,

$$A_1\omega^5 + iA_2\omega^4 + (A_3 + iA_4)\omega^3 + (A_5 + iA_6)\omega^2 + (A_7 + iA_8)\omega + (A_9 + iA_{10}) = 0, \quad (5.4.10)$$

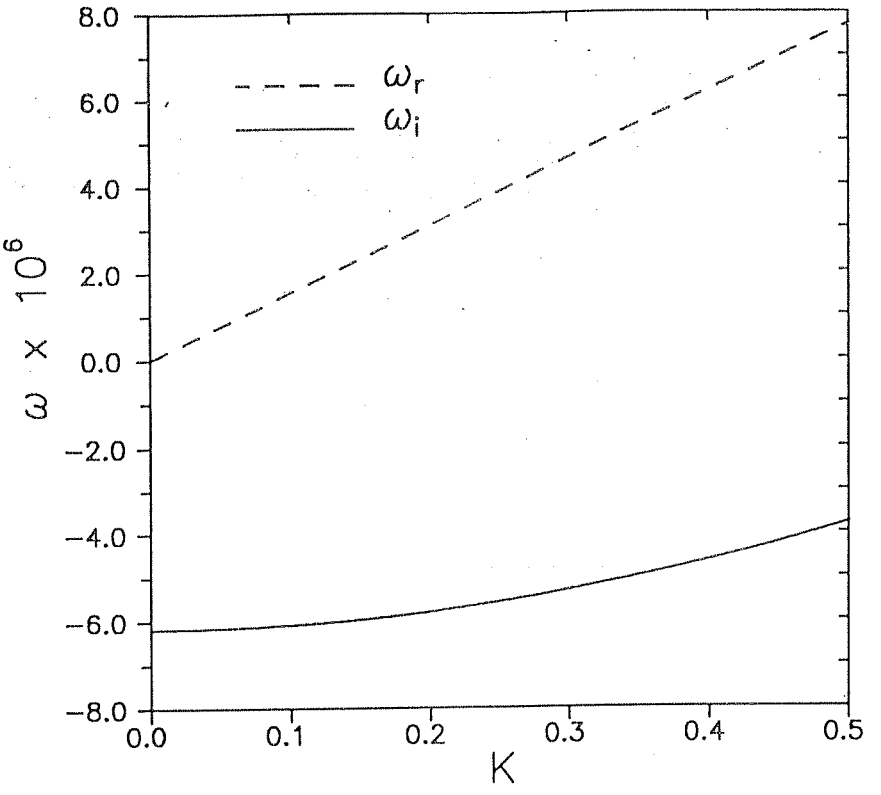

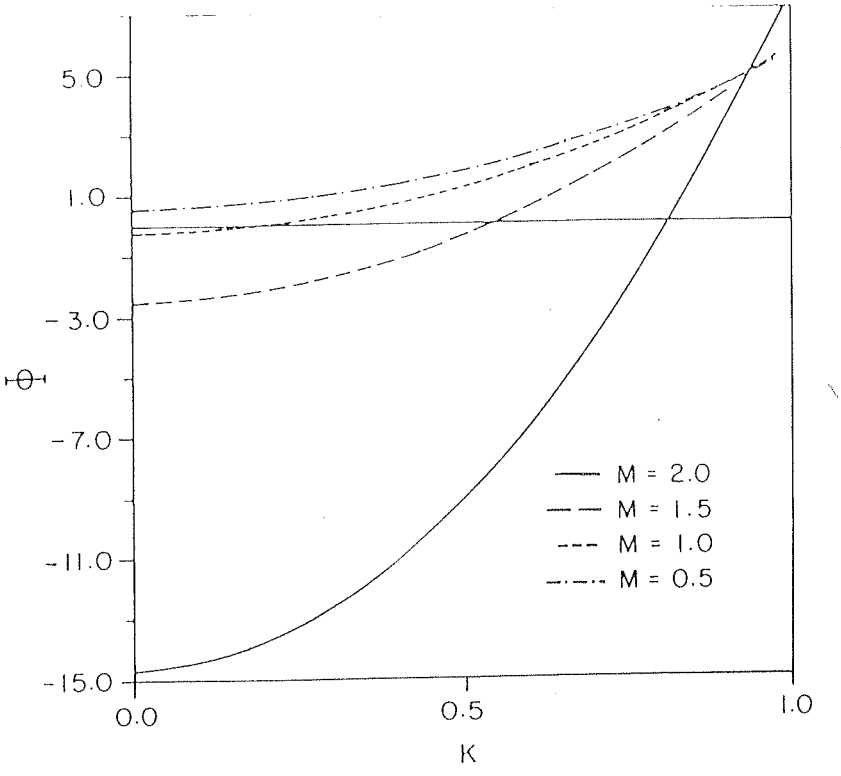

Figure 5.1: The normalized growth rate (ω_i) and normalized dispersion curve (ω_r) for the electromagnetic mode ($Q_1 = 0$).

Figure 5.2: Variation of ϕ as a function of k for different values of magnetic Mach number M (M = V_A/C_s).

where the coefficients A_1, A_2, ...*etc* are defined in Appendix B. We first solve the dispersion relation, analytically, under two different approximations and subsequently solve the complete DR numerically.

5.4.2.1 Kelvin-Helmholtz mode

Let's assume that $\omega \ll 1$ and $\omega\sigma \leq 1$. Under this approximation, the higher powers of ω may be neglected and the dispersion relation (5.4.10) reduces to,

$$(A_7 + iA_8)\omega + (A_9 + iA_{10}) = 0. \tag{5.4.11}$$

Writing $\omega = \omega_r + i\omega_i$, the solution of (5.4.11) in compact notation is written as

$$\omega_r = -\frac{A_7A_9 + A_8A_{10}}{A_7^2 + A_8^2}, \tag{5.4.12}$$

$$\omega_i = -\frac{A_7A_{10} - A_8A_9}{A_7^2 + A_8^2}. \tag{5.4.13}$$

Explicitly ω_i can be written as,

$$\omega_i = -\frac{2}{\alpha\sigma V_a^2(1+4K^2\alpha^2)}\left[DP\left\{1 + 3K^2\alpha^2 + k^4\alpha^4 + \frac{V^{\phi^2}}{(1+V_a^2)}\left(2 + K^2\alpha^2 - k^4\alpha^4\right)\right\} - \frac{\alpha k^2 C_s^2}{2M^2}\Phi\right], \tag{5.4.14}$$

where

$$M = \frac{V_a}{C_s} \tag{5.4.15}$$

$$DP = \frac{(\gamma-1)}{\rho_0 c^2}\frac{dP}{d\alpha} \tag{5.4.16}$$

$$\Phi = \frac{6(1+k^2\alpha^2)}{1+V_a^2}V^{\phi^2}M^2 + k^4\alpha^4(M^2+1) + 2K^2\alpha^2(M^2+1.5) + M^2 - 4, \tag{5.4.17}$$

where M signifies the magnetic Mach number. As negative ω_i is the signature of the instability, this would occur when the pressure gradient term (1st term in equation 5.4.14) is positive. The stabilizing role of the acoustic term (2nd term in (5.4.14)) depends on the value of M, where the critical value is given by, $M_c < \sqrt{2}$. Thus, for $M^2 > 2$, this term destabilizes the system in the absence of the pressure gradient. Our analysis of the equilibrium configuration in Chap. 4 shows M = 0.5 and this implies that the accoustic term stabilizes the disc structure. A plot of Φ as a function of k for different values of M is depicted in Fig. 5.2 which demonstrates that for higher values of M (M > M_c), longer wavelengths are destabilized while the shorter wavelengths are stabilized.

The variation of growth rate versus k with n as a parameter, where n is the angular momentum parameter (*cf.* Chap. 4) is depicted in Fig. 5.3a. It is observed that the system is unstable for n > 0.1, which is in good agreement with the equilibrium pressure profile (Fig. 4.5). Since, in the absence of velocity shear ($dV_0/dr = 0$), the instability vanishes, we conclude that this mode is driven by the velocity shear and is of Kelvin-Helmholtz in nature. It is to be emphasized that in our analysis the velocity shear arises due to the differential rotation of the disc and not due to the velocity discontinuity between the disc and the magnetosphere as discussed by many authors (Scharlemann [44], Anzer & Börner [86] and references there in). In addition, there could be a jump in the azimuthal velocity at the inner edge. In fact, from the turning point behaviour of the pressure profiles near the inner edge, we had already postulated the existence of instability (see, page 81). This mode which is propagating in the radially inward direction reveals that the growth rate is large for higher values of n and one can also notice that the validity of the local approximation is limited to very small range of k values near the cutoff

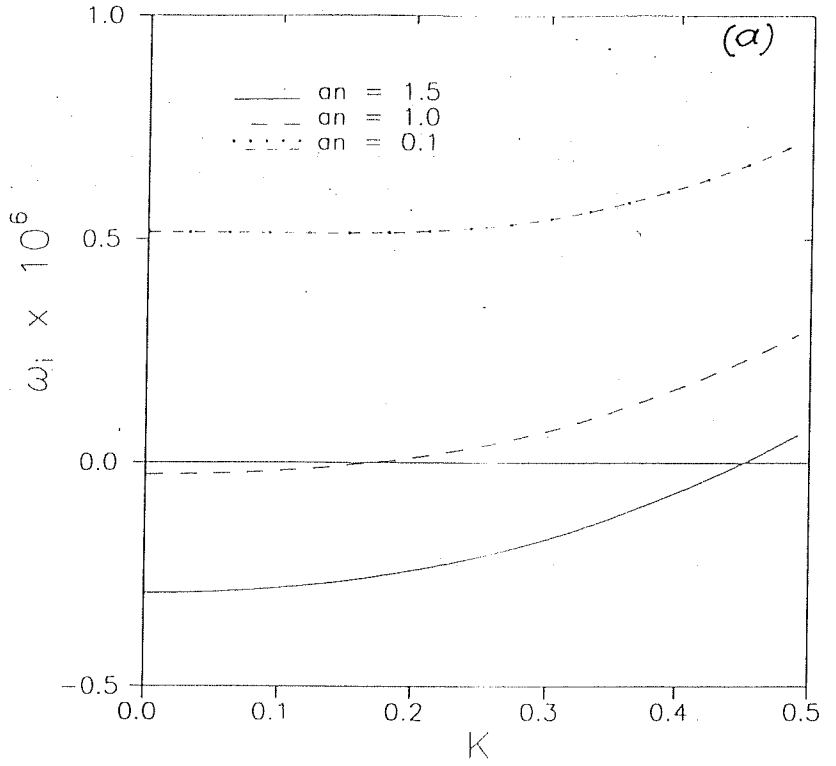

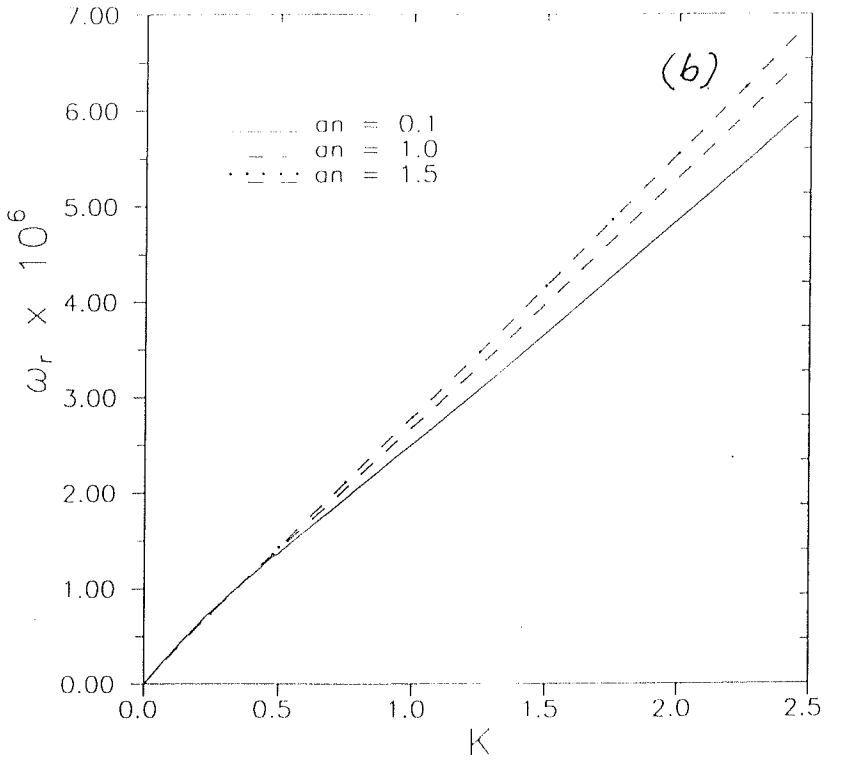

Figure 5.3: (a) The normalized growth rates and (b) normalized dispersion curve for K-H instability for different values of n, where n is the angular momentum (L) parameter ($L^2 = \mathrm{nGM}/r_{in}$).

(Fig. 5.3a). The dispersion curves for different n values are plotted in Fig. 5.3b.

Considering conductivity as a parameter, the instability growth rate as a function of the wave number is plotted in Fig. 5.4. It is seen that the growth rate is directly proportional to the resistivity *i.e.* the higher value of conductivity lowers the growth rate of K-H. However, some earlier studies of KHI (Shivamoggi [109], Chhajlani & Vyas [111]) have reported that the growth rate varies as 1/3 rd power of the resistivity. The discrepancy may be attributed to the variation in equilibrium configurations and geometry that one has considered.

As mentioned earlier, the above study was carried out for a case where the equilibrium density was assumed to be constant. However, the preliminary perturbation analysis with the effect of density gradient reveals that the inhomogeneity in density destabilises K-H instability. The instability which is excited even in the absence of velocity shear, is identified as Rayleigh-Taylor like instability. This nomenclature is due to the fact that this mode is propagating along the direction of density gradient whereas the usual R-T mode propagates transverse to the density gradient.

5.4.2.2 Magnetosonic mode

Under the approximation, $1 \leq \omega \leq \sigma$ and $\omega\sigma \geq 1$, the dispersion relation (5.4.10) simplifies to,

$$\omega^2 = -\frac{(A_7 + iA_8)}{A_3}. \tag{5.4.18}$$

As done earlier, separating ω into real and imaginary parts, we obtain

$$\omega_i = \pm\frac{1}{2}\left(\frac{A_7}{A_3}\right)^{\frac{1}{2}}\left[1 \pm \left\{1 + \left(\frac{A_8}{A_7}\right)^2\right\}^{\frac{1}{2}}\right]^{\frac{1}{2}} \tag{5.4.19}$$

$$\omega_r = -\frac{A_8}{2A_3\omega_i}. \tag{5.4.20}$$

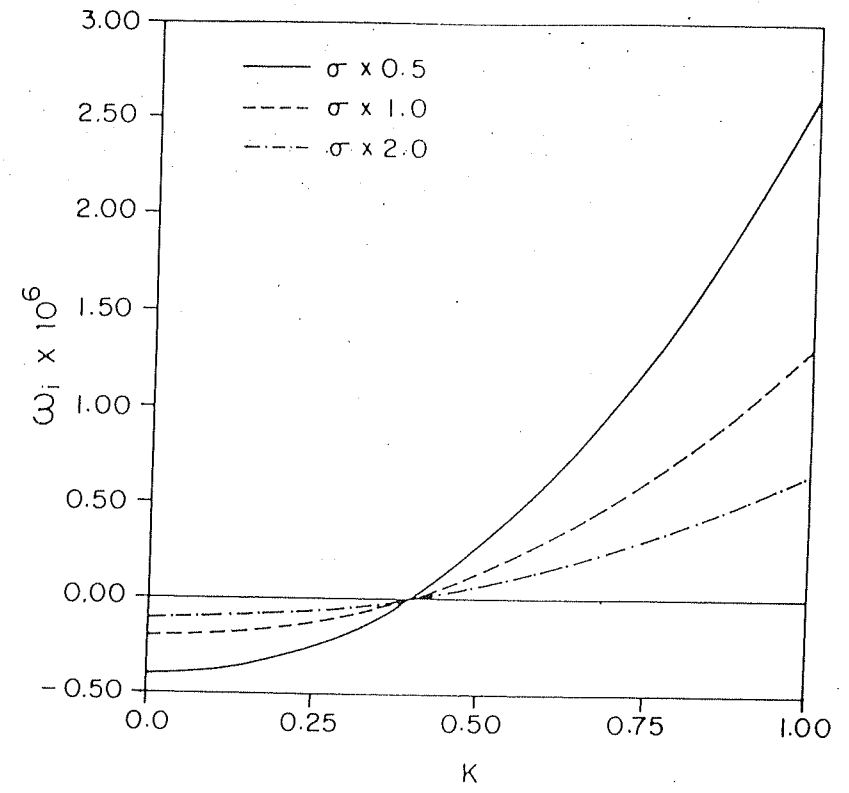

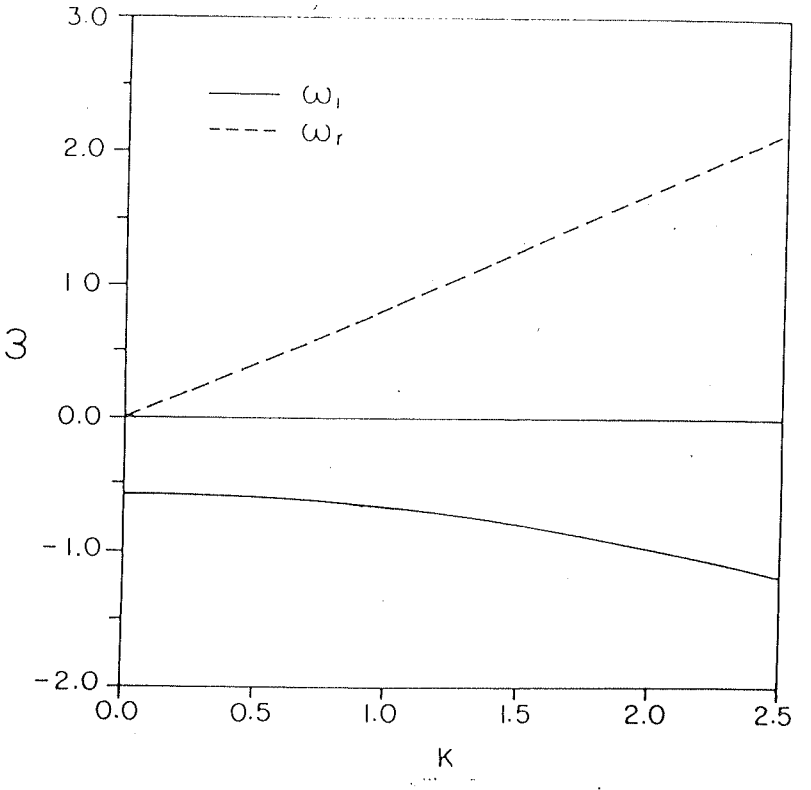

Figure 5.4: The normalized instability growth rate for K-H instability for different conductivity (σ) values, where $\sigma = 10^8\ s^{-1}$.

Figure 5.5: The normalized growth rate (ω_i) and normalized dispersion curve (ω_r) for the magnetosonic mode.

It is clear that the value of ω_i with the negative sign in the front describes the unstable mode. The form of ω_r identifies the instability to be magnetosonic in nature. We also find that this instability is independent of conductivity and is propagating in the radially inward direction. The growth rate and the dispersion curve are plotted in Fig. 5.5.

5.4.3 Numerical results

The complete fifth order dispersion relation (5.4.10) is solved numerically using complex routine ZROOTS from the Numerical Recipes (Press *et al.* [112]). Out of the five possible roots only two are associated with instabilities (corresponding to negative ω_i values). These are graphically presented in Fig. 5.6. The analytical and numerical growth rates for K-H and magnetosonic modes are presented in Fig. 5.7. It can be observed that the results agree fairly well with each other.

5.4.4 Discussion

The present analysis deals with the one-dimensional instability studies at the inner edge of an accretion disc around a compact object taking into account the effect of finite conductivity, inhomogeneous magnetic field and velocity shear. Considering only the radial perturbation of the resistive MHD equations, the calculations show that there exist three different modes namely Kelvin-Helmholtz, magnetosonic and resistive electromagnetic, which, under appropriate conditions, become unstable as described in the text. The KHI exists only for velocities slightly lower than the Keplerian value. In the absence of the pressure gradient forces arising due to the velocity shear (dV_0/dr), KHI gets stabilized whereas the other two instabilities still exist. The analytical expressions of the growth rate for K-H and electromagnetic

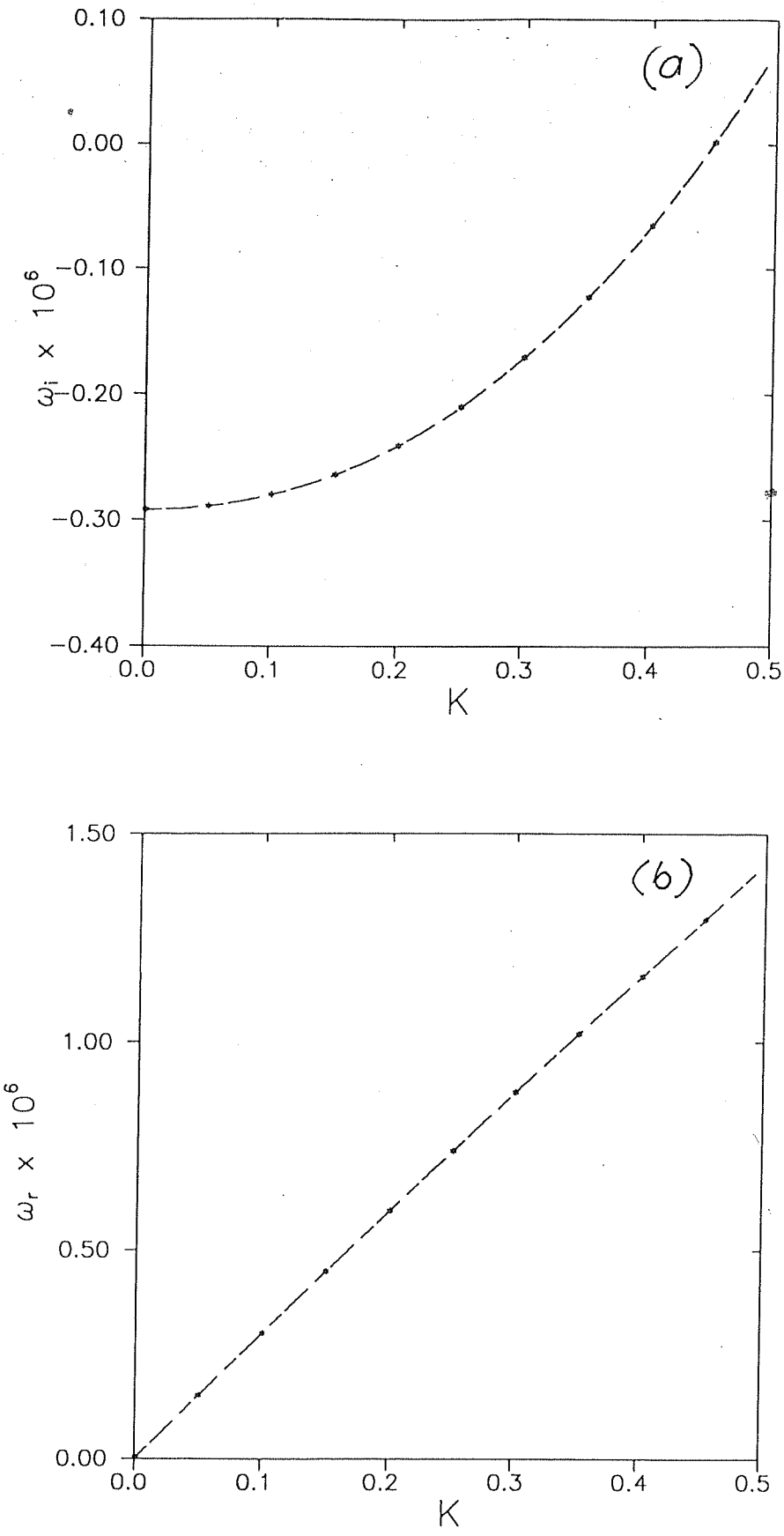

Figure 5.6: (a) The normalized growth rate (ω_i) and (b) normalized dispersion curve (ω_r) for the K-H instability obtained numerically by the method of finding complex roots.

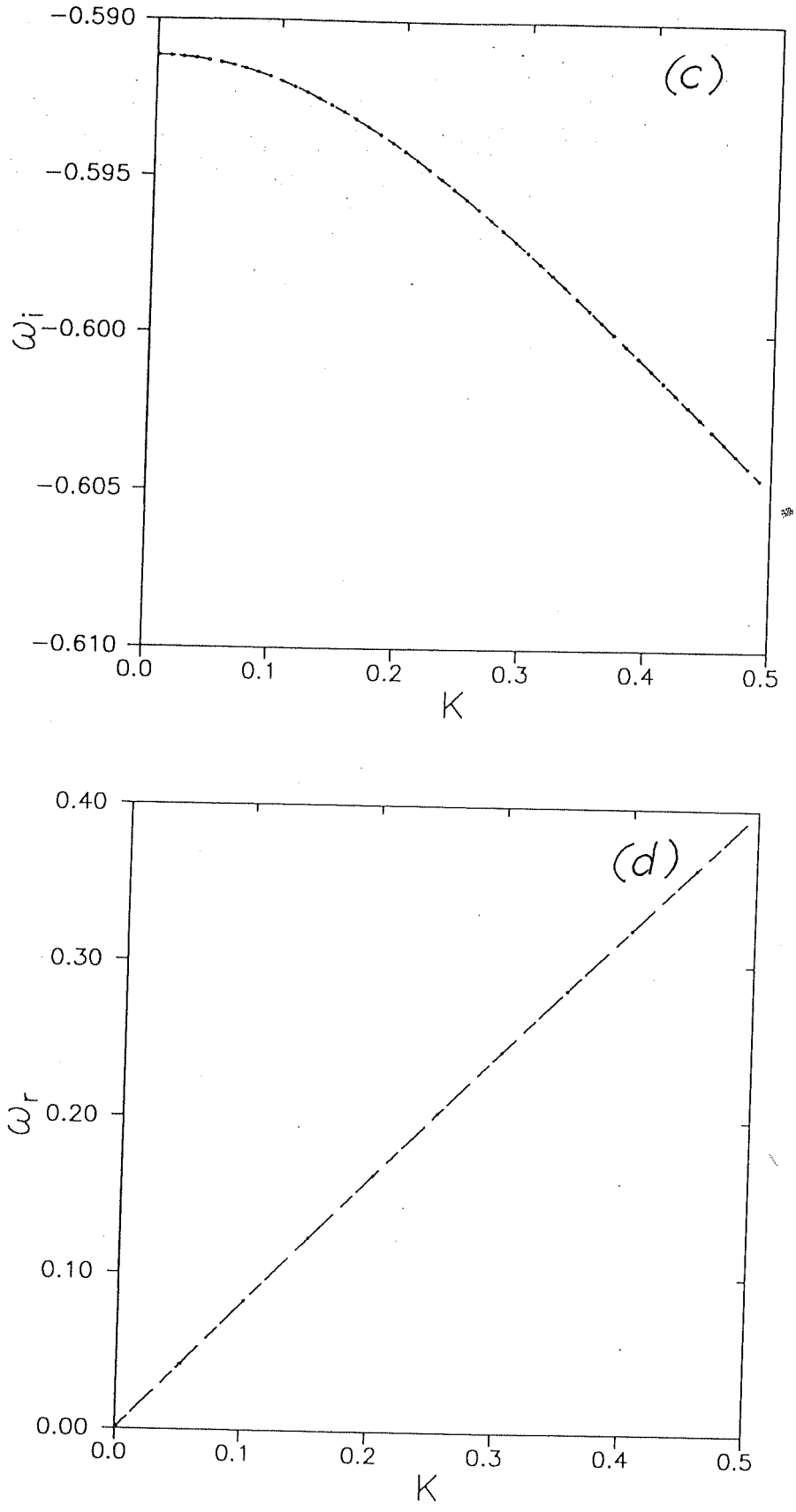

Figure 5.6: (c) The normalized growth rate (ω_i) and (d) normalized dispersion curve (ω_r) for the magnetosonic mode obtained numerically by the method of finding complex roots.

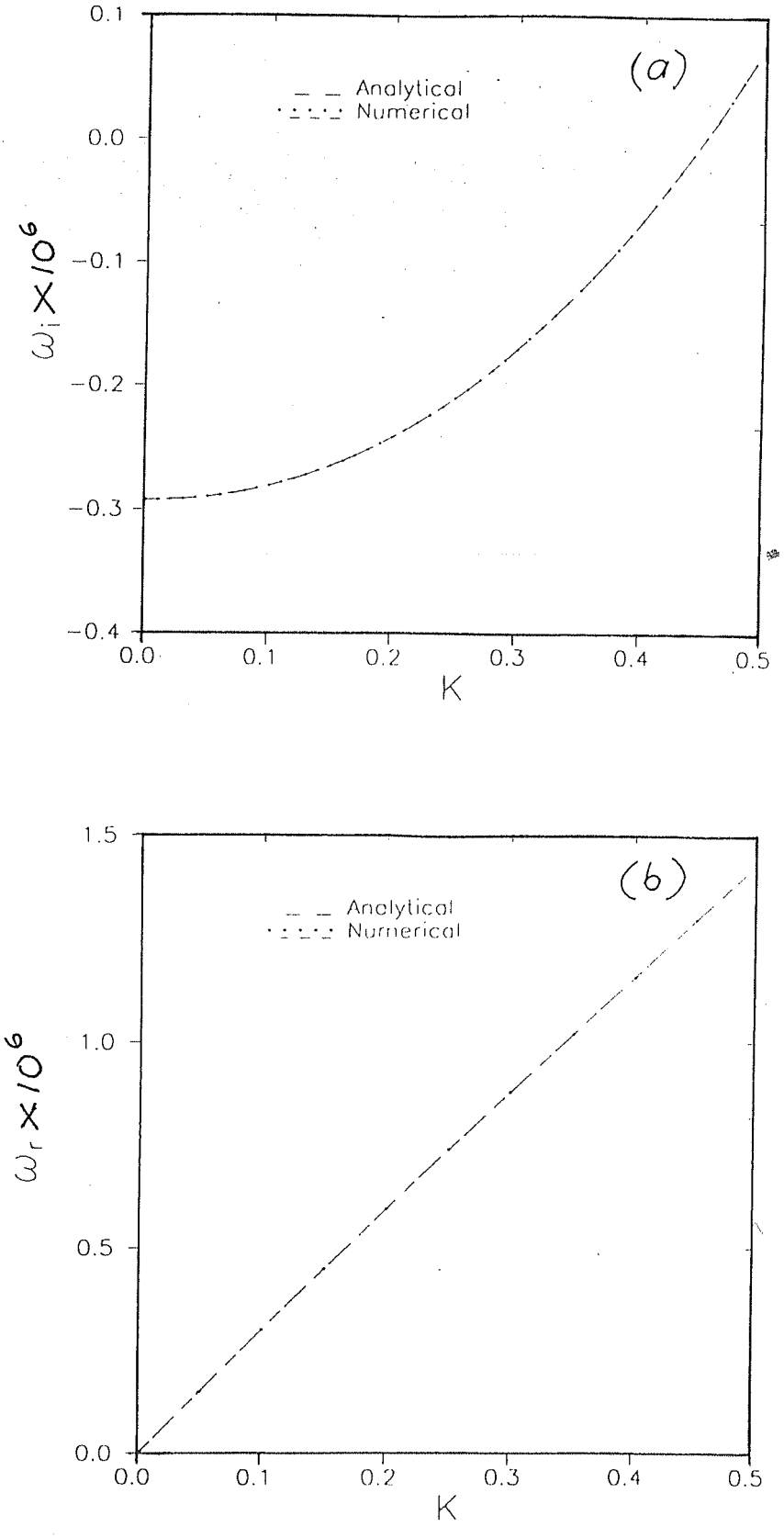

Figure 5.7: Comparison of normalised growth rate of K-H mode by two different methods (a) analytical (b) numerical.

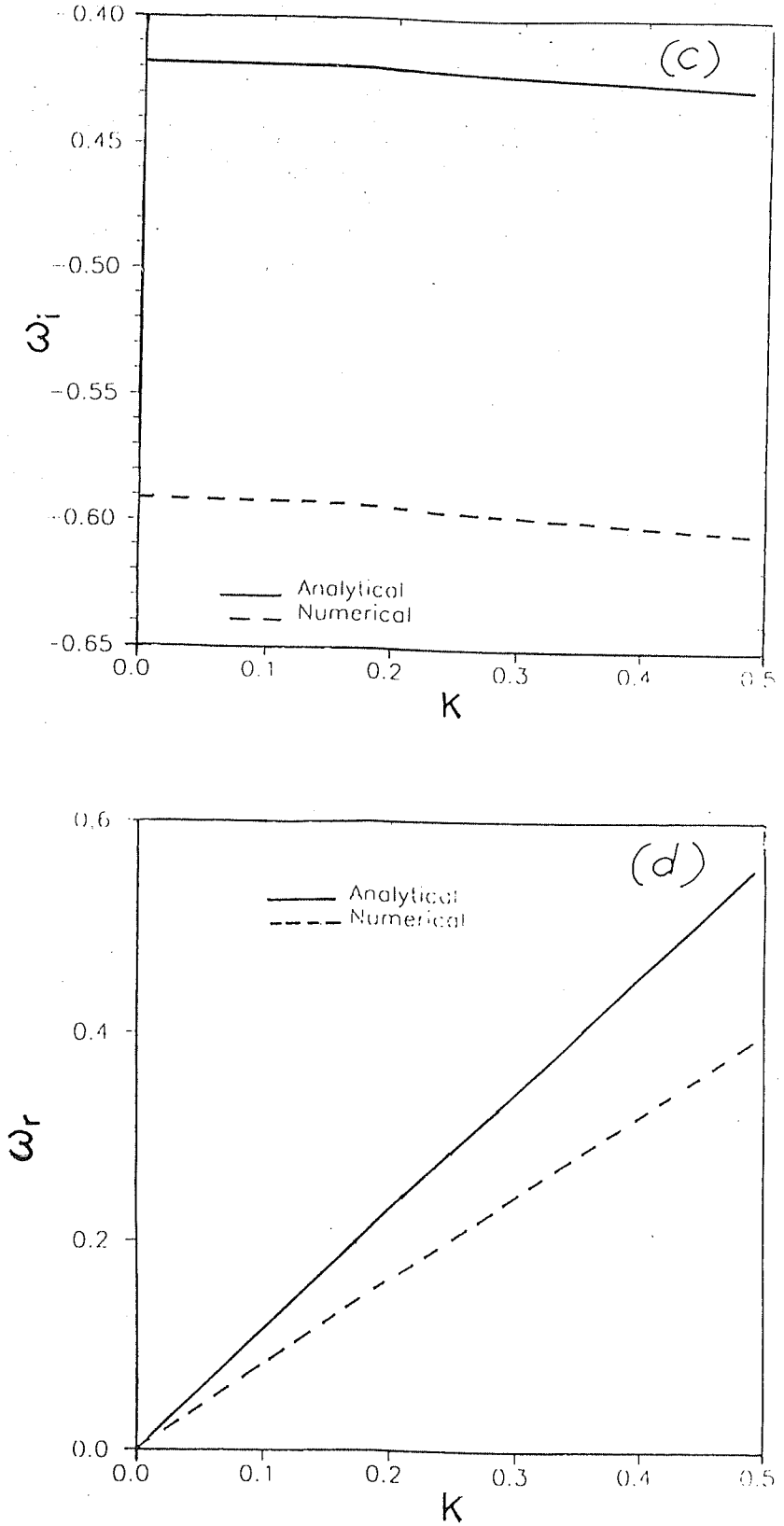

Figure 5.7: (c) Comparison of normalised growth rate and (d) dispersion curve of magnetosonic mode by two different methods.

instability reveal that the growth rates are inversely proportional to the conductivity. It is also to be noted that the compressibility lowers the growth rate of these two modes, which is in agreement with the known results (Miura & Pritchett [108]). However, the magnetosonic instability is unaffected by the finite conductivity of the medium. Also, the preliminary investigation of the effect of density gradient on KHI shows that the density inhomogeneity destabilises KHI and excites R-T like modes at the inner edge of the disc.

5.5 Eigenvalue techniques

It is evident from the above calculations that the process of deriving and solving an exact dispersion relation is a cumbersome exercise and involves tedious algebra. We, now solve the same set of equations taking a different but simple approach and subsequently use this technique to study two-dimensional perturbations. The method as outlined by Simonutti [113] consists of converting the system of linearised equations into the form of an algebraic matrix eigenvalue problem

$$(A_r + iA_i)\,X = \omega(B_r + iB_i)X, \tag{5.5.1}$$

where A and B are square matrices of finite dimension n and its elements are defined in terms of the independent variables of the problem. X is a column vector of dimension n and is a scalar and each of these quantities may be complex. It is well known that the eigenvalue will represent the dependant variable of the dispersion relation and the elements of the eigenvector will represent the selected dynamic variables of the system. With the eigen system formulation, it is possible to directly determine the solutions of the dispersion relation by calculating the eigenvalue and the eigenvectors. The eigenvectors contain information concerning the nature of the

dynamic variables *i.e.* polarizations *etc.* for each mode of oscillations. This elegant method is very much simpler compared to the earlier method described in Sect. 5.4.

5.5.1 Comparison of results

We have applied this method to the foregoing calculations of the radial stability analysis by considering the time dependence of the perturbations as

$$\Psi_1(r,t) \;=\; \psi \; exp(\nu t \;+\; ikr) \qquad (5.5.2)$$

This change in time dependence is made with the objective of keeping the matrix B as purely real which makes the numerical computation easier. For computing the eigenvalues and eigenvectors of the complex eigenvalue problem (equation 5.5.1), we use the well known EISPAK routines (Smith *et al.*[96]. The results agree quite well with our earlier calculations (Figs. 5.8, 5.9 and 5.10a,b). In addition, we also obtained the eigenvector for different modes and are presented in Figs.5.10c & 5.11. The mode structures as a function of k gives the distribution of energy over the possible wavelengths. The eigenmode structures for KHI (Fig. 5.10c) reveal that the energy is mainly distributed over the longer wavelengths and this matches with the earlier calculations. This is also true in the case of the magnetosonic mode (Fig. 5.11). From these analyses, we conclude that the eigenmode structures of various instabilities over k-space match consistently with their corresponding growth rate curves.

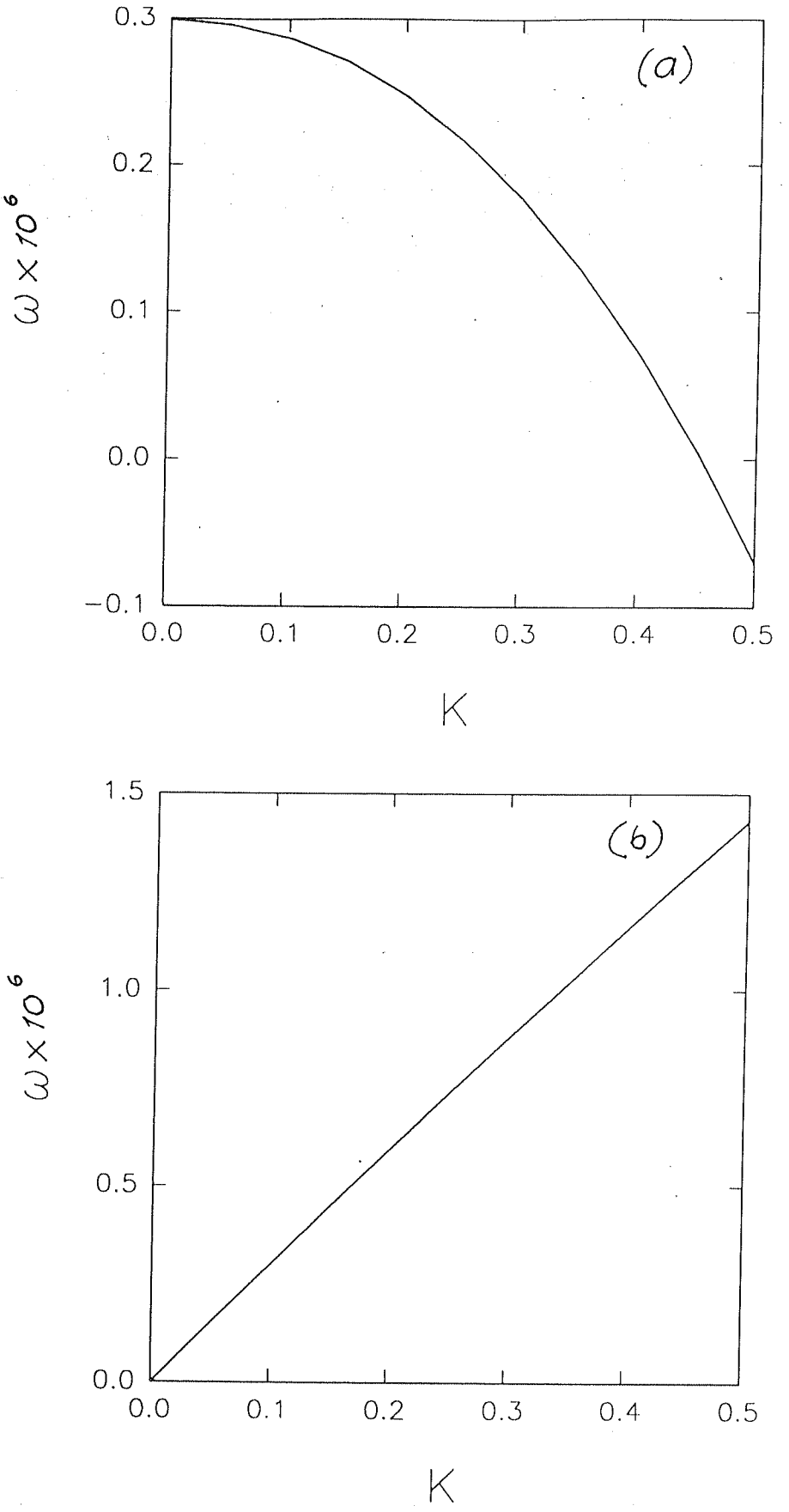

Figure 5.8: (a) The normalised growth rate and (b) dispersion curve of K-H mode by the method of eigenvalue techniques.

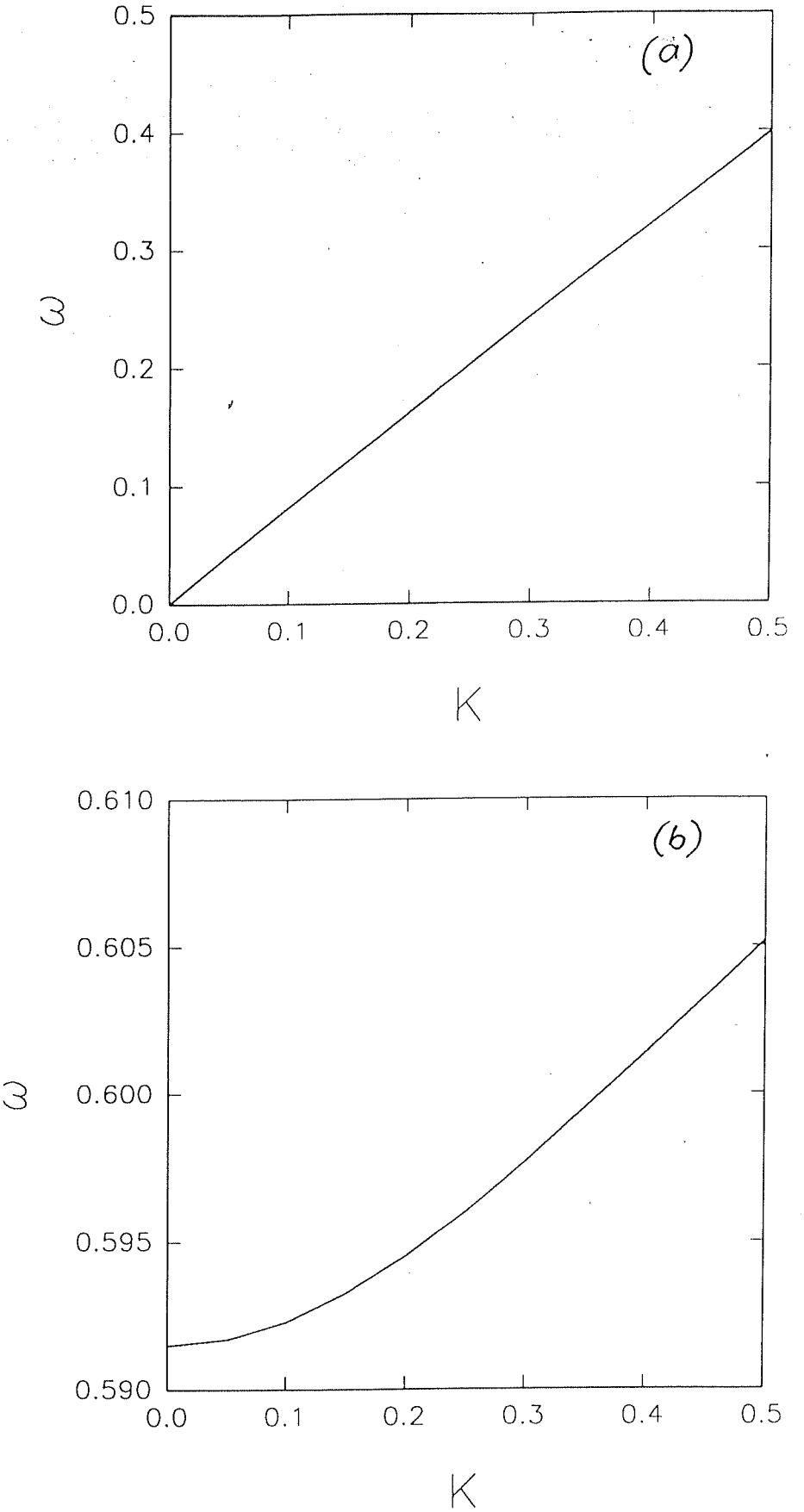

Figure 5.9: (a)The normalised growth rate and (b) dispersion curve of magnetosonic mode by the method of eigenvalue techniques.

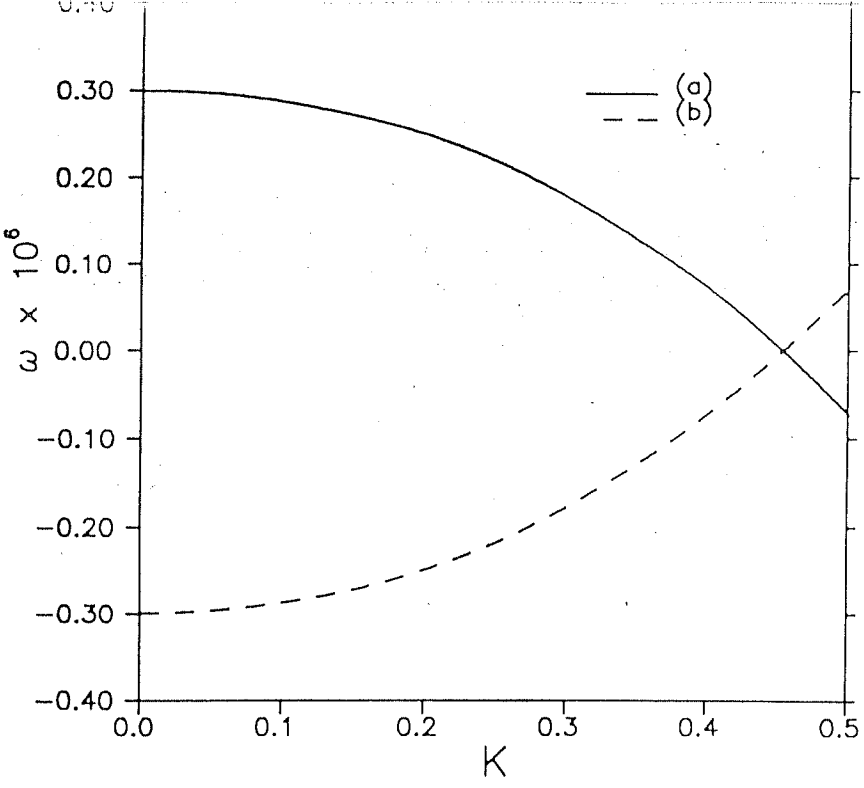

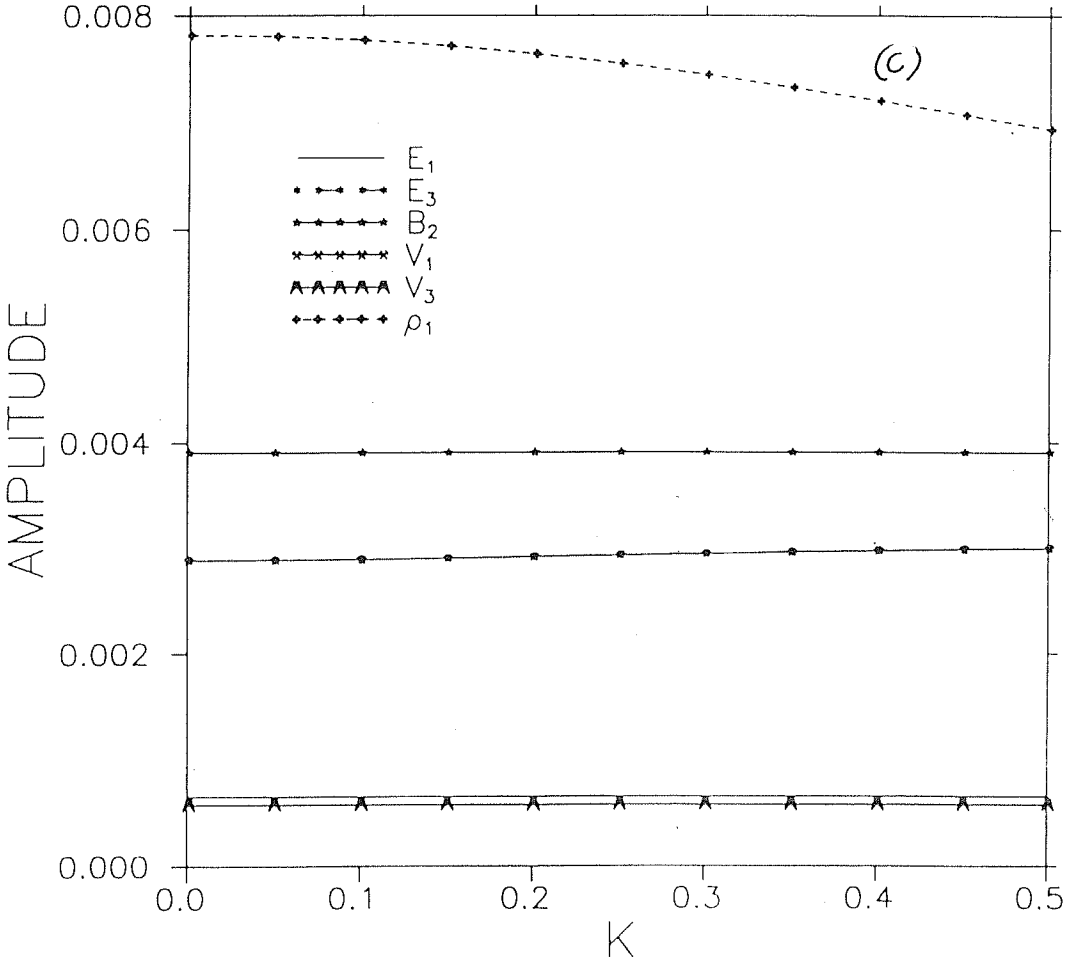

Figure 5.10: Comparison of normalised growth rate for K-H mode by two different methods (a) eigenvalue techniques (b) complex root finding. (c) eigen mode structures for K-H instability for different perturbed quantities by the method of eigenvalue techniques.

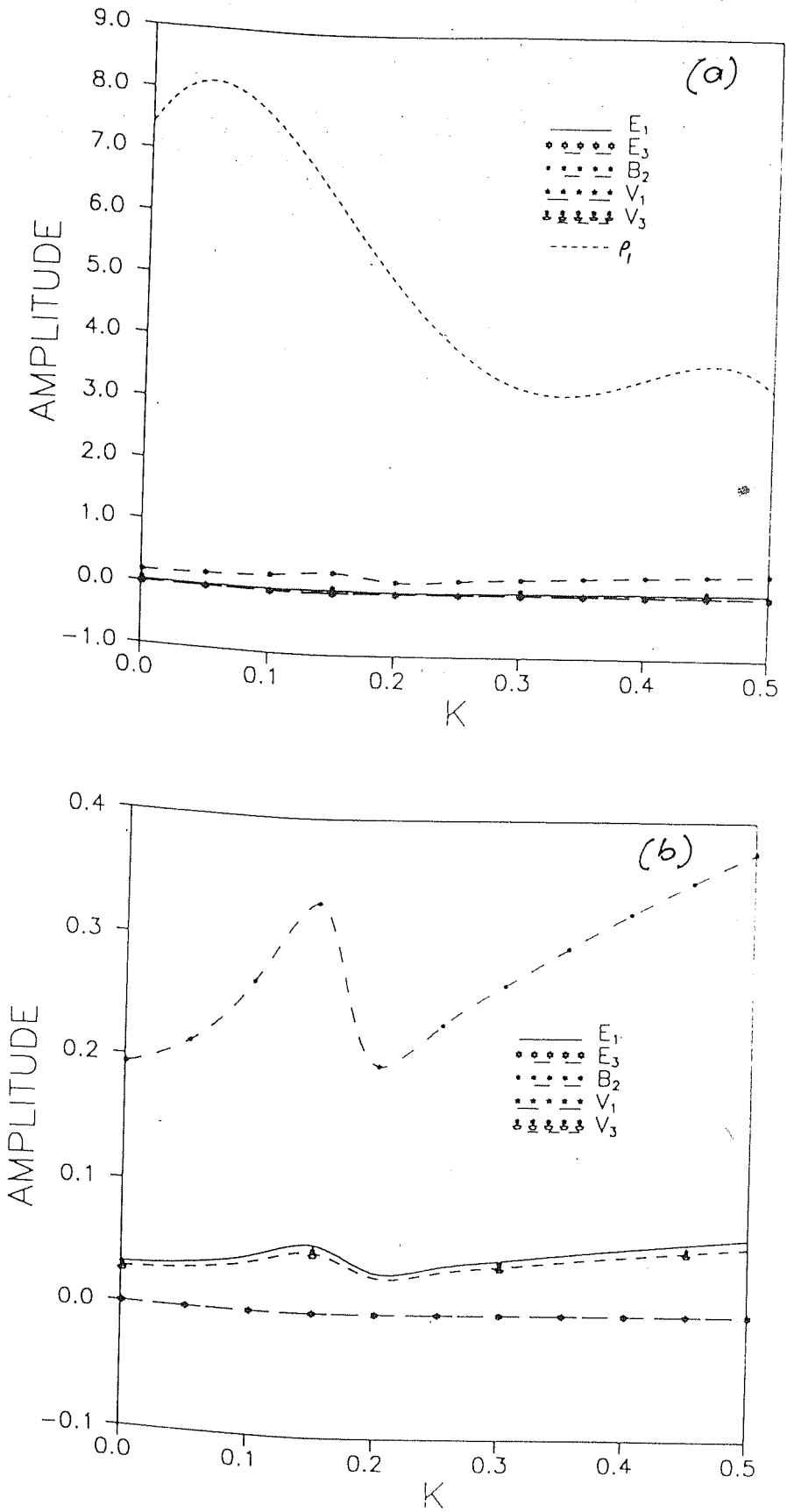

Figure 5.11: Eigen mode structures for magnetosonic mode by the method of eigenvalue techniques for (a) all the perturbed quantities (b) without perturbed density.

5.6 Two dimensional perturbation analysis

We report, in this section, the results obtained by carrying out a two dimensional (radial-azimuthal) perturbation analysis under local approximation using the eigenvalue techniques. The problem at hand consists of solving ten equations in ten variables and forms a closed system. As carried out earlier, we separate the complete equations into two groups and solve them separately in order to obtain better numerical results. Thus, equations (5.3.3,5.3.5, & 5.3.7) involving the variables E_2, B_1, and B_3 constitute one eigenvalue problem while the remaining seven equations with seven variables (E_1, E_3, B_2, V_1, V_2, V_3 and ρ_1) form the second eigenvalue problem.

5.6.1 Results and discussions

In this section, we discuss the numerical results obtained in the case of radial-azimuthal perturbation by the method of eigenvalue techniques. The analyses reveal the existence of three basic instabilities *viz.*, K-H, fast magnetosonic (FMS) and slow magnetosonic modes (SMS). A comparison of the growth rates (Figs. 5.12a & 5.13a) of these modes shows that FMS mode is most unstable with a higher growth rate whereas KHI is least unstable with a normalized growth rate of the order 10^{-6}. From the dispersion curves for K-H and MS modes (Figs. 5.12a & 5.13b), it is found that longer wavelengths of K-H and shorter wavelengths of MS modes are more unstable. It is also to be noted that KHI exists only for purely radial perturbation and gets stabilized if the wave propagation in the azimuthal direction is included ($m \neq 0$) in the analysis. But, the finite azimuthal mode number excites slow MS mode which was absent in the one dimensional analysis.

The phase velocity calculation of slow and fast magnetosonic modes show the

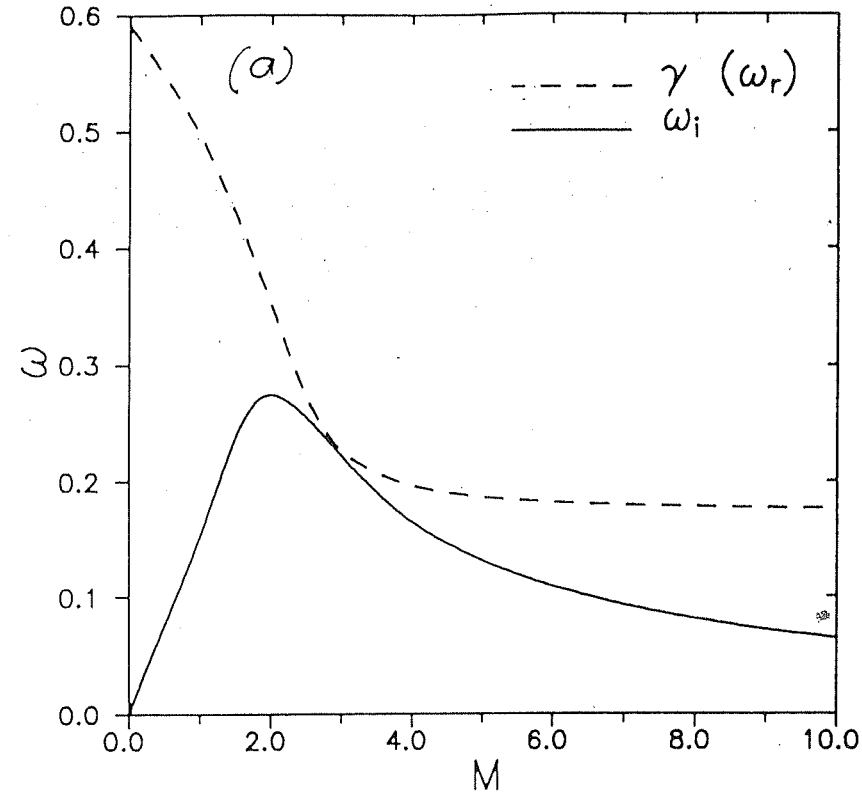

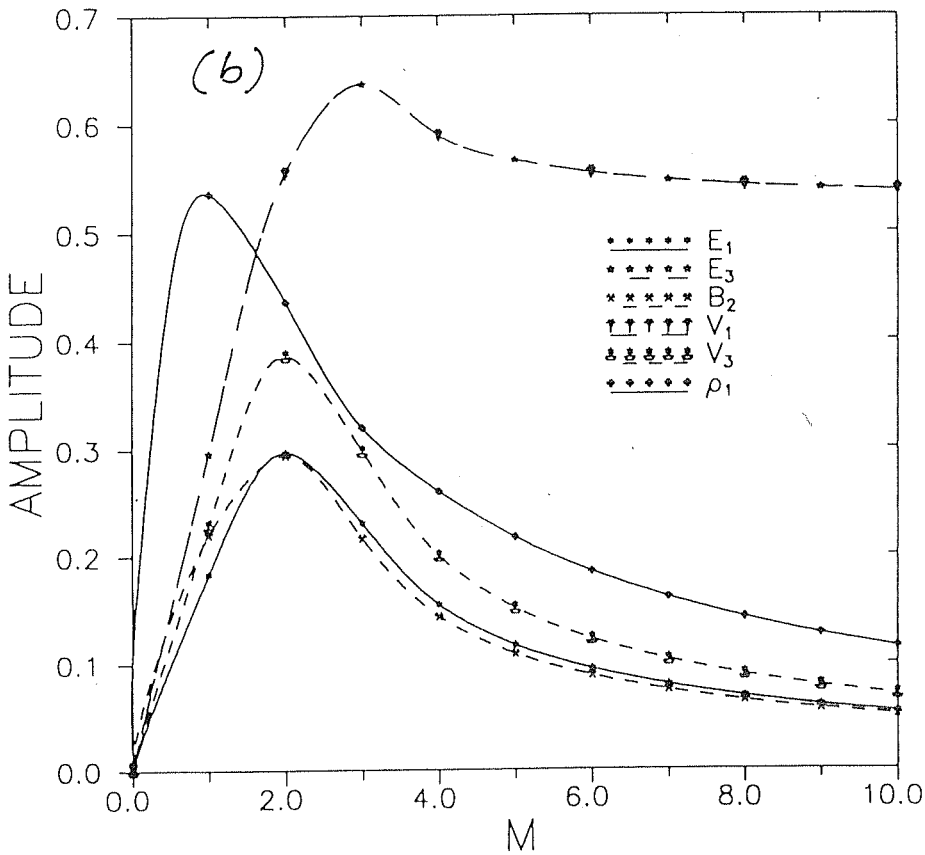

Figure 5.12: (a) The normalised growth rate and dispersion curve and (b) the eigenmode structures for the fast magnetosonic mode for k = 0.

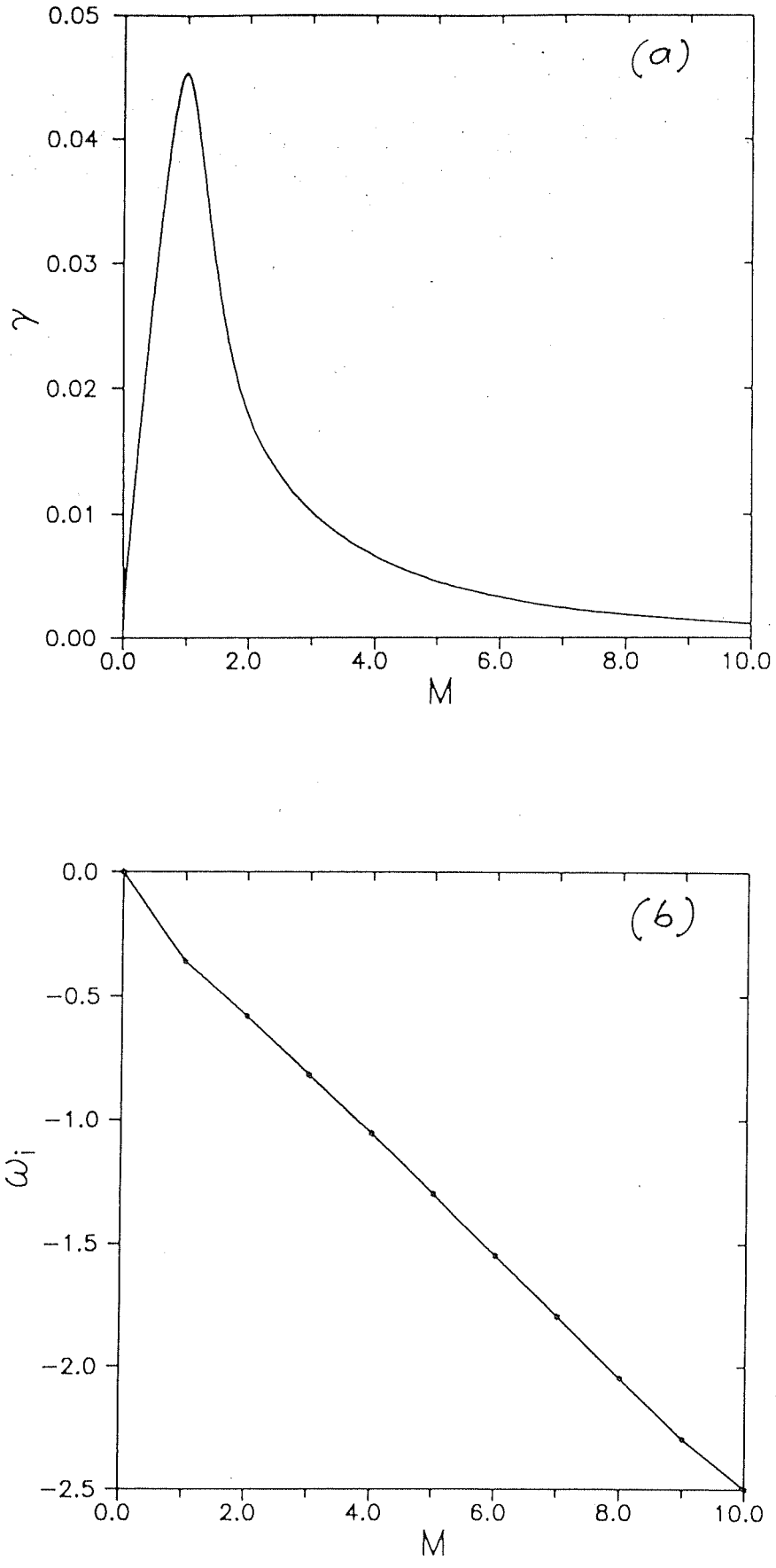

Figure 5.13: (a) The normalised growth rate and (b) dispersion curve for the slow magnetosonic mode for k = 0.

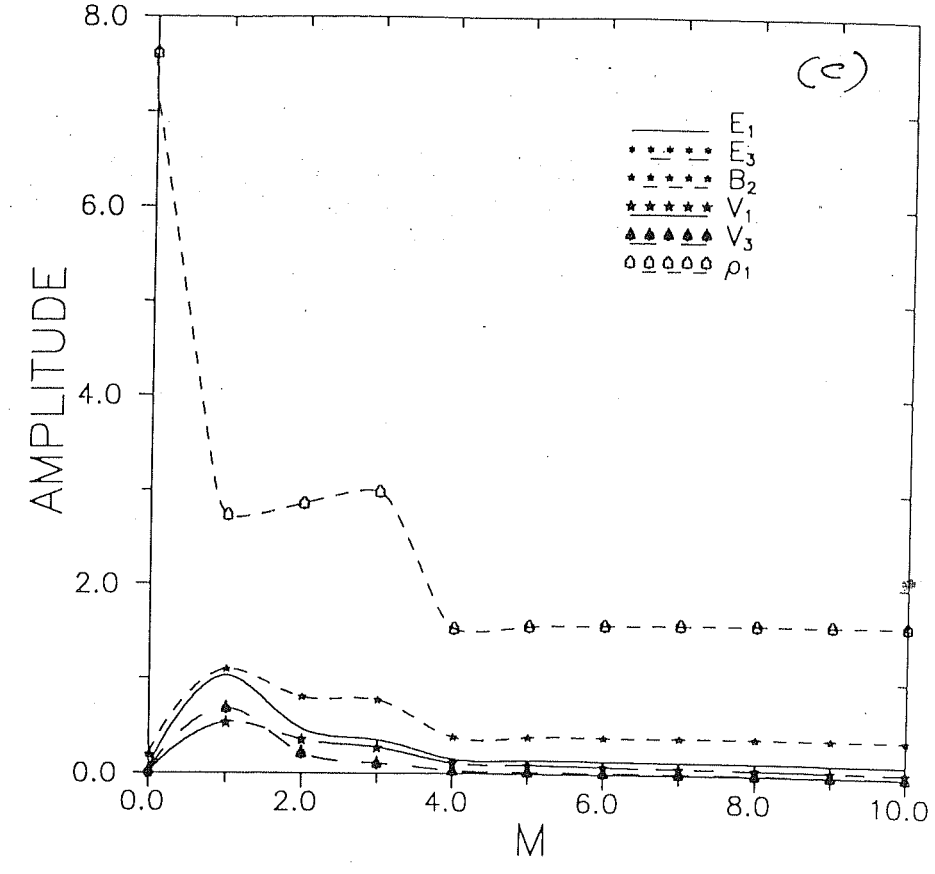

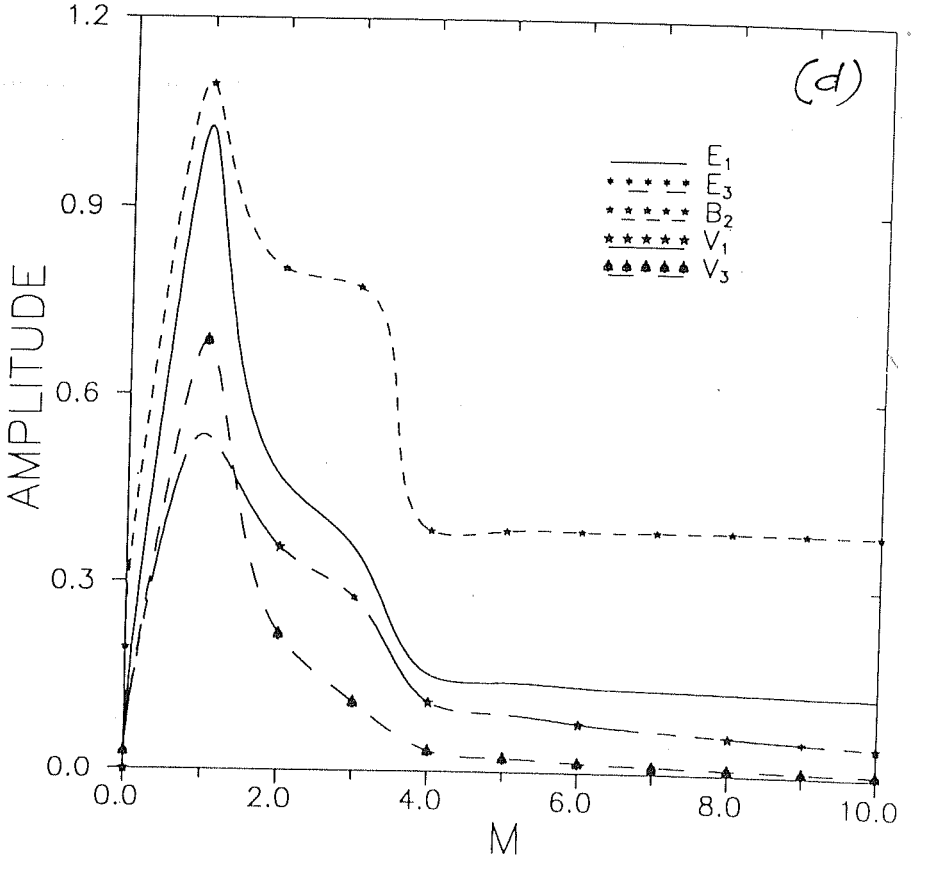

Figure 5.13: Eigen mode structures for slow magnetosonic mode by the method of eigenvalue techniques with k = 0 for (c) all the perturbed quantities (d) without perturbed density.

direction of propagation of these modes and we find that FMS and SMS propagate in opposite direction to each other. For purely azimuthal perturbation (k $= 0$) FMS propagates in azimuthal direction but opposite to the direction of plasma flow while SMS propagates along the flow direction. The effect of higher m-mode numbers on these instabilities is depicted in Figs. 5.14 & 5.15. These diagrams show that higher m values reduce the growth rates of the fast and slow MS modes.

The investigation of the dispersion characteristics of these modes reveal that the FMS modes are non-dispersive along the radial direction but dispersive in azimuthal direction. Contrary to this, the SMS modes are weakly dispersive along radial direction and non-dispersive in azimuthal direction. Dispersion is found to be significant for smaller k (higher wavelength) values and for Alfvenic mach number M_A ($M_A = V^{\phi}/V_A$) ≥ 0.3. The growth rates of these instabilities are found to be more for subsonic and sub-alfvenic plasma flows (Figs. 5.16-5.18). The nature of the growth rate curves is in qualitative agreement with the work of Miura & Pritchett [108] where they find that the growth rate is reduced due to the stabilizing effects of the finite value of k_z, where k_z is the perturbation along the z direction in cylindrical co-ordinate system. However, in their case the growth rate becomes zero beyond some value of the wave number k_z. But, our study shows that SMS mode gets completely stabilized for higher mode numbers whereas the fast one grows with a constant growth rate. MS modes are found to be independent of the finite conductivity of the fluid as in the case of radial perturbation analysis.

The K-H instability which exists only in radial direction becomes prominent for higher flow velocity *i.e.* higher Alfvenic and sonic mach numbers (Fig. 5.3). For lower Alfvenic and sonic mach numbers, the growth rate of the instability shifts towards the longer wavelength. Existence of a threshold value of plasma flow for the

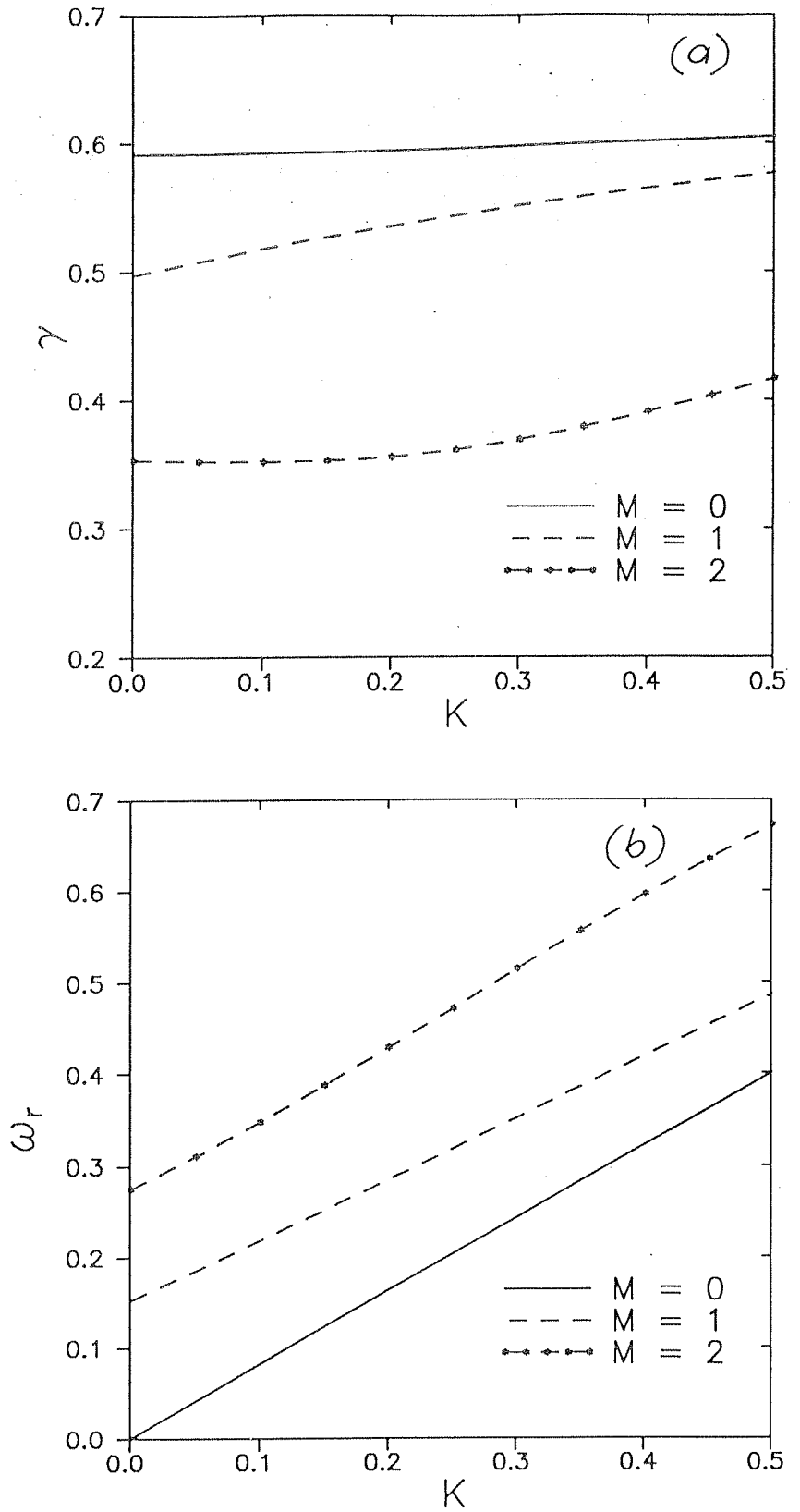

Figure 5.14: (a) The normalised growth rate and (b) normalised dispersion curve for fast magnetosonic mode with azimuthal mode number m as a parameter.

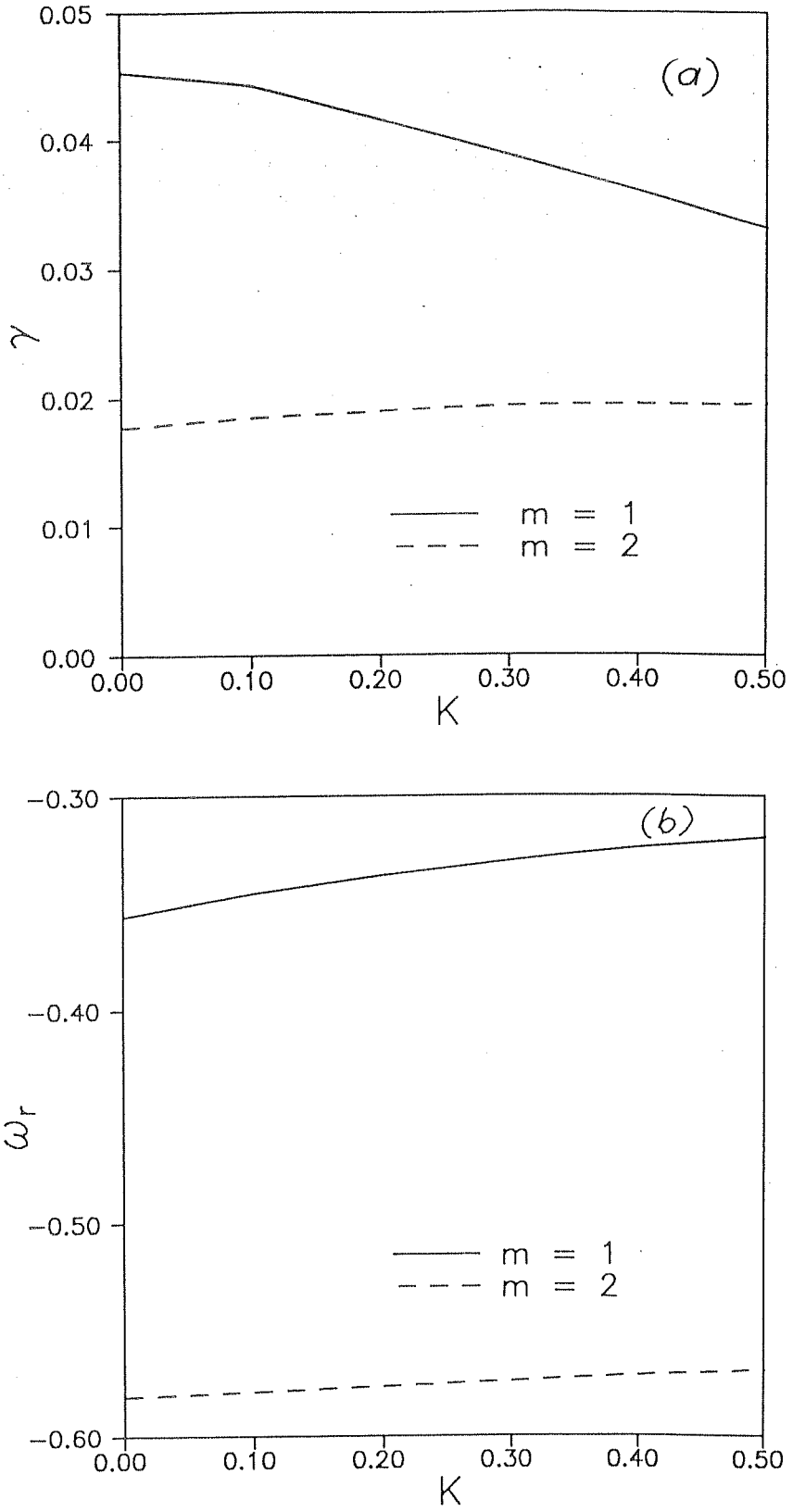

Figure 5.15: (a) The normalised growth rate and (b) normalised dispersion curve for slow magnetosonic mode with azimuthal mode number m as a parameter.

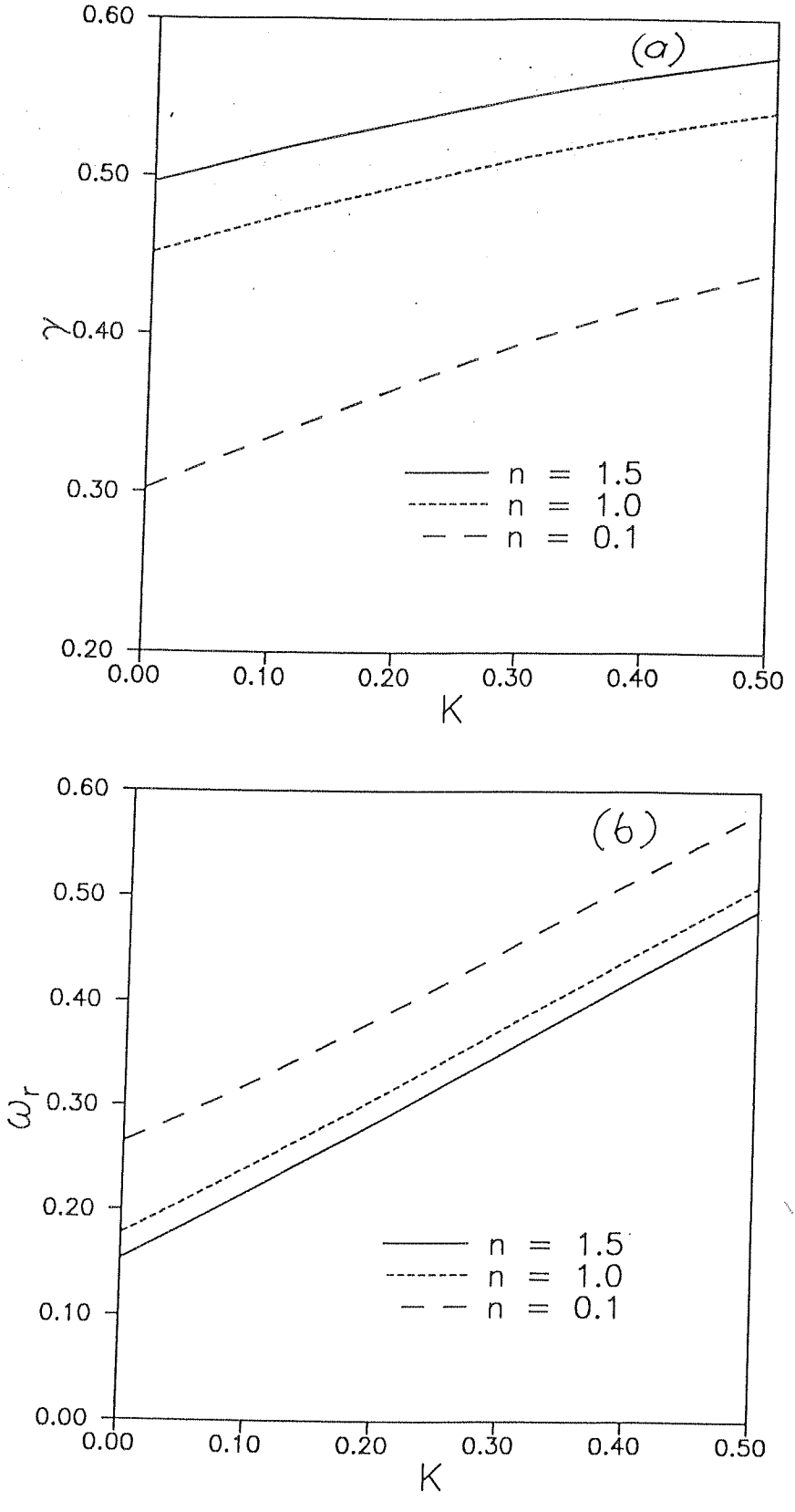

Figure 5.16: (a) The normalised growth rate and (b) normalised dispersion curve for fast magnetosonic mode with V^{ϕ} as a parameter for m = 1.

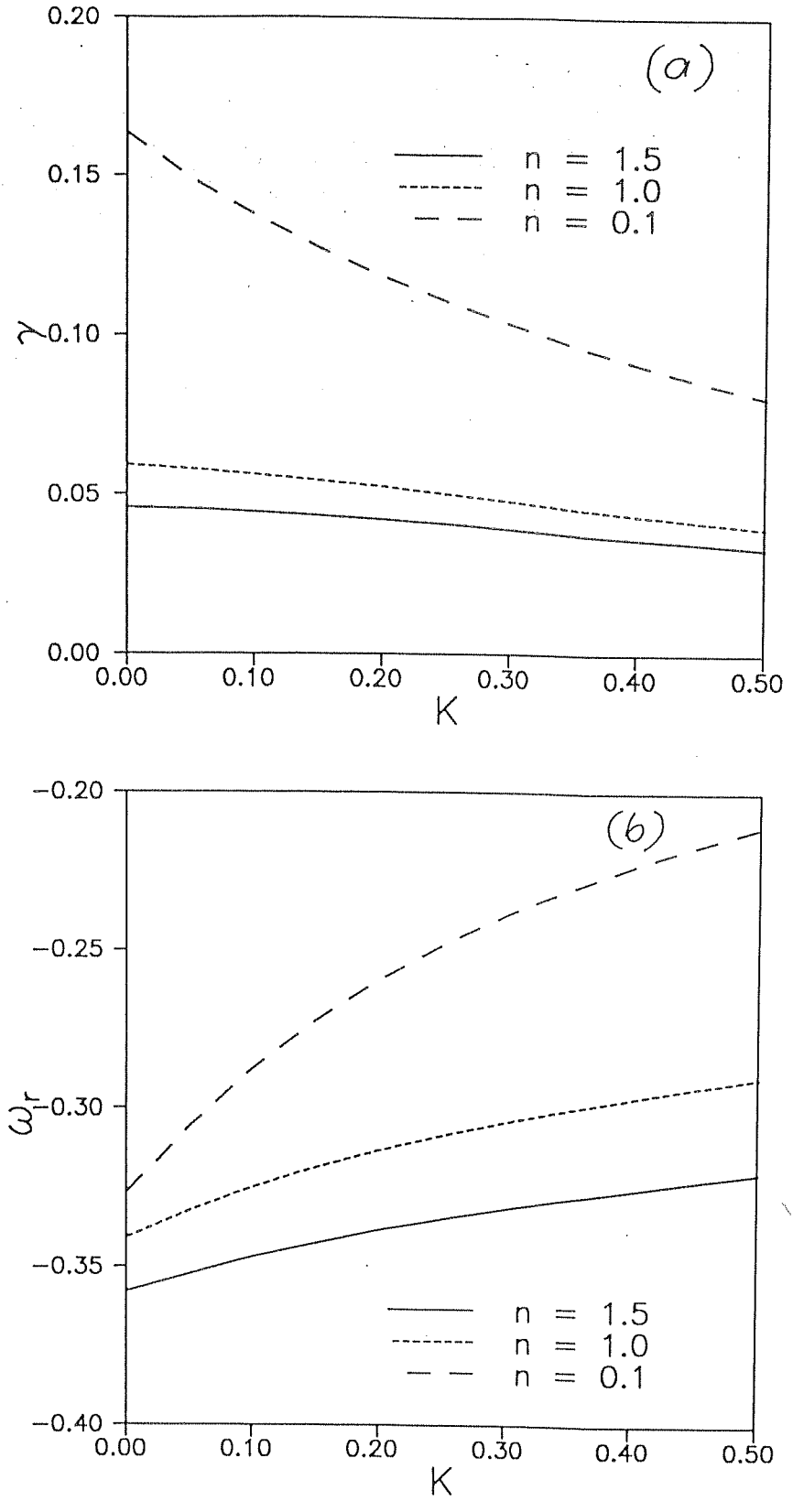

Figure 5.17: (a) The normalised growth rate and (b) normalised dispersion curve for slow magnetosonic mode with V^{ϕ} as a parameter for m = 1.

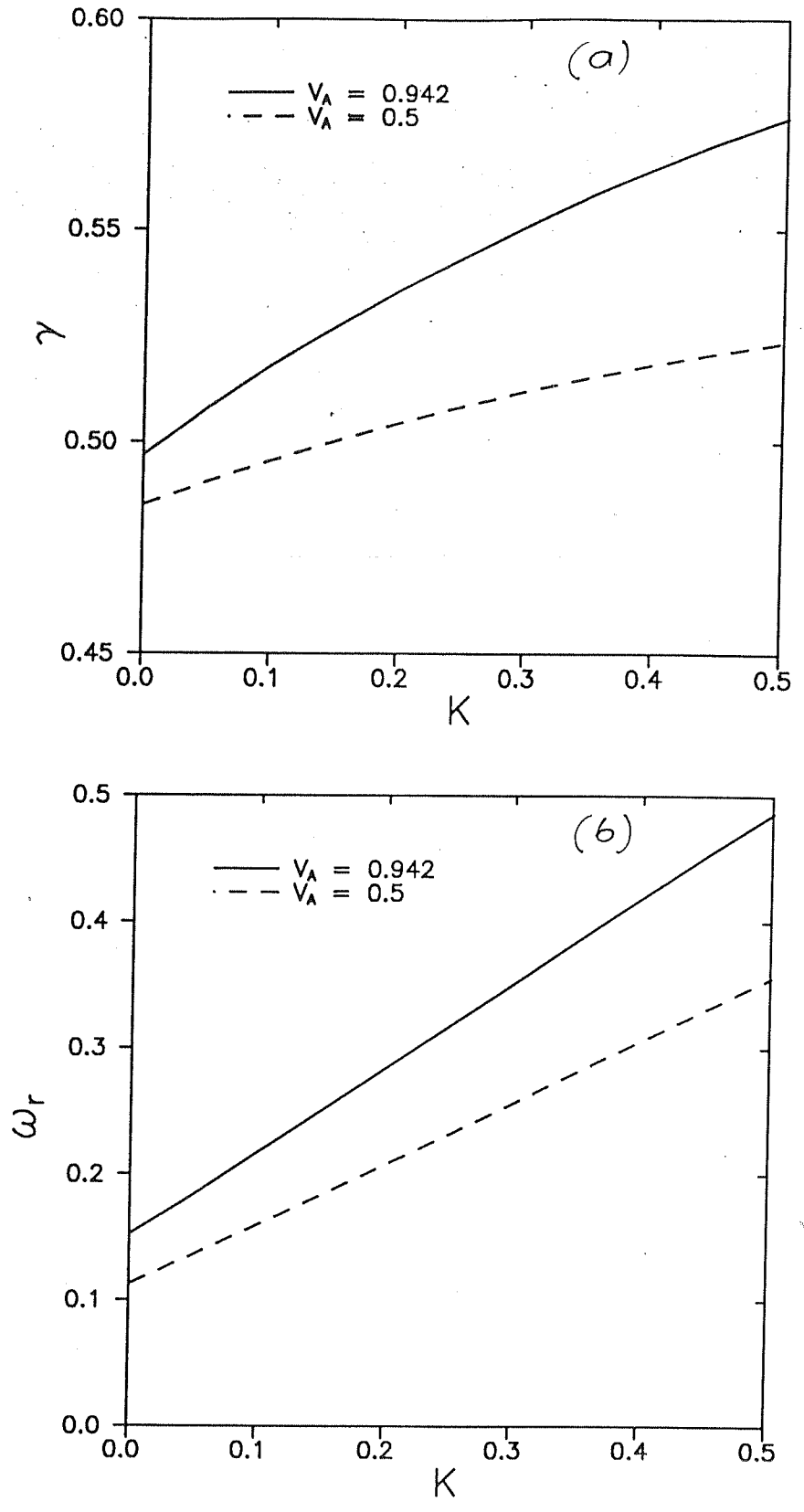

Figure 5.18: (a) The normalised growth rate and (b) normalised dispersion curve for fast magnetosonic mode with V_A as a parameter for m = 1.

excitation of KHI is found to be consistent with our equilibrium results. In contrast, the MS modes are weakly dependent on the value of V^{ϕ} and exists even for static case ($V^{\phi} = 0$, Figs. 5.16 & 5.17). The analysis of these modes further demonstrate that FMS (SMS) mode depends on V_A (C_s) and the instability is switched off for zero value of these parameters (Figs. 5.18-5.21).

We now turn to the discussion of the eigenmode structure of these instabilities. Figs. 5.11b, 5.12b & 5.13 show the amplitudes of perturbed electric, magnetic, velocity and density fields as a function of m with the parameter $V^{\phi} = 0.316$, $V_A = 0.942$, $C_s = 0.4394$. The amplitude of density perturbation of these two instabilities has a broad maximum which falls off monotonically with higher mode number. However, the rate of decrease is different for the fast and slow MS modes. It is interesting to note that for a given instability, the distribution of the amplitudes of all the fields and the corresponding growth rates as a function of wavenumber have identical patterns. This implies that our analysis is consistent.

The analysis of the other three equations in the framework of the eigenvalue analysis reveals the existence of one more instability which is purely electromagnetic in nature. This mode propagates radially inward and is suppressed by higher m values ($m \geq 2$) (Fig. 5.22). As discussed in case of radial perturbations (Sect. 5.4.2), this mode is believed to arise due to the finite conductivity of the plasma (see, Shivamoggi [109]). We further conjecture that this mode may be modified if one considers the finite thickness of the accretion disc, since it is known that finite thickness stabilizes some of the growing modes (Miura & Pritchett [108]).

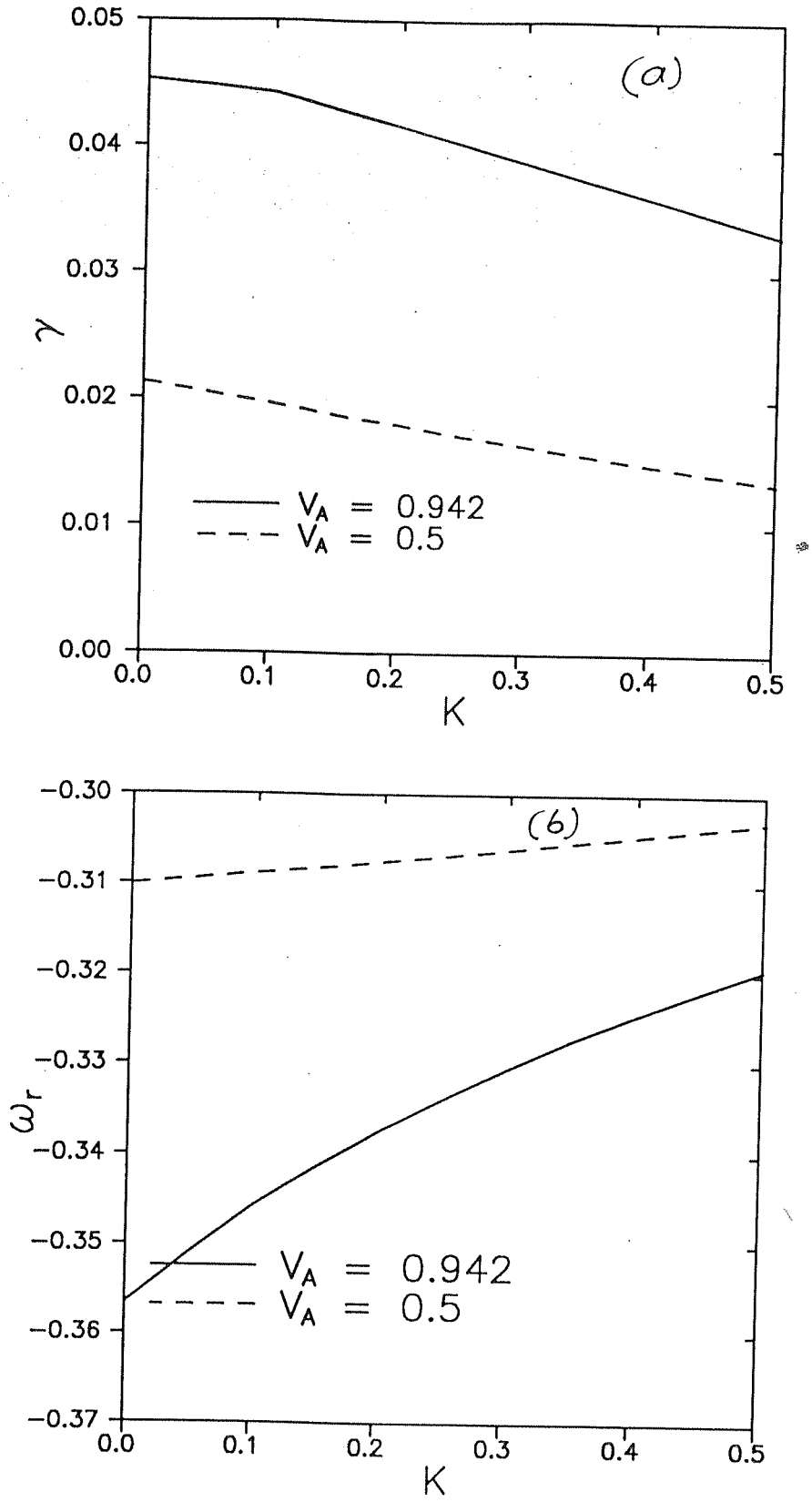

Figure 5.19: (a) The normalised growth rate and (b) normalised dispersion curve for slow magnetosonic mode with V_A as a parameter for m = 1.

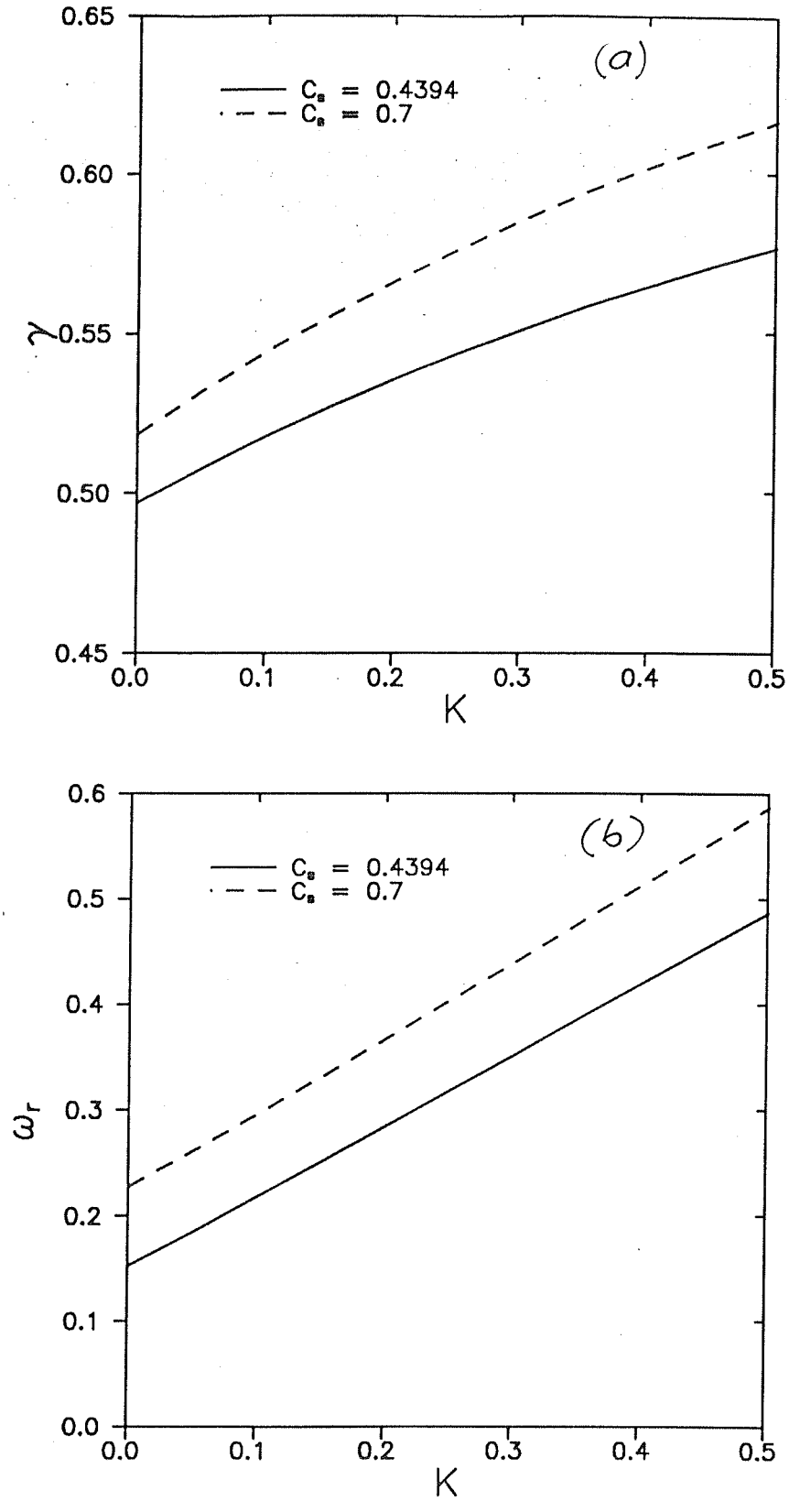

Figure 5.20: (a) The normalised growth rate and (b) normalised dispersion curve for fast magnetosonic mode with C_s as a parameter for m = 1.

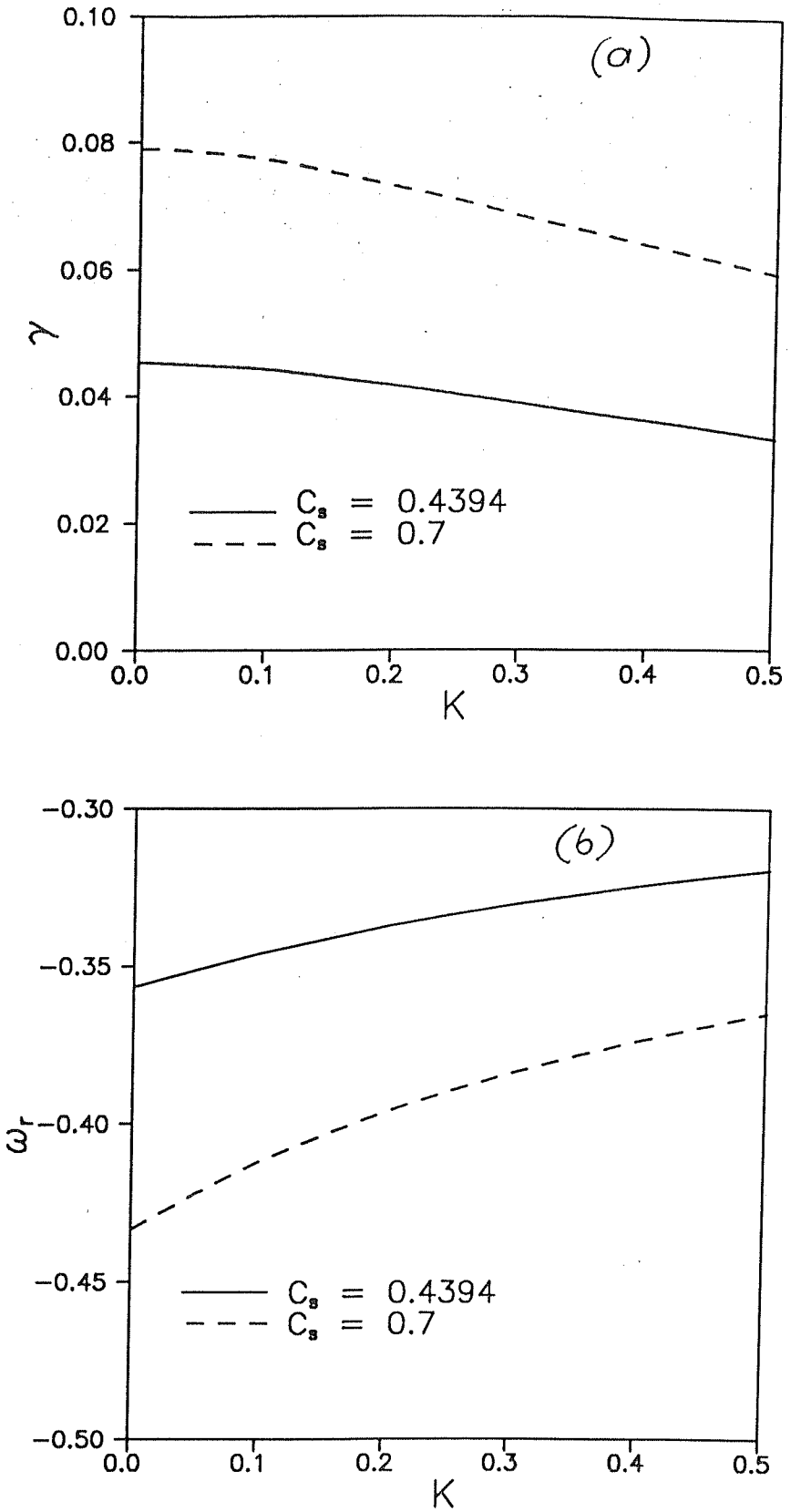

Figure 5.21: (a) The normalised growth rate and (b) normalised dispersion curve for slow magnetosonic mode with C_s as a parameter for m = 1.

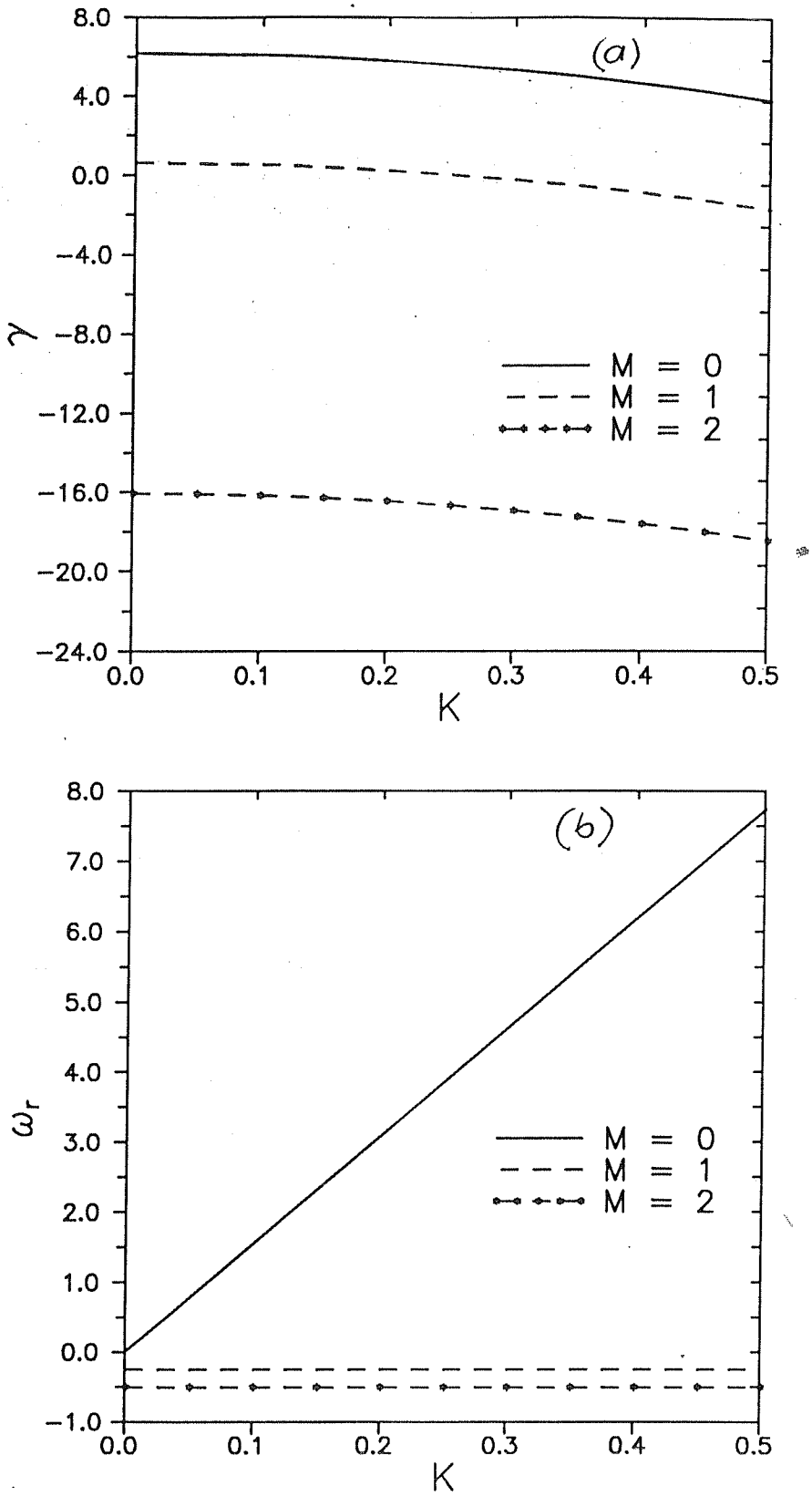

Figure 5.22: (a) The normalised growth rate and (b) normalised dispersion curve for electromagnetic mode for different azimuthal mode number m.

5.6.2 Non-local analysis

In earlier studies, as described in Sect. 5.4 and 5.6.1, we carried out the perturbation analysis in the frame work of a local approximation and obtained results which are in fairly agreement with the work of other investigators. The approximation of local stability analysis which breaks down for smaller values of radial wave number (k) points out the need to carry out a non-local (global) analysis. In the framework of global analysis, in this section, we carry out a preliminary perturbation analysis of the equilibrium solution given in Chap. 4.

The governing equations for this analysis are given in Sect. 5.3. We perform a radial perturbation analysis (m = 0) using these dynamical equations (5.3.2-5.3.11). The set of 10 differential equations with 10 variables are solved as an eigenvalue problem using the techniques outlined in Sect. 5.5. The numerical method that converts the differential equations into a set of linear and homogeneous algebraic equations uses a second order finite difference method.

In this analysis, we consider N-grid points in the α interval [1.25,8.75]. Central differencing is used at the inner grid points (J = 2,3, ...N-1) and a forward differencing is used at the inner edge of the disc (J = 1). Thus, we have 10(N-1) algebraic equations for N-1 perturbed quantities. We apply these N equations at each grid points, J = 1, 2, ...N-1 and the resulting set of equations will have N $\times$ N-1 closed set of equations. Since, we have a system of N first order differential equations, we have to specify N boundary conditions which provides the remaining N equations of the N $\times$ N closed set of equations. The boundary conditions assume that all the perturbed quantities *viz.* E_i, B_i, V_i and ρ_1 where i = 1,3, vanish at the outermost boundary (r = r_{out} and J =Nth grid point). Now, we have to find the eigenvalues ω_r and ω_i by requiring a zero value for the determinant of the coefficient

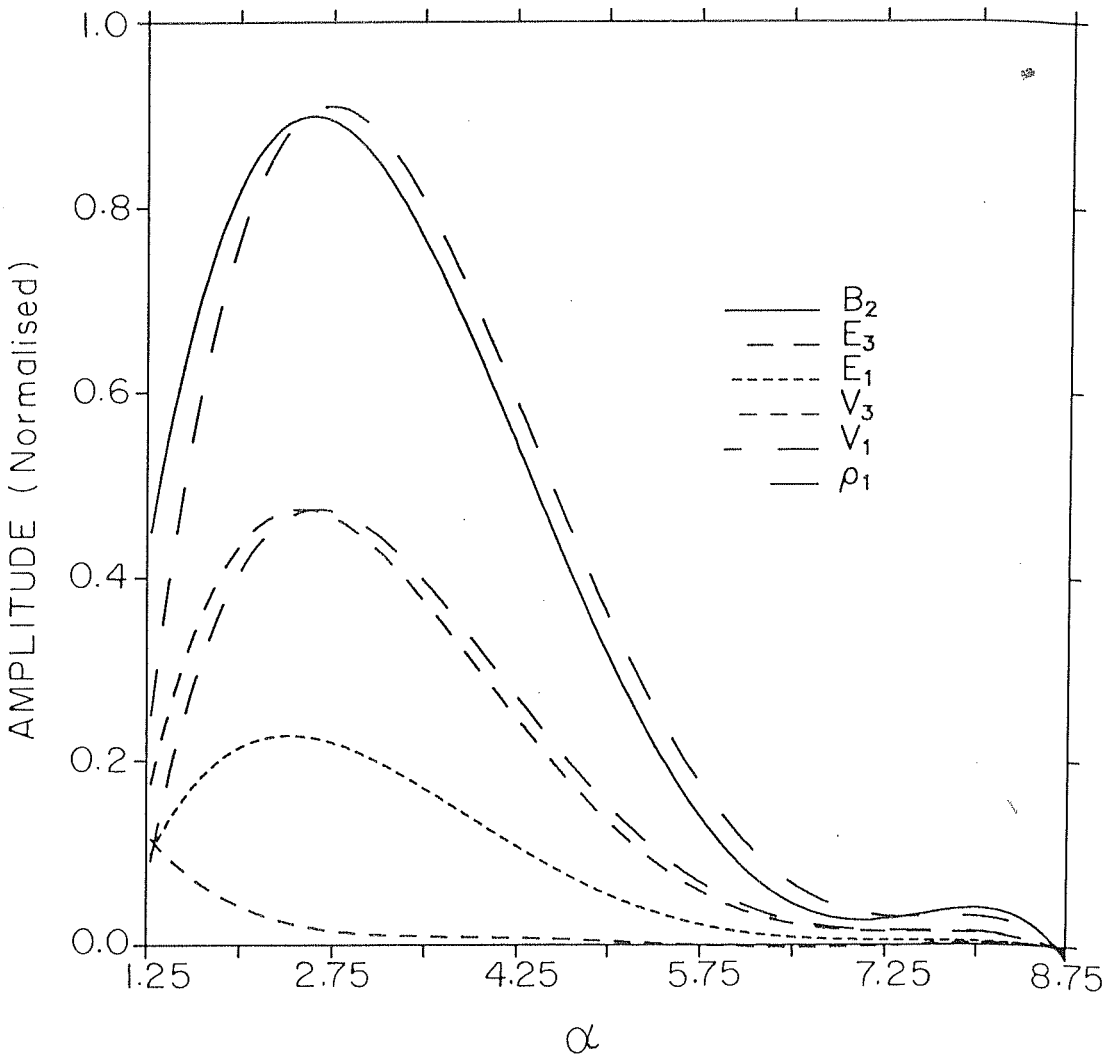

Figure 5.23: The normalised eigenmode structures for Kelvin-Helholtz instability in the framework of a non-local (global) analysis.

matrix. We have used the previously mentioned EISPAK routines (Smith *et al.* [96]) to obtain the solutions.

The numerical study shows the presence of three modes which agrees with our earlier calculation of radial perturbation in the framework of local approximation. The normalized eigenmode structure elucidates that the perturbation is localized near the inner edge of the accretion disc. The maximum growth also coincides with the pressure profile (Fig. 4.5) where the gradient is maximum. A typical eigenmode plot for KHI is depicted in Fig. 5.23. However, this analysis is far from complete. It is well known that one has to test the convergence of the eigenvalues by carrying out a sensitivity study by changing the matrix size. But, due to the large matrix size involved in our calculation, and due to the limitation of computational facilities, we have not been able to satisfy the convergence criterion to the limit of satisfaction. However, the eigenvalues are localized around N = 100 and do not vary by more than a few percent.

5.7 Conclusion

In this chapter, we have investigated the plasma instabilities at the inner edge of the accretion disc around a compact object under the local and non-local approximations. This analysis is based on the equilibrium solution presented in Chap. 4. The one-dimensional perturbation analyses reveal the presence of resistive-electromagnetic, K-H and magnetosonic modes which under appropriate conditions become unstable. The K-H mode propagating in a radially inward direction becomes stable for azimuthal velocity slightly lower than the Keplerian velocity. This mode also gets stabilized in the absence of velocity shear. The electromagnetic mode is conjectured to be the consequence of the finite conductivity of the plasma

and may get modified due to the finite thickness of the disc, which is neglected in this study. It is also found that the compressibility lowers the growth rate of these two modes which is in agreement with the known results. The analytical expressions (5.4.8 & 5.4.14) for the growth rate of these two instabilities clearly show that the growth rates are inversely proportional to the finite conductivity. However, the magnetosonic modes are independent of conductivity. The density inhomogeneity excites R-T like modes. These modes which are present even in the absence of velocity shear is believed to play an important role in pushing the matter inside the inner edge. The consistency of these analyses are verified by adopting another approach to solve the same problem. This approach employs the technique of eigenvalue formulation to solve the linearised equations which are Fourier transformed under the local approximation. The results of both the approaches agree perfectly with each other. In addition, this method illustrates the eigenmode structures of the unstable modes and reveals that the density perturbation has the maximum amplitude. The nature of the mode structure has the same pattern as their growth rates which further demonstrates the consistency of our calculation.

This investigation in the frame work of eigenvalue technique is further extended to two dimensional perturbation analysis of the same equilibrium configuration. The study highlights the stabilizing effects of the perturbation with finite azimuthal mode number. We notice that KHI gets stabilized for $m > 0$. But the finite m number excites slow magnetosonic mode and this mode also gets stabilized for higher m-mode number ($m \geq 2$). In contest, the fast magnetosonic mode attains a constant growth rate for higher m values. An investigation is also carried out to analyze the effects of different parameters on the instability. The study concludes that the growth rates of all the modes are higher for subsonic and subalfvenic plasma

flows. The study also shows the differences in the propagation and dispersion characteristics of magnetosonic modes. These two modes which propagate in opposite directions have contrasting dispersive characteristics. FMS are non-dispersive along the radial direction and dispersive in azimuthal direction whereas SMS is dispersive in radial direction and non-dispersive in azimuthal direction. As, in case of one dimensional perturbation analysis, MS modes are further found to be independent of conductivity. The computation of the eigenmode structures which has the same pattern as the corresponding growth rates implies the consistency of our calculation.

We have also carried out a preliminary survey of one-dimensional perturbation analysis in the framework of global analysis. Considering the appropriate boundary conditions at the outer edge, the equations are solved by the method of eigenvalue techniques using a finite difference scheme. The results show the existence of three different modes and confirms our earlier study of radial perturbation in the framework of local approach.

Although, our results qualitatively agree with the instability studies of earlier investigators, we find that our results have some quantitative differences. We attribute this to the following factors. The basic difference lies in our geometry. We recall that our analysis started with the study of dynamics and structure of equilibrium configurations in relativistic formalism. Thus, we have adopted a spherical geometry which is the natural co-ordinate system to describe gravity. This coordination system is also adopted for the stability analysis. The second point to be stressed is our equilibrium solution which is quite rigorous and involves many physical parameters compared to equilibrium configuration adopted by others. Thirdly, our equilibrium configurations of magnetic and velocity fields have smooth profiles in contrast to equilibrium solutions adopted by other investigators where a jump

was invariably considered. Further, we have considered the propagation of the wave along the direction of velocity shear in contrast to the usual studies where the direction of propagation is taken transverse to the shear along with the boundary conditions. In addition, under local approximations we have not considered any boundary conditions and thus our modes represent body modes. However, for purely azimuthal mode (k = 0), the instability characteristics partially coincide with the other known results.

Thus, our work where we have tried to improve upon the earlier approaches, presents the stability properties of a resistive plasma flow configuration around a compact object. The novelty of this research lies in the fact that the present perturbation analysis corresponds to physically relevant and self-consistent equilibrium solutions which describe a more realistic configuration of magnetic accretion discs around plasma magnetospheres. It is probable that the two dimensional behaviour of the above instabilities can modify the accretion flow pattern. We also conjecture that as a result of these instabilities, the incoming matter can penetrate the magnetic field of the central star and can push the inner edge of the disc nearer to the compact object. Consequently, disc luminosity would be enhanced. It is also believed that the instability could explain the variability of AGN's and X-ray binaries. However, more effort is needed to associate these instabilities to explain the observable features of the astrophysical plasmas and our work presents a systematic progress towards this goal.

Chapter 6

CONCLUDING REMARKS AND OPEN PROBLEMS

The study of structure of magnetosphere around accreting compact objects is important for the understanding of a wide variety of cosmic high energy sources. Most of the energy emitted by these sources is in the form of X-rays with energy output in the range of 10^{36} ergs-s^{-1} to 10^{38} ergs-s^{-1} and is supplied by the accretion of matter to the surface of the compact objects like neutron stars or black holes. If the central compact object has an intrinsic magnetic field, the magnetic field influences the incoming magnetofluid and eventually the motion is completely governed by the field and the matter ends up on the surface of the central star either by flowing along the field lines or by diffusing across the field lines due to the turbulence or instabilities. If the matter being attracted have angular momentum with respect to the central body, it forms a disc around it. The large scale structure and the dynamics of such discs is important physically, as many of the observable properties like pulse shapes, spectra, spin-up rate and intensity fluctuations depend on it. On the other hand, the interaction between the magnetosphere of a neutron star and a

surrounding accretion disc is important with regard to the formation of binary radio pulsars and the origin of quasi-periodic oscillations from low mass X-ray binaries. In this context, it is necessary to understand the different modes of instabilities that could arise in discs supported by the gas and magnetic pressure around compact objects under general perturbations.

With this motivation, we have developed the dynamical equations for a magnetofluid surrounding a central compact object in a curved background geometry. These general set of equations can fit into any astrophysical plasma studies including jets observed from extragalactic radio sources. But, our aim in this thesis have been to analyze and show the existence of equilibrium structures around compact objects and subsequently study their stability characteristics. Thus, we have investigated the dynamical equilibrium and stability of few configurations. The analyses and the conclusions are briefly summarized below.

1. Considering the background spacetime to be the Schwarzschild geometry and the electromagnetic field as well as the matter distribution to be stationary and axisymmetric, a fairly simple analytical solution for an incompressible matter having only azimuthal component of velocity was obtained. The analysis showed that the self-consistent calculation of fully relativistic equations demand the flow velocity to be Keplerian (sub-Keplerian) for thin (thick) disc configurations (Prasanna *et al.* [115]).

2. With the understanding that a velocity greater than Keplerian distribution is not consistent with the generalized equations, we next, investigated a more complicated equilibrium structure for a resistive plasma disc having a poloidal magnetic field and all velocity components. For a better understanding of the underlying physical mechanisms and for the sake of mathematical simplicity,

this study was carried out in Newtonian limit. The analysis revealed that equilibrium configurations could exist only for certain combination of physical parameters. Thus, this study obtained limits on physical variables like seed magnetic field of the compact object, outer disc density and finite conductivity of the plasma. The study shows that the magnetic field of the central star is of the order of 10^8 gauss. As the estimation of magnetic fields for some of the X-ray binaries fall in this range, our model appears to be promising. The study also revealed that for certain combination of numerical values, the pressure distribution shows turning point behaviour indicating the presence of large pressure gradients around these points. The presence of such large pressure gradients is known to give rise to instabilities (Tripathy *et al.* [116]).

3. As the presence of large pressure gradients near the inner edge indicated the presence of instabilities, we have also carried out stability analysis of the plasma flow around compact objects, both in the framework of local and non-local approach. We first carried out one-dimensional perturbation investigation along the direction of the velocity shear (radial direction) and subsequently extended it into two dimension to include the direction of plasma flow (azimuthal direction). This problem has been investigated both analytically and numerically by the method of finding complex roots. One of the key features of this investigation is the existence of Kelvin-Helmholtz and Rayleigh-Taylor type of instabilities which opens up possibilities for the matter to flow across or along the magnetic field lines. The absence of velocity shear switches off the KHI but R-T like instability still exists. We have also obtained resistive electromagnetic modes which are, probably, due to the finite conductivity of the plasma. The results of this analysis have been subsequently verified by

solving the matrix eigenvalue problem by using numerical techniques. Using, the same eigenvalue technique, the radial-azimuthal perturbation analyses have revealed the presence of fast and slow magnetosonic modes which get stabilized in the absence of V_A and C_s respectively. A preliminary study in the framework of non-local analysis presented the eigenmode structures and the results indicated that the instability is localized at the inner edge of the disc. The presence of all the three modes in this frame work also verified the consistency of our local approximation. However, in order to get a good correlation between the theory and observation, more detailed analysis would be required. (Tripathy *et al.* [118]).

As the steady state solutions are inhomogeneous in spatial coordinates r and θ, it is necessary to perform a global stability analysis of the above mentioned equilibrium configurations with proper boundary conditions at the inner edge of the accretion disc. The break down of local approximation for longer wavelengths of unstable modes also necessitates a non-local study. This problem as clear from the above considerations, is very difficult to tackle analytically and has to be solved numerically. The following questions would be addressed in this study.

- Nature of instabilities that exist in a thick disc having a self-consistent magnetic field.
- The role of instabilities in radiation processes.
- The mechanism and amount of angular momentum and torque transported to the central star.

In our investigation of self-consistent equilibrium configurations, we have assumed the disc to have a poloidal component of the magnetic field only. But, the

motion of ions and electrons in the plasma environment going around the central star would produce currents and associated magnetic fields in the toroidal direction also. As a result of the generation of this toroidal field, angular momentum is exchanged between the star and the disc. It is believed that the toroidal component of the magnetofluid plays an important role in the generation of jets in astrophysical objects. Thus, it is important to analyze the equilibrium structure of a thick accretion disc including the self consistent magnetic field in the toroidal direction.

APPENDIX A

Here, we show that the magnetic fields inside the disc are constant in nature and do not depend on the value of k. Using spherical polar co-ordinates (r,θ,ϕ), the equation for magnetic field lines dx/ds = B/|B| can be written in component form as

$$\frac{dr}{ds} = \frac{B_r}{|B|}. \tag{A1}$$

$$r\frac{d\theta}{ds} = \frac{B_\theta}{|B|}. \tag{A2}$$

Dividing equation (A1) by (A2), we obtain

$$\frac{dr}{d\theta} = -r\ \cot\theta, \tag{A3}$$

which on integration yields r sinθ = A. Transforming this into the cartesian coordinate system with X = r sinθ, where θ = 0 denotes the pole, we have the equation of field line as X = A. This represents the constant field lines parallel to the Y axis which is shown in Fig 4.1.

APPENDIX B

$$Q_1 = \omega^2 - i\omega\hat{\sigma} - (k^2 - \alpha^{-2} - 2ik\alpha^{-1}) \tag{B4}$$

$$Q_2 = \omega(1 + V_A^2 + i\omega\hat{\sigma}^{-1}) \tag{B5}$$

$$Q_3 = -V^{\phi}(k - i\alpha^{-1}) \tag{B6}$$

$$Q_4 = -2V^{\phi}\alpha^{-1}(1 + i\omega\hat{\sigma}^{-1}) \tag{B7}$$

$$\begin{aligned} Q_5 &= \left[\frac{V_A^2}{\omega}F + \frac{i}{\hat{\sigma}}\right] + \hat{\sigma}V_A^2 + \frac{2V^{\phi 2}}{\alpha\omega}(k - i\alpha^{-1}) \\ &- \left[ikC_s^2 + DP\right](k - 2i\alpha^{-1})\frac{F}{\hat{\sigma}\omega^2} \end{aligned} \tag{B8}$$

where

$$F = 2k\alpha^{-1} + i(k^2 - \alpha^{-2}) - i\omega^2 - \hat{\sigma}\omega \tag{B9}$$

$$DP = \frac{(\gamma - 1)}{\rho_0 c^2}\frac{dp}{d\alpha} \tag{B10}$$

APPENDIX C

$$A_1 = -\frac{1}{\sigma^2} \tag{C11}$$

$$A_2 = \frac{2(1+V_A^2)}{\sigma} \tag{C12}$$

$$A_3 = (1+V_A^2)^2 + \sigma^{-2}\left[k^2(1+C_s^2) - 2\alpha^{-1}(DP) - \alpha^{-2}\right] \tag{C13}$$

$$A_4 = -k\sigma^{-2}\left[2\alpha^{-1}(1+C_s^2) + DP\right] \tag{C14}$$

$$A_5 = -k\alpha^{-1}\sigma^{-1}\left[2(1+2V_A^2) + (2+V_A^2)(2C_s^2 + \alpha DP)\right] \tag{C15}$$

$$A_6 = \sigma^{-1}\left[(1+2V_A^2)(\alpha^{-2} - k^2) + (2+V_A^2)(2\alpha^{-1}DP - k^2C_s^2)\right] \tag{C16}$$

$$A_7 = (1+V_A^2)\left[2\alpha^{-1}DP + V_A^2\alpha^{-2} - k^2(V_A^2 + \sigma^{-2}C_s^2)\right] + 2V_a^2V^{\phi^2}\alpha^{-2} \tag{C17}$$

$$+ C_s^2k^2(\alpha\sigma)^{-2}\left[5 - k^2\alpha^2\right] + 2k^2\alpha^{-1}\sigma^{-2}DP\left[2 - k^{-2}\alpha^{-2}\right] \tag{C18}$$

$$A_8 = (1+V_A^2)\left[\frac{2k}{\alpha}(V_A^2 + C_s^2) + kDP\right] + \frac{2k}{\alpha}\left[2k^2C_s^2 + V_A^2V^{\phi^2}\right] \tag{C19}$$

$$- \frac{k}{\alpha^3\sigma^2}\left[2C_s^2 + \alpha DP(5 - k^2\alpha^3)\right] \tag{C20}$$

$$A_9 = (1+V_A^2)\frac{k}{\sigma\alpha^2}\left[DP(k^2\alpha^2 - 5) - \frac{2C_s^2}{\alpha}(1 - 2K^2\alpha^2)\right] \tag{C21}$$

$$A_{10} = \frac{(1+V_A^2)}{\alpha^3\sigma^1}\left[2DP(1 - 2k^2\alpha^2) + \alpha k^2C_s^2(k^2\alpha^2 - 5)\right] \tag{C22}$$

Bibliography

[1] Gold T., 1959, J. Geophys. Res., **64**, 1219.

[2] Schreier E., Levinson R., Gursky H., Kellogg E., Tananbaum H. & Giaconni R., 1972, Astrophys. J., **172**, L79.

[3] Tananbaum H., Gursky H., Kellogg E.M., Levinson R., Schreier E. & Giaconni R., 1972, Astrophys. J., **174**, L143.

[4] Hoyle F. & Lyttleton R.A., 1939, Cam. Phil. Soc., **35**, 405.

[5] Bondi H., 1952, Mon. Not. R. astr. Soc., **112**, 195.

[6] Vasyliunas V.M., 1979, Space. Sci. Review, **24**, 609.

[7] Börner G., 1980, Phys. Rep., **60**, 151.

[8] Hayakawa S., 1985, Phys. Rep., **121**, 327.

[9] Wiita P.J., 1985, Phys. Rep, **123**, 117.

[10] Fumiaki Nagase, 1989, Pub. Astron. Soc. Japan, **41**, 1.

[11] Prasanna A.R., 1991, Pramana-J.Phys., **36**, 445.

[12] Zeldovich Y.B., 1964, Sov. Phys. Doklady, **9**, 195.

[13] Salpeter E.E., 1964, Astrophys. J., **140**, 796.

[14] Bisnovyati-Kogan G.S., 1979, Rev. de. Nuovo. Cimento, **2**, 1.

[15] Prasanna A.R., 1980, Rev. de Nuovo Cimento, **3**, (iv).

[16] Prasanna A.R. & Varma R.K., 1977, Pramana - J. Phys., **8**, 229.

[17] Chakraborty D.K. & Prasanna A.R., 1982, J. Astrophys. Astr., **3**, 193.

[18] Abramowicz M.A., Jarozynski M. & Sikora M. 1978, Astron. Astrophys., **63**, 221.

[19] Galeev A.A., Rosner R. & Vaiana G.S., 1979, Astrophys. J., **229**, 318.

[20] Lynden-Bell D., 1978, Phys. Scr., **17**, 185.

[21] Lovelace R.V.E., 1976, Nature, **262**, 349.

[22] Blandford R.D., 1976, Mon. Not. R. astr. Soc., **176**, 465.

[23] Blandford R.D. & Znajek R.L. 1977, Mon. Not. R. astr. Soc., **179**, 443.

[24] Malkan M. A., 1983, Astrophys. J., **268**, 582.

[25] Paczynski B., 1987, Nature, **327**, 303.

[26] Hayakawa S. & Matsuoka M., 1964, Prog. Theo. Phys. Supp., **30**, 204.

[27] Novikov I.D. & Zeldovich Y.B., 1966, Nuovo. Cim. Supp., **4**, 810.

[28] Shklovsky I.S., 1967, Astrophys. J. Lett., **148**, L1.

[29] Prendergast K.H. & Burbidge G.R., 1968, Astrophys. J. **151**, L83.

[30] Lynden-Bell D., 1969, Nature, **226**, 64.

[31] Lynden-Bell D. & Rees M.J., 1971, Mon. Not. R. astr. Soc., **152**, 461.

[32] Giacconi R., Guesky H., Kellogg E., Schreier E. & Tananbaum H., 1971, Astrophys. J. Lett. **167**, L67.

[33] Shakura N.I. & Sunyaev R.A., 1973, Astron. Astrophys., **24**, 337.

[34] Frank J., King A.R. & Raine D.J., 1985, *Accretion Power in Astrophysics*, Cambridge University Press, Cambridge.

[35] Novikov I.D. & Thorne K.S., 1973, in *Black Holes*, ed. C. DeWitt & B. DeWitt Gordon and Breach, London and New York.

[36] Thorne K.S., 1974, Astrophys. J. **191**, 507.

[37] Treves A., Maraschi L. & Abramowicz M. A., 1989, *Accretion- A collection of influential papers*, World Scientific, Singapore.

[38] Pringle J.E. & Rees M.J., 1972, Astron. Astrophys., **179**, 585.

[39] Davidson K. & Ostriker J.P., 1973, Astrophys. J., **179**, 585.

[40] Lamb F.K., Pethick C.J. & Pines D., 1973, Astrophys. J., **184**, 271.

[41] Baan W. A. & Treves A., 1973, Astron. Astrophys., **22**, 421.

[42] Elsner R.F. & Lamb F.K., 1976, Nature, **262**, 356.

[43] Ghosh P., Lamb F.K. & Pethick C.J., 1977, Astrophys. J. Lett., **148**, L129.

[44] Scharlemann E.T., 1978, Astrophys. J., **219**, 617.

[45] Ichimaru S., 1978, Astrophys. J., **224**, 198.

[46] Lamb F.K., 1979, in Sydney Chapman conference on magnetospheric boundary layers (Preprint).

[47] Ghosh P. & Lamb F.K., 1978, Astrophys. J. Lett., **223**, L83.

[48] Ghosh P. & Lamb F.K., 1979, Astrophys. J., **232**, 259.

[49] Ghosh P. & Lamb. F.K., 1979, Astrophys. J., **234**, 296.

[50] Kaburaki O., 1986, Mon. Not. R. astr. Soc., **220**, 321.

[51] Aly J.J., 1980, Astron. Astrophys, **86**, 192.

[52] Horiuchi R. & Tomimatsu A., 1978, Prog. Theor. Phys., **60**, 1933.

[53] Horiuchi R. & Tomimatsu A., 1979, Prog. Theor. Phys., **62**, 408.

[54] Horiuchi R., 1982, Prog. Theor. Phys., **68**, 541.

[55] Anzer U., Bröner. G. & Meyer-Hofmeister E., 1987, Astron. Astrophys., **188**, 85.

[56] Kaburaki O., 1987, Mon. Not. R. astr. Soc., **229**, 165.

[57] Lightman A.P. & Eardley D. M., 1974, Astrophys. J. Lett., **187**, L1.

[58] Bisnovyati-Kogan G.S. & Ruzmaikin A.A., 1974, Astrophys. Space. Sci, **28**, 45.

[59] Bisnovyati-Kogan G.S. & Ruzmaikin A.A., 1976, Astrophys. Space. Sci, **42**, 401.

[60] Lovelace R.V.E., Mehanian C., Mobarry C.M. & Sulkanen M.E., 1986, Astrophys. J. Suppl., **62**,1.

[61] Mobarry C.M. & Lovelace R.V.E., 1986, Astrophys. J. ,**309**, 455.

[62] Prasanna A.R. & Chakraborty D.K., 1981, J. Astrophys. Astr., **2**, 1.

[63] Chakrabarty D.K. & Prasanna A.R., 1981, J. Astrophys. Astr., **2**, 421.

[64] Prasanna A. R. & Bhaskaran P., 1989, Astrophys. Space. Sci., **153**, 201.

[65] Bhasakaran P. & Prasanna A.R., 1989, Astrophys. Space. Sci., **159**, 109.

[66] Bhasakaran P. & Prasanna A.R., 1990, J. Astrophys. Astr. **11**, 49.

[67] Bhaskaran P., **Tripathy S. C.** & Prasanna A.R., 1990, J. Astrophys. Astr., **11**, 461.

[68] Abramowicz M.A., Calvani, M. & Madau, P., 1987, Comments Astrophys., **12**, 67.

[69] Fishbone L.G. & Moncrief V., 1976, Astrophys. J., **207**, 962.

[70] Paczynski B. & Wiita P.J., 1980, Astron. Astrophys., **88**. 23.

[71] Jaroszynski M., Abramowicz M.A. & Paczynski B., 1980, Acta. Astron., **30**, 1.

[72] Abramowicz M.A., Calvani M. & Nobili L., 1980, Astrophys. J., **242**, 772.

[73] Paczynski B., 1980, Acta. Astron., **30**, 447.

[74] Paczynski B. & Abramowicz M.A., 1982, Astrophys. J., **253**, 897.

[60] Lovelace R.V.E., Mehanian C., Mobarry C.M. & Sulkanen M.E., 1986, Astrophys. J. Suppl., **62**,1.

[61] Mobarry C.M. & Lovelace R.V.E., 1986, Astrophys. J. ,**309**, 455.

[62] Prasanna A.R. & Chakraborty D.K., 1981, J. Astrophys. Astr., **2**, 1.

[63] Chakrabarty D.K. & Prasanna A.R., 1981, J. Astrophys. Astr., **2**, 421.

[64] Prasanna A. R. & Bhaskaran P., 1989, Astrophys. Space. Sci., **153**, 201.

[65] Bhasakaran P. & Prasanna A.R., 1989, Astrophys. Space. Sci., **159**, 109.

[66] Bhasakaran P. & Prasanna A.R., 1990, J. Astrophys. Astr. **11**, 49.

[67] Bhaskaran P., **Tripathy S. C.** & Prasanna A.R., 1990, J. Astrophys. Astr., **11**, 461.

[68] Abramowicz M.A., Calvani, M. & Madau, P., 1987, Comments Astrophys., **12**, 67.

[69] Fishbone L.G. & Moncrief V., 1976, Astrophys. J., **207**, 962.

[70] Paczynski B. & Wiita P.J., 1980, Astron. Astrophys., **88**. 23.

[71] Jaroszynski M., Abramowicz M.A. & Paczynski B., 1980, Acta. Astron., **30**, 1.

[72] Abramowicz M.A., Calvani M. & Nobili L., 1980, Astrophys. J., **242**, 772.

[73] Paczynski B., 1980, Acta. Astron., **30**, 447.

[74] Paczynski B. & Abramowicz M.A., 1982, Astrophys. J., **253**, 897.

[75] Kuwahara F., 1988, Prog. Theo. Phys., **80**, 449.

[76] Kuwahara F., 1989, (Preprint).

[77] Pringle J.E., 1981, Ann. Rev. Astron. Astrophys., **19**, 137.

[78] Pringle J.E., 1973, Nature, **243**, 90.

[79] Shakura N.I. & Sunyaev R.A., 1976, Mon. Not. R. astr. Soc., **175**, 613.

[80] Hoshi R. 1979, Prog. Theo. Phys., **61**, 1307.

[81] Bath G.T. & Pringle J.E., 1982, Mon. Not. R. astr. Soc., **199**, 267.

[82] Abramowicz M.A., 1981, Nature, **294**, 235.

[83] Elsner R.F. & Lamb F.K., 1977, Astrophys. J., **215**, 897.

[84] Arons J. & Lea S.M., 1976, Astrophys. J., **207**, 914.

[85] Anzer U., Börner, G., 1980, Astron. Astrophys., **83**, 183.

[86] Anzer U., Börner, G., 1983, Astron. Astrophys., **122**, 73.

[87] Papaloizou J.C.B. & Pringle J.E, 1984, Mon. Not. R. astr. Soc., **208**, 721.

[88] Papaloizou J.C.B. & Pringle J.E, 1985, Mon. Not. R. astr. Soc., **213**, 799.

[89] Blaes O.M., 1987, Mon. Not. R. astr. Soc., **227**, 975.

[90] Goodman J. & Narayan R., 1988, Mon. Not. R. astr. Soc., **231**, 97.

[91] Frank J. & Robinson J., 1987, (Preprint).

[92] van der Klis M., Stella A., White N., Jansen A. & Parmar A.N., 1986, Astrophys. J., **316**, 411.

[93] Treves A., Maraschi L. & Abramowicz M.A., 1988, Pub. Astron. Soc. Pacific, **100**, 427.

[94] Prasanna A.R. in *Gravitation & Relativistic Astrophysics*, 1982, Eds. A.R. Prasanna, J.V. Narlikar & C.V. Vishveshwara, World Scientific, Singapore.

[95] Chandrasekhar S. 1961., *Hydrodynamic and Hydromagnetic stability*, Oxford University Press, London.

[96] Smith B.T., Boyle J.M., Garbow B.S., Ikobe Y., Klema V.C. & Moler C.B., 1974, *Lecture Notes in Computer Science*, **6**, Springer Verlag, Berlin.

[97] Garbow B.S., Boyle J.M., Dongarra J.J. & Moler C.B., 1977, *Lecture Notes in Computer Science*, **51**, Springer Verlag, Berlin.

[98] Uchida Y. & Low B.C., 1981, J. Astrophys. Astr., **2**, 405.

[99] Pringle J.E. & Rees M.J., 1972, Astron. Astrophys., **179**, 585.

[100] Greenberg P.J., 1971, Astrophys. J., **164**, 589.

[101] Bisnovayti-Kogan G.S. & Blinnikov S.I., 1972, Astrophys. Space. Sci. **19**, 119.

[102] Taam R.E. & vanden Heuvel E.P.J., 1986, Astrophys. J., **305**, 235

[103] Shields G.A., Wheeler, J.C., 1976, Astrophys. J., **17**, 69.

[104] Abramowicz M.A., Livio M., Soker N. & Szuszkiewicz E., 1990, (MPA Preprint).

[105] Choudhury S.R. & Lovelace R.V.E., 1986, Astrophys. J., **302**, 188.

[106] Pietrini P. & Torricelli-Ciamponi G.,1989, Phys. Fluids., **B1**, 923

[107] Corbelli E. & Torricelli-Ciamponi G., 1990, Phys. Fluids., **B2**, 828.

[108] Miura A. & Pritchett P.L., 1982, J. Geophys. Res., **87**, 7431.

[109] Shivamoggi B.K., 1981, Phys. Scr., **24**, 49.

[110] Rognlien T.D. & Weinstock J., 1974, J. Geophys. Res., **79**, 4733.

[111] Chhajlani R.K. & Vyas M.K., 1990, Astrophys. Space. Sci., **173**, 109.

[112] Press W.H., Flannery B.P., Teukolsky S.A. & Vetterling W.T., 1988, *Numerical Recipes - The art of scientific computing*, Cambridge University Press, New York.

[113] Simonutti M.D., 1976, Phys. of Fluids., **19**, 636.

[114] Pringle J.E., Rees M.J. & Pacholcyzk A.G., 1973, Astron. Astrophys., **29**, 179.

[115] Prasanna A.R., **Tripathy S.C.** & Das A.C. 1989, J. Astrophys. Astr. **10**, 21.

[116] **Tripathy S.C.**, Prasanna A.R. & Das A.C., 1990, Mon. Not. R. astr. Soc., **246** ,384.

[117] **Tripathy S.C.**, Dwivedi C.B, Das A.C. & Prasanna A.R., 1991, PRL-TH/91-1 (Preprint).

[118] **Tripathy S.C.**, Dwivedi C.B, Das A.C. & Prasanna A.R., 1991, (in preparation).